STUDIES OF THE JANUARY 31, 1986 NORTHEASTERN OHIO EARTHQUAKE

A Report to the
U.S. Nuclear Regulatory Commission

Prepared by the
U.S. Geological Survey

R.L. Wesson and C. Nicholson
editors

Open-file Report 86-331

Reston, Virginia
1986

TABLE OF CONTENTS

I. EXECUTIVE SUMMARY

This report describes the results of investigations of the northeastern Ohio earthquake of January 31, 1986 undertaken by the U.S. Geological Survey at the request of the Nuclear Regulatory Commission. These investigations include a study of the mainshock, its aftershocks, and previous seismicity; an assessment of the degree to which the deep fluid injection wells in the area may have influenced the recent earthquake activity; and an investigation of the high frequency nature of the seismograms recorded from both the mainshock and its aftershocks.

Analysis of the mainshock and aftershocks indicates no obvious structure or fault with which the January 31 earthquake can be associated. Locations of aftershocks obtained to date are permissive of the interpretation of a fault striking somewhat east of north, but as most of the aftershocks are tightly clustered in space, they provide only very weak evidence for the orientation of such a structure.

Estimates of stress inferred from commercial hydrofracturing measurements suggest that the state of stress in northeastern Ohio is close to the theoretical threshold for small earthquakes as predicted by the Mohr–Coulomb failure criterion. Given this state of stress, triggering of small earthquakes by fluid injection would not be surprising. However, the distance of the January 31 earthquake and its aftershocks from the wells (with the exception of the very small earthquake on March 12), the lack of any small earthquakes detected near the bottom of the wells, the history of small to moderate earthquakes in the region prior to the initation of injection, and the attenuation of the pressure field with distance from the injection wells, all argue for a "natural" origin for the earthquake. Therefore, although triggering remains a possibility, the probability that the injection played a significant role in triggering the earthquake, based on the information currently available, must be regarded as low. The analysis of the possible relation between the injection wells and the January 31 earthquake has indicated nothing to suggest the occurrence of an earthquake larger than that expected for the broad region, or the activation of a major structure closer to the wells or near the power plant.

High-resolution (up to 96 dB), broadband (< 200 Hz) recordings of the aftershock sequence show that seismic signals as high as 130 Hz were resolvable above noise levels

for the larger aftershocks (m_b 2.2; 2.5) at hypocentral distances up to 18 km. Signals relatively rich in high frequencies were also observed on the strong-motion records of the mainshock for frequencies up to the upper bandwidth limit of the recorders (30 Hz). Based on the aftershock data, spectral ratios computed to estimate the amplitude response of local site conditions at a site near the Perry Nuclear Plant (site GS01) show exaggerated vertical ground shaking near 4–7 Hz and near 20 Hz. The peaks in spectral ratios near these frequencies appear to be attributable, at least in part, to resonances in the near-surface soil layers. Smaller, but apparently significant, resonances are also indicated in the spectral ratios for horizontal motions.

Investigations to date have suggested the value of additional studies in several areas. Continued earthquake monitoring in the vicinity of the epicenter of the January 31 earthquake would be of considerable value both for the generic problem of trying to understand earthquakes in the eastern United States and from the point of view of continued investigation into the question of a possible relationship between the January earthquake and fluid injection. Additional geophysical investigations, particularly using the seismic reflection technique and research–quality measurements of stress in boreholes, would also be useful in attempting to understand the structural and tectonic conditions that led to the earthquake. Generic studies of site resonances, including field and numerical studies, would help in assessing the potential levels of exaggerated ground shaking and their significance for engineering purposes.

II. INTRODUCTION

On January 31, 1986, at 11:46 EST an earthquake of magnitude 4.9–5.0 [NEIS] occurred about 40 km east of Cleveland, Ohio, and about 17–18 km south of the Perry Nuclear Power Plant. The earthquake was felt over a broad area including 11 states, the District of Columbia, and parts of Ontario, Canada, caused intensity VI–VII at distances of 15 km, and generated relatively high accelerations (0.18 g) of short duration at the plant. Because of the nature of this event and its proximity to a critical facility, a rapid response by the seismological community was triggered. The result was some 47 stations occupying 64 sites were deployed by 7 agencies or institutions. These included Lamont–

Doherty Geological Observatory, the Tennessee Earthquake Information Center, St. Louis Univeristy, the University of Wisconsin, the U.S. Geological Survey, Weston Geophysical Corporation and Woodward–Clyde Consultants. Analog portable seismographs were operating within 10 hrs of the mainshock, and broadband wide-dynamic range digital GEOS instruments were recording within 27. Thirteen aftershocks were detected as of April 15th, with six occurring within the first 8 days. The latest was on March 24th. Two of the aftershocks were felt. Coda magnitudes for the aftershocks ranged from -0.5 to 2.5. Focal depths for all the earthquakes range from 2 to 7 km.

Of concern was whether the mainshock indicated a level of seismic hazard in excess of that previously believed to exist in the region. The January 31st earthquake was the largest to occur in the northeast Ohio region since records of earthquake activity began, however, approximately 30 earthquakes of smaller magnitude were previously recorded in this area. The largest of these prior earthquakes was of comparable magnitude (m_b = 4.5–4.7) and occurred in 1943.

Another aspect of this sequence was the possibility that the recent earthquakes were induced by deep injection well activities. Three wells that penetrate the basement are currently operating within 15 km of the earthquakes and there was concern expressed that the wells may have played a significant role in triggering the earthquake activity.

Although the attenuation of seismic waves is less severe in the eastern as opposed to the western United States, unusually high frequencies were recorded at considerable distances for both the mainshock and its aftershocks. A question arose as to whether these high frequencies were a result of regional path effects, unusual source characteristics, or specific site resonances.

This report discusses the results of three lines of investigation carried out by the U.S. Geological Survey and includes compilations of data from a number of different sources. The first is a basic study of the mainshock and its aftershocks, and includes locations, focal mechansims and information on previous historical seismicity. The second involves an investigation of the deep fluid injection wells, and an assessment on the degree to which the wells may have influenced the recent earthquake activity. The third study concerns the character of the earthquake seismograms, principally from the aftershocks,

and the nature of the high frequency content of the recorded ground motion, particularly at the Perry Nuclear Power Plant.

ACKNOWLEDGMENTS

This study was conducted on behalf of, and with financial support from, the Office of Nuclear Reactor Regulation, U. S. Nuclear Regulatory Commission.

The authors acknowledge and appreciate the cooperation, exchange of data, and discussions with the following agencies and individuals:

Calhio Chemical Company

William Toth

Cleveland Electric Illuminating Company

Eilleen Buzzelli, Frank Stead, Mike Hayner

Electric Power Research Institute

Carl Stepp

Lamont–Doherty Geological Observatory

Nano Seeber, John Armbruster, Keith Evans, David Simpson

Geauga County Disaster Services Agency

Dale Wedge, Pat Linn

Geoscience Services

Joseph Fischer

John Carroll University

William Ott, S.J.

Nuclear Regulatory Commission

Leon Reiter, Phyllis Sobel

Ohio Geological Survey

Horace Collins, Mike Hansen

Ohio Division of Oil and Gas

Dennis Crist

Ohio Environmental Protection Agency

Gerry Myers

Petro Evaluation Services Company

Jay Henthorn

Resouce Services, Inc.

Warren Latimer

St. Louis University

Steve Nyers, Robert Herrmann

Tennessee Earthquake Information Center

Jer-Ming Chiu

University of Wisconsin

Doug Christensen

Weston Geophysical Corporation

Richard Holt, Gabriel LeBlanc, Preston Turner

Woodward–Clyde Consultants

Tom Statton, Richard Quittmeyer, Kathy Mroteck

III. HISTORICAL SEISMICITY

Compilations of historical earthquakes in northeastern Ohio based on felt reports extend back to at least the mid-1850's. Instrumental recordings of local and regional earthquakes began in northeastern Ohio when John Carroll University, located in the outskirts of eastern Cleveland, started operation of its observatory in 1904. A seismicity map for Ohio (Figure 1, Stover *et al.*, 1979) indicates about 30 earlier earthquakes in the northeastern region of the state. Since 1850, the repeat time for felt earthquakes is about 9 years, although earthquakes large enough to cause damage (intensity VI) are rare. The largest event known prior to 1986 was a magnitude 4.5–4.7 earthquake that occurred in 1943. This 1943 earthquake was recently relocated using the same velocity model as was used to locate the 1986 mainshock (J. Dewey, written communication, 1986). Its revised location (41.628° N ± 14 km, 81.309° W ± 10 km) is just slightly west of the 1986 event. Thus, the earthquake of 1986 should not be considered unusual.

Appendix A contains an expanded, updated version of the seismicity catalog for the state of Ohio. Only those earthquakes with epicenters within the boundary of the state

are listed, even though additional earthquakes in bordering states or in Canada may have been felt or have caused damage in Ohio. Most notable of these are the Attica, New York earthquake of 1929 (m_b = 5.2), and the northern Kentucky (Sharpsburg) earthquake of 1980 (m_b = 5.2). The largest event in Ohio was part of an earthquake swarm near Anna in 1937, and had a magnitude between 5 and 5.5. Another earthquake of particular interest is the 1983 event (m_{bLg} = 2.7) near Perry, the location of which is unfortuately rather uncertain (Appendix A). In November of 1983, an earthquake of about magnitude 2.5 was observed by stations operated by the University of Western Ontario (G. LeBlanc, personal communication). Its position is unknown, however, its seismogram is similar in many respects to the January, 1983 event. Its absence from the U.S. earthquake catalogs implies a detection threshold for this part of Ohio at or above magnitude 2.5.

IV. MAINSHOCK

The earthquake of January 31, 1986 occurred at 11:46 EST. There was no immediate foreshock sufficiently large to record on the instruments at John Carroll University, although there is a suggestion of two earlier events, one on January 23rd and the other on January 30th, based on comparison of the daily seismograms with that of the largest aftershock (J. Armbruster, personal communication, 1986). The mainshock was felt over a wide area and as far away as northern Virginia. The magnitude of the event was m_b = 4.9 (NEIS) based mostly on data from Europe, or m_{bLg} = 5.0 (SLU) from surface waves.

By holding the focal depth fixed at 10 km, the mainshock epicenter was located at 41.650° N latitude and 81.162° W longitude, using P-wave arrivals from 41 stations. All of the stations utilized in the location procedure were within 10° of the earthquake, the closest station being CLE (John Carroll University) at 0.32°, and the farthest was POW (Powhatan, Arkansas, SLU) at 9.55°. The velocity model developed by Nuttli *et al.*[1969] from earthquake travel-times in the central United States was used in the location process and resulted in a maximum horizontal standard error in location of ±4.6 km, based on a 90% confidence ellipsoid.

Within the resolution of the data, moment of the mainshock is estimated to be about 3×10^{23} dyne–cms, based on inversion of surface waves, with a focal depth of 8 km and a

focal mechanism that is either right-slip (N20° E) or left-slip (N290° W) on nearly vertical nodal planes (A. Dziewonski, R. Herrmann, personal communication, 1986). A body-wave moment tensor inversion was attempted, but amplitudes were too small for sufficient resolution (J. Nabelek, personal communication).

Both the U.S. Geological Survey and Weston Geophysical Corporation conducted intensity studies immediately following the mainshock (Figures 2 and 3). Most notable of the earthquake effects were: the fairly widespread region of panic in Painesville and Mentor (including the temporary evacuation of several public buildings); the collapse of a ceiling, a broken water main, significant damage sustained by the city sewer lagoon, and a large number of chimneys thrown down in Chardon; a large area of disturbed wells and a damaged trailer near Hambden; cracks that developed in the Thompson High School (causing a temporary evacuation); damage to the foundations of the Amish School and City Hall in Huntsburg; and a broken gas line as far away as South Russell (Geauga County Disaster Services Agency, 1986). Fifteen people were reported to have suffered minor injuries. Isolated intensities approached VII (Figure 3) although in general the maximum intensity was VI (Figure 2). The intensity at the Perry Nuclear Power Plant was V.

Preliminary intensities reported by the USGS (Figure 2) were determined during a canvas of the epicentral area on February 4–11, 1986. The highest intensities found (Modified Mercalli intensity VI) occurred up to 15 km away from the instrumental epicenter. Two areas defined by the intensity VI isoseismal are identified. One, which includes the earthquake epicenter, is somewhat elongated in a northeast-southwest direction with an additional lobe to the northwest. Such elevated levels of intensity toward the lake are not unexpected, as site resonances within lake sediments often amplify strong ground motion (*c.f.*, Section VII). The other area of intensity VI is off to the southeast. Damage within intensity VI isoseismals consisted primarily of wall cracks, cracked or fallen plaster, fallen ceiling tiles, damaged chimneys, disturbed wells, items fallen off shelves, broken pipe seals and cracked windows. Fallen plaster generally occurred in older buildings. Disturbed ceiling tiles, usually along the juncture of the ceiling with an outside wall, occurred where the intensity based on other indicators was V to VI.

The isoseismals shown in Figure 2 are dashed because additional data will soon be available from a more systematic survey involving USGS intensity questionnaires. When the new data are included, configurations of present isoseismals may change although major modifications are not expected. At present, however, an area that encompasses most of the intensity V isoseismal may be defined by an ellipse with semi-major and semi-minor axes of 100 and 60 km, respectively, and oriented in a northeast direction. The "valley" of low intensities (primarily III–IV) found within this area of intensity V's has no apparent correlation with regional bedrock geology, although the southwest section of the intensity low does correspond to an area of kames and eskers. Futher work is needed, however, to establish more definitive relationships, once the more complete data are available.

V. AFTERSHOCKS

This discussion covers aftershocks recorded during the period 31 January to 15 April, 1986, and describes analysis of data collected by field teams from the U.S. Geological Survey, as well as the analysis of arrival time and first motion data obtained from the other cooperating groups listed above. Most instrumentation consisted of single-component high-frequency analog recorders. However, the U.S. Geological Survey deployed 10 broad–band, high–dynamic range digital GEOS instruments with internal clocks synchronized to radio time code (WWV). These stations started operation on February 1st, and several were still in operation as of April 3rd. Station locations, time histories, Fourier amplitude spectra, preliminary aftershock locations as well as discussions of the deployment and instrument capabilities of the GEOS stations are given in Borcherdt [1986]. Including both analog and digital recording by all of the groups and agencies, some 47 stations operating at 64 sites were deployed. Table 1 lists station names, affiliations and locations for the sites occupied during the aftershock study.

As of 15 April, some 13 aftershocks were located. Most of these events occurred within the first 8 days; two were felt. Coda magnitudes ranged from -0.5 to 2.5 based on a formula developed for earthquakes in the northeastern United States [Chaplin *et al.*, 1980]. Figure 4 presents seismograms of some of the earthquakes recorded on the analog instruments. It is obvious that in many cases the events are very small. Because of the

dense network of stations (Figure 5), however, even the smallest event was reported by at least 6 stations.

In addition to the aftershocks, several events believed to be quarry blasts were also recorded (Figure 6). These events all occurred on weekdays during working hours, generated nearly the same signals at the recorders, had lower frequency content content, and exhibited an air wave. Two of these events were located as a matter of course (Figure 9) and were found to occur near a sand and gravel pit south of Thompson and east of Rt. 528.

Three preliminary velocity models were used to locate the earthquakes and are given in Table 2. The first is a simple two-layer model to accommodate the Paleozoic section over the granitic basement. It is essentially the same model used by Weston Geophysical to initially locate earthquakes in their aftershock survey. The second is somewhat more complex and is based on a surface-wave inversion across the Cincinnati Arch by Herrmann [1969]. The third is a composite from several different sources and consists of 5 sedimentary layers over crystalline basement at a depth of 2.1 km. The interfaces are based on an extensive compilation of information from wells drilled at least as far as the top of the PreCambrian basement (Cleveland Electric Illuminating Company, 1982). An average of down-hole and cross-hole velocity logs were used to determine the P and S wave velocities in the upper 0.5 km. Velocities in the basement, lower crust and mantle are based on regional earthquake travel-time studies [Nuttli *et al.*, 1969]. Velocities in the Paleozoic section are inferred from refraction studies in adjacent areas [Press, 1966]. All three models should be considered preliminary. With the exception of the near-surface P and S velocities in the third model, the velocities used in the models are not based on actual *in situ* measurements in the epicentral region, and several are only estimates from a limited set of available data. Furthermore, none of the models takes into consideration the slight dip of the top of the PreCambrian interface, which near the shore of Lake Erie is about 1830 meters (6,000 feet) deep but near the epicentral region, it is about 2130 meters (7,000 feet).

The earthquakes were located using HYPOELLIPSE [Lahr, 1985] and as many of the available arrival-times as were internally consistant. Arrivals based on the digitally recorded GEOS intruments were given preferential weight because of the higher precision

of timing, the greater resolution in picking the arrivals and the greater confidence in identifying the shear-wave arrival on the three-component instruments. A serious complication in the earthquake locations was that many of the single-component stations reported secondary arrivals that were often a converted phase (S to P). Figure 7 shows a composite Wadati diagram for vertical stations operated by the USGS. The slope is 1.68 indicating that many of the secondary arrivals plotted as S traveled part of their ray paths as P waves. Preliminary studies of these phases [R. Borcherdt, L. Seeber] indicates that the arrival times are consistent with conversion taking place at either the base of the Paleozoic section (P to S) or the base of the unconsolidated surface sediments (S to P). Thus, in order not to mix both converted and direct shear arrivals, two sets of locations are given. The first set utilizes only the data from the USGS instruments (Figure 8) and is shown in Figure 9. S arrivals from the GEOS three-component stations are used and the earthquakes are located using the simplest velocity model (model #1). These locations give the results from a fairly homogeneous data set for which a high degree of confidence is associated with each arrival. For comparative purposes, a second set is given that utilizes all the available data. In this second set (*e.g.*, Figure 13), there is better station coverage and therefore greater precision, however, accuracy is somewhat degraded because of slight variations in internal timing within each of the networks included and because some of the additional stations had poorer resolution in identifying arrival times off analog records. The second set also gives preferential weight to the GEOS instrument readings and employs the prefered 7–layer velocity model (model #3). It is apparent, however, that even with different velocity models or different procedures used in the location process, the earthquake epicenters do not vary by much (Table 3). Only the focal depths are significantly affected, with systematic biases of up to a kilometer when separate models are used.

Aftershock Locations

One of the more notable features of the aftershock sequence was that it contained so few events. No aftershocks were detected in the first 26 hrs and only thirteen were reported by April 15th. Whereas, with the Sharpsburg, Kentucky, earthquake of 1980, 60

aftershocks were located within the first 16 days; and in the case of the Goodnow, New York, earthquake ($M_L = 5.2$) of 1983, almost 100 aftershocks were recorded in the month following the mainshock. In addition, most of the early aftershocks of the 1986 event occurred within a very small source volume. Figures 9 through 11 show the locations of the first 6 aftershocks using only the USGS stations. These earthquakes describe a very small source region that could be considered an ellipse with semi-major and minor axes of 1.2 and 1.0 kms. The vertical extent of the activity is confined to a narrow seismogenic zone between 4 and 7 kms deep. If only this initial seismicity is used, there is not sufficient resolution or spatial extent in activity to define any preferred fault structure, and indeed, activity originating from a single point source can not be precluded. Vertical cross sections shown in Figure 11 demonstrate that independent of the observation point, no particular planar feature is evident.

Using all the available data, however, some evidence of a fault structure emerges. Figure 12 shows all the available aftershock locations as well as station coverage within the immediate vicinity. Although the initial aftershock activity remains in a very small cluster, there was an event on March 24th that is located about a kilometer outside the immediate source region of the mainshock (Figure 13). Its location to the SSW, coupled with a poorly resolved trend in the earthquake epicenters, suggests a short fault segment oriented 15° to 20° east of north, consistent with one of the nodal planes observed in the preliminary focal mechanism of the mainshock. Vertical cross sections taken perpendicular and parallel to a strike of N20° E (Figure 13, B and C), suggest that rupture may have occurred at depth on a nearly vertical fault with a NNE orientation.

In addition to the tight cluster of aftershocks, one small earthquake was detected near station GS02 (Figure 12) on March 12^{th}. Its relative proximity to the Calhio injection wells, suggests that at least this single event may be a candidate for having been induced. This event is discussed further in Section VI.

Focal Mechanism Solutions

Single-event focal mechanism solutions (lower hemisphere equal-area projections) were constructed using polarity data from nearly all the temporary stations deployed. Readings

from both sets of USGS instruments, Lamont, TEIC, Weston Geophysical and Woodward–Clyde were combined to produce the results shown in Figures 14–17. For those few events that were too small to yield a sufficient number of first motions to determine a single-event solution, a composite of the first motions of these smaller events is given along with the focal mechanism solution of the largest aftershock (Figure 18). As expected, the largest events give the most consistent results. These earthquakes exhibit focal mechanism solutions with NNE and WNW striking nodal planes (Figure 14). If the NNE-striking nodal plane is taken as the fault orientation, then motion during the earthquake is oblique right-slip. Other focal mechanisms (Figures 15-17) exhibit significantly different nodal plane orientations. Although it is certainly true that for some of these smaller events, the actual first-motion may have been lost in the background noise, the consistent change in large numbers of first-motions observed at various stations (while preserving the specific radiation pattern of a double-couple source) lends credence to the interpretation that the focal mechanism for all the aftershocks is not the same. For some, a large component of normal faulting is observed in the fault plane solution (*e.g.*, 860210), while others exhibit nodal planes with significantly different orientations (*e.g.*, 860207). In general, however, most of the focal mechanisms are consistent with a maximum horizontal stress field striking ENE. The observation that different focal mechanisms are found throughout the aftershock sequence suggests that more than one favorably oriented fracture is being reactivated. Furthermore, because the orientations in slip vary from predominantly strike-slip to oblique slip with a large component of normal faulting, this implies ratios of the principal stresses such that the vertical stress is intermediate, but very close to the maximum horizontal stress.

VI. POSSIBLE ROLE OF FLUID INJECTION

Motivation and Background

It has been conclusively demonstrated that under some conditions, the increase in fluid pressure in the earth's crust as the result of the injection of fluid or the impoundment of a reservoir, can trigger earthquakes [*c.f.*, Raleigh *et al.*, 1976]. In view of the deep waste disposal wells in operation near the epicenter of the January 31 Northeastern Ohio

earthquake, a study was undertaken to determine, to the extent possible, whether the waste injection wells may have played some role in triggering the earthquake. In addition, the possible role of solution mining for salt, previously active in the area, was also considered.

Well-documented examples of earthquake activity induced by fluid injection include earthquakes triggered by waste injection near Denver [Healy *et al.*, 1968; Hsieh and Bredehoeft, 1981], by secondary recovery of oil near Rangely, Colorado [Raleigh *et al.*, 1976] and in West Texas [Davis, 1985], and by solution mining for salt in western New York State [Fletcher and Sykes, 1977]. Other cases of induced seismicity, owing to either fluid injection or reservoir impoundment were recently reviewed and discussed by Simpson [1986]. In each of these cases it is possible to show two characteristics of the induced earthquakes. First, there is a very close geographic association between the bottom of the injection wells and the locations of the earthquakes in the resulting sequence. Second, it is possible to perform calculations based on the measured or inferred state of stress in the earth's crust and the measured injection pressure to determine whether the theoretical threshold for the occurrence of an earthquake is met. These calculations are referred to as the determination of the state of "effective stress" and its relation to the "Mohr–Coulomb failure criteria," [see, for example, Jaeger and Cook, 1976].

Two deep injection wells near Perry, Ohio, are the most likely candidates for possible earthquake triggering in view of their depth, injection pressure and length of operation. The first of these wells, Calhio #1, was completed in 1971 [Natural Resources Management Corp., 1971]. Full-scale injection of waste into the well began in 1975. A second well, Calhio #2, was completed in 1981, and has been used as a backup to the first well since that time [Resource Services Inc., 1980]. The two wells are located somewhat less than 1 km apart, therefore at distances more than a few kilometers away, the wells can be considered as a single point source of fluid. More than 1.19 billion liters (315 million gallons) of fluid have been injected into the two wells, principally into Calhio #1 (Figure 19)[Ohio EPA, written communication, 1986]. Both wells are about 1800-m deep, extending a short distance into the PreCambrian crystalline basement. The basement in this region is overlain by a section of essentially flat-lying sedimentary rocks of Paleozoic age. The formations of principal interest in this study are the basal sandstone (Mt. Simon formation) and the overlying

Rome and Maynardsville formations. The Mt. Simon formation was the targeted injection zone, but initial drill stem and injection tests indicated a lower than expected permeability. Consequently, both wells are open to both the Mt. Simon and Maynardsville formation [Natural Resources Management Corp., 1971]. Typical injection pressure at an injection rate of 320 liters/min (85 gals/min) have reached a maximum of 110 bars (1620 psi) at the wellhead. The corresponding pressure at the bottom of the well is the sum of the wellhead pressure plus the hydrostatic pressure caused by the weight of the fluid in the well itself. This amounts to an additional 181 bars (2658 psi) or a total pressure of 291 bars (4278 psi), taking 1.025 as the average density of the injected fluid.

As described in the previous section, the mainshock of the January 31 earthquake, and all its immediate aftershocks are rather tightly clustered about 5 km north-northwest of Hambden, Ohio. As shown in Figure 20, the deep injection wells near Perry, Ohio, are about 12 km farther to the north. There was, however, one small (coda magnitude -0.2) earthquake located close to the wells on March 12^{th}. Figure 21 shows the seismogram of this event as recorded by station GS02. Subsequent examination of all the available records proved that this earthquake was recorded by at least 5 other stations. The location of this earthquake is about 1 km west of station GS02 and about 3 km SSW of the Calhio wells (Figure 20). Furthermore, its focal depth was determined to be 2 km. This corresponds to the base of the Paleozoic section and is the same depth at which fluid is injected from the Calhio wells. Although this one earthquake could be a random event, its depth and position relative to the injection wells is suggestive. Whether additional earthquakes, triggered by well injection, have occurred is uncertain. Although no known earthquake is located immediately adjacent to the wells, the detection threshold for earthquakes near the well prior to the installation of portable equipment following the January 31 earthquake (relying on the seismograph at John Carroll University in Cleveland) is estimated to be somewhat greater than magnitude 2.5. Consequently, it is conceivable that additional small earthquakes could have occured nearer to the wells between the initiation of injection operations and the January 31 earthquake.

In the best documented case of injection induced seismicity, at the Rocky Mountain Arsenal near Denver, small earthquakes began near the bottom of the injection wells, then

migrated out along a northwesterly trend for a distance of about 6–7 km [Healy *et al.*, 1968]. After the sequence had been in progress for 5 years (18 months after well operations ceased), the earthquakes continued to occur near the base of the wells but primarily in a linear zone 4–6 km away and at a depth of 4–6 km. The occurrence of the one small earthquake near the well, as shown in Figure 20, gives some support to the possibility that other earthquakes, including the 1986 mainshock, may also have been triggered by injection activities.

Estimation of the State of Stress

The principle sources of information about crustal stress in the epicentral area are: measurements of the instantaneous shut-in pressure (ISIP) made during commercial hydrofracture operations (these indicate the magnitude of the least compressive stress), breakdown pressures during well stimulation (these provide estimates on a combination of both the maximum compressive stress and the tensile strength of the rock being fractured), fracture re-opening pressures (which provide estimates of the maximum compressive stress alone), and focal mechanism orientations which provide some indication of the ratios between all three principal stresses. In the case of Lake County, Ohio, data from three wells (the two Calhio wells and the Diamond Alkalai brine disposal well near Painesville) can be used to set bounds on many of the critical values necessary to make a proper evaluation of the degree to which stress conditions may have been affected as a result of well operations.

In addition, K. Evans (written communication, 1986) has compiled a number of ISIP measurements into a map showing the ratio of overburden stress to the minimum compressive stress for the Appalachian Basin. Several of the measurements included in his data set were made expressly for the purpose of determining the state of stress in the rock and not simply for well stimulation. These data show that below the regional evaporite layer, this ratio is uniform throughout much of the northern Appalachian basin. These stress ratios vary from about 0.6 to 0.7, with values tending to decrease slightly toward the south. Stress ratios smaller than unity suggest that the vertical direction is either the intermediate or greatest principal stress, and therefore that hydrofrac operations in this region open vertical fractures perpendicular to the horizontal least compressive stress.

For those hydrofrac operations that were performed for the purpose of stress measurement, the direction of maximum compressive stress is NE to East. Although a shallow stress measurement was in fact made very near the disposal well site (at the Perry Nuclear Power Plant), the unusually high stress ratio found is probably attributable to decoupling above the evaporite layer and consequently not representative of the basement stress-field magnitude ratios (K. Evans, written communication).

The horizontal NE striking maximum compressive stress obtained by hydrofrac measurements is consistent with the preliminary focal mechanism for both the 1986 mainshock and many of its aftershocks. An important implication, however, of the focal mechanisms is that because the predominant style of faulting observed is nearly pure strike-slip, the maximum compressive stress is horizontal and greater than the overburden. The fact that some of the earthquakes exhibit large components of normal faulting, however, implies that the stress difference between the vertical and maximum horizontal compressive stress is not large.

State of stress at bottom of injection wells

Table 4 lists relevant values for principal stress available from both existing well data and regional variations. The calculations or extrapolations are done in bars (1 bar = 14.7 psi), and represent the best estimates presently available. It should be noted that there is a large uncertainty in many of these values (particularly the maximum horizontal compressive stress), mainly because commercial measurements are ill–suited for this analysis and because accurate detailed measurements within the epicentral region are not available. In nearly all cases, some assumptions and interpretations of the existing well records had to be made to determine the values calculated. Thus, the values presented in Table 4 should be considered very preliminary. The preferred values listed at the bottom of the table are not simple averages of all the available estimates for that particular value, but represent our considered opinion as to the most likely estimate.

The vertical stress can be calculated once the weight of the overburden is known. Density logs taken in the Calhio wells indicate an average density of 2.6 g/cm^3 (K. Evans, written communication). This implies a density gradient of .255 bar/meter or 459 bars at

the bottom of the well. Nearly identical values of overburden stress were measured in a deep Michigan hole drilled through similar materials [Haimson, 1978].

Values for the least principal stress at the base of the Paleozoic section (bottom of the wells) can be estimated from the instantaneous shut-in pressure (ISIP) recorded while each of the wells was hydrofractured. The actual measurement of this pressure is made at the top of the hole, so it has to be corrected by adding to it the pressure of the weight of the fluid column in the drill string. Some uncertainty is introduced by this correction because although most of the wells were stimulated with fresh water (specific gravity 1.0 g/cm^3), the presence of other material in the injected fluid (acid, sand, waste, brine, etc.) will make the density of the fluid somewhat higher. To simplify matters, a standard value of 180 bars is assumed for the correction to the bottom of the wells (1800 meters), unless specific information was available to indicate a different value was more appropriate. In several cases, values for the ISIP are measured both early and late into the hydrofrac procedure. Table 4 lists both values. Since the value measured after extended pumping is often not a true indication of the least principal stress, initial values of ISIP are assumed to be more valid. Initial values, corrected to the bottom of the well, range from 262 to 302 bars. If regional values of the stress ratio are used (assuming 460 bars for the vertical stress), the minimum stress ranges from 275 to 321 bars. Thus, these two independent estimates yield similar values. Extrapolations from downhole measurements made at regional distances (Michigan and western New York) range as high as 370 bars [Haimson, 1978; Hickman *et al.*, 1985]. The preferred value is taken to be 300 bars. This is on the conservative side, as small values of ISIP (and therefore the minimum horizontal compressive stress) imply a larger stress differential relative to the maximum horizontal compressive stress, and thus a greater likelihood for shear failure along preexisting favorably-oriented fractures.

Formation pore pressure is measured directly during drill stem tests. Table 5 lists values of pore pressure measured in both the Mt. Simon and Maynardville formations from the two Calhio wells. The two sets of measurements were made about 9 years apart. Those made in the Calhio #2 well indicate a change in the formation pore pressure since extensive pumping began in the Calhio #1 well four years earlier (1975). The apparent increase in pore pressure with time found in the Maynardsville is consistent with calculated effects of

fluid injection in the adjacent well. The apparent decrease in pore pressure found in the Mt. Simon, however, is anomalous and may reflect the imprecision of the measurements. In any case, the values obtained are all close to hydrostatic if the density of the connate water is assumed to be 1.2 g/cm^3.

From the preliminary focal mechanism solutions, the maximum horizontal compressive stress is at or above the vertical stress (i.e., $\geq$ 460 bars). Values extrapolated from regional downhole measurements are in excess of 500 bars [*e.g.*, Hickman *et al.*, 1985]. Estimates derived from formation breakdown pressures during well stimulation in the Calhio wells give lower values, but they need to be corrected for the effective tensile strength of the rock. This would revise these estimates upwards by anywhere from 40 to 100 bars, as tensile strength can vary over a considerable range. Measurements derived from well records made during the stimulation of the brine well near Painesville are suspect, since the hydrofrac procedure was done through perforated casing [Petro Evaluation Services Inc., 1985]. Of all the measurements, the value of the maximum compressive stress is the least well known. Accurate assessment of this value is critical to evaluations of the effects of the injection wells. Larger values imply a larger stress differential, and thus a greater potential for failure of the rock. It must be emphasized that because of the large uncertainties in the value of the maximum principal stress, no definitive statement regarding the potential for failure can be made at the present time, however, estimates based on the lower bound to the maximum horizontal compression (*i.e.*, the vertical stress of 460 bars) are useful, as they would represent conservative estimates on how close to failure conditions are at the top of the basement.

Using the preferred values given in Table 4, it appears that without fluid injection, the conditions are near but do not exceed failure at the bottom of the wells. Figure 22a is a graphical representation of the Mohr–Coulomb failure criterion. Shear failure is likely to occur when the shear stress (τ) exceeds values defined by the linear relation $\tau = \tau_0 + \mu\sigma_n$, where τ_0 is the effective tensile strength, μ is the coefficient of friction, and σ_n is the stress normal to the plane of slip. For a preexisting fracture with no cohesion, τ_0 is zero. Shear stress along fractures of various orientations are linear combinations of the maximum and minimum compressive stresses, and are defined by the locus of points

around the Mohr circle, whose center is the average between the maximum and minimum principal stresses (right circle, Figure 22a). Larger stress differences between the maximum and minimum, result in larger Mohr circles and larger available shear stresses for favorably oriented fractures. In the presence of a fluid, the effective stress levels are reduced by the amount of the formation pore pressure, which moves the Mohr circle to the left (middle circle, Figure 22a). This condition is close to but does not exceed the failure criterion for a fracture with no cohesion. At a nominal injection pressure of 110 bars, however, this would bring the zone immediately surrounding the well bottom to an effective stress state near critical for favorably oriented preexisting fractures having a cohesive strength of as much as 40 bars and friction coefficient near 0.6 (left circle, Figure 22a). Preliminary focal mechanisms and hydrofrac stress measurements suggest that vertical planes striking NNE and ESE would be most favorably oriented for failure. And since the overburden is only a lower bound for the estimate of the maximum compressive stress, the actual conditions for failure would be more critical than the situation shown.

Because fluid injection could have brought at least the region near the bottom of the well into a critical stress state, the absence of any known earthquakes in the immediate vicinity of the well suggests that there are no favorably oriented weak fractures near the well. Thus, either existing fractures have cohesion strengths greater than 40 bars, or if weaker fractures do exist, they are not favorably oriented for failure in the existing stress field. The predominant dip of fractures observed in a core taken from the injection zone in Calhio well #2 is 20 degrees. Such fractures would not be favorably oriented for failure according to the forgoing analysis, as shear stress is maximum only for near vertical faults.

State of stress in the hypocentral region

Estimation of the preexisting state of stress at the hypocenter requires extrapolation of measurements to a depth of 5 to 8 km, a procedure that is somewhat controversial. McGarr (1980) shows that although it is permissible to extrapolate individual stress components to depth in laterally homogeneous environments, the linear extrapolation of principal stresses is not theoretically justified.

In the epicentral region, the compilation by K. Evans indicates a stress ratio of about

0.63 determined in hydrofrac operations in the Silurian Clinton–Medina sandstone. If the same ratio is applied at the hypocentral depth of 5 km, then the overburden pressure of about 1300 bars corresponds to a minimum compressive stress of 820 bars. Hydrostatic fluid pressure at 5 km depth would be 590 bars, assuming a density of 1.2 g/cm^3 for the connate brines. This state of effective stress is plotted on the Mohr circle diagram in Figure 22b. This figure again indicates a near-critical stress state for favorably oriented pre-existing fractures.

Fluid Pressure Changes in Epicentral Area Due to Fluid Injection

Estimation of the fluid pressure change near the earthquake hypocenters is inconclusive because we lack detailed information about the nature of the reservoir into which the waste is being injected. The characteristics of the reservoir in the vicinity of the well are known from measurements made during well completion. Using these characteristics, three alternate reservoir models were evaluated in order to determine what the increase in fluid pressure at the hypocenter may have been. The first model is an infinite isotropic reservoir; the second two are reservoirs of rectangular cross section, extending to infinity in the third direction, which is assumed to be in the direction connecting the well and the hypocenters. These models are for the purpose of studying how fluid pressure propagated horizontally from the well and do not address the question of how the fluid migrated downward 3 km from the injection horizon to the approximate hypocentral depth of 5 km.

Reservoir properties

The wastes are injected into both the Maynardville and Mt. Simon formations that lie just above the PreCambrian granitic basement. Table 6 lists properties of these formations obtained from the UIC permit application for well number 2. It is stated in the report from Resources Services [1980] that these two zones are very similar in wells numbers 1 and 2. A representative transmissivity for the entire injection zone is 4.2E–6 m^2/s. Although the storativity, which gives the amount of fluid released per unit column of aquifer for a unit decline in head, is unknown, a minimum value can be obtained by neglecting the compressibility of the reservoir. For a formation having the thickness of the Maynardville and Mt. Simon formations combined, and a porosity of 0.08, the minimum

storativity is 2.2E–5. An assumption of minimum storativity results in a maximum value for the cone of impression surrounding a source. A more realistic value of 5.4E–5 for the storativity is obtained by assuming a reservoir compressibility of 3.5E–6 per bar. Although the storativity does not have a great effect on the infinite reservoir calculations, it does have a significant effect on the strip reservoir calculations.

For purposes of calculating pressure 12 km from the well, it suffices to use an average fluid injection rate. The total volume injected into both wells is 1.17 billion liters (310 million gallons) during the period from March 1975 through November, 1985. For purposes of the following analysis, this amount was assumed to be injected over the total lifetime of the well (i.e, 1972–1986, or about fourteen years), corresponding to an average injection rate of 6.7 million liters/month. This assumption slightly underestimates the pressure affect of the wells. Because the distance between the wells (about 0.5 km) is small compared to the distance from the wells to the hypocenter, the two wells have been modeled as a single fluid source.

Infinite reservoir model (radial flow)

In order to maintain injection pressure of 110 bars or less for the assumed 14-year period of operation of the injection wells, a slight increase in transmissivity to 4.5E–6 m^2/s was assumed. Figure 23 shows pressure versus distance for different time periods after initiation of injection at 7 million liters/month into an infinite reservoir with a transmissivity as specified and a storage coefficient of 5.4E–5. Figure 24 is a plot of pressure versus time at the well bore for the same model. The infinite reservoir model yields an estimate of slightly less than 2 bars for the increase in fluid pressure 12 km from the well, which is where the January 31^{st} earthquake occurred.

Infinite strip reservoir model

The pressure falloff with distance is greatest for the infinite reservoir because fluid is free to flow in all directions. However, if fluid flow is confined to a narrow reservoir trending from the wells to the hypocentral region, then the pressure at a given distance from the well will be higher. This type of model was used by Hsieh and Bredehoeft [1981] to calculate the pressure distribution around the Rocky Mountain Arsenal well implicated

in the 1960's Denver earthquake sequence. In the case of the Cleveland earthquakes, there is no independent evidence that the injection zone has a long, narrow configuration. However, the calculations are useful in that they illustrate how large a pressure buildup at epicentral distances is possible, and because they show that the injection pressure history at the well bore may be diagnostic of the shape of the reservoir.

Figures 25 and 26 show pressure versus distance for several times after the beginning of injection for two strip reservoir models. The model used for Figure 25 has transmissivity equal to that assumed for the infinite reservoir model, and a width of 7.5 km. The model used for Figure 26 has a higher transmissivity of 2.0E–5 m^2/s, and the reservoir is 1 km wide. For the wider strip, pressure at the epicentral distance is comparable to that for the infinite reservoir. However, for the narrow strip, pressure at the epicentral distance is about 38 bars 15 years after beginning injection.

Injection pressure

Figure 24 shows the injection pressure versus time record that would have been observed at the wellhead for the three different reservoir models. In each case, pressure at the well bore is always less than the maximum injection pressure of 110 bars for the first 14 years of injection, but the time history of the injection pressure is different in each case. A detailed analysis of the injection pressure history would be able to discriminate between the cases of an infinite reservoir and a narrow strip, and might thus place more constraints on the amount of pressure buildup at the hypocenter. Preliminary analysis of injection pressures with time at the Calhio #1 and #2 wells indicate that the pressure buildup (i.e., resistence to flow) at the wells is consistent with a radial flow model (Ohio EPA, written communication, 1986).

The effect of ceasing injection

Figure 27 shows pressure versus distance for the three reservoir models assuming that injection is stopped after 15 years. In each case, although the pressure near the well falls steadily, the fluid pressure at the epicentral distance, as well as at greater distances, continues to rise for at least 10 years after cessation of injection. The pressure at the wellhead would vary with time as shown in Figure 28 if injection were stopped; the rate of

pressure decline would be diagnostic of the configuration of the reservoir, possibly within a year after cessation.

Conclusions

With our present information, it is not possible to confirm or reject the hypothesis that injection of waste into the Calhio wells triggered the earthquake activity near Painesville. If the state of stress in the hypocentral region is comparable to that at the bottom of the injection wells, then it appears that elevating the pressure by 110 bars would have resulted in a state of effective stress that would be judged critical on the basis of the Mohr–Coulomb failure criterion. The actual state of stress at the bottom of the well, however, is likely to be closer to failure than this estimate because the stress regime appears to be one in which the overburden underestimates the maximum compressive stress. Thus, because these stress estimates are uncertain, and also because they are not based on measurements made at the hypocenter, it is not possible to specify a level of pressure below which seismicity could not have been induced.

The actual pressure elevation in the hypocentral region due to the injection operation is certainly less than 110 bars, and probably less than about 40 bars. Whatever this pressure is, it will continue to rise whether or not injection continues, unless an extraction operation is undertaken.

However, in light of the fact that the mainshock and most of the aftershocks occurred at considerable distance from the active wells, the pressure fall-off with distance from the wells, the occurrence of small to moderate earthquakes in this region prior to initiation of injection, the lack of large numbers of small earthquakes (commonly observed in cases of induced seismicity) and the lack of earthquakes immediately below the wells all argue for a "natural" origin for the earthquake on January 31st. Thus, although triggering remains a possibility, the probability based on existing data that the injection wells played a significant role in causing the earthquake sequence is considered low.

Solution Mining and Earthquakes in Northeastern Ohio

The association of solution mining with the occurrence of small earthquakes in western New York State [Fletcher and Sykes, 1977], and the extensive salt mining operations in northeastern Ohio [Clifford, 1973], motivated a study of possible correlations between recent historical earthquakes and solution salt mining in Ohio. Solution mining for salt began in northeastern Ohio in 1889 (Figure 29a) [Clifford, 1973] and continues to the present, although several previously active operations have been closed down. The location of solution mining operations and additional locations of deep fluid injection [Clifford, 1975] are compared with the location of felt earthquakes in Figure 29b. Based on the spatial proximity and temporal association with active solution mining activities, it could be argued that the 1906 and 1930 earthquakes, 15 and 35 km southeast of Cleveland, respectively, could be associated with solution mining operations. Other earthquakes east of Cleveland, might be associated with well activities, if the reported locations for these events are in substantial error, and their actual locations are much closer to the well operations. However, in view of the large number of earthquakes reported prior to the initiation of solution mining, and the apparent occurrence of at least some earthquakes in northeastern Ohio beyond the range of expected influence from mining operations, it seems reasonably clear that at least some of the earthquakes are natural and that solution mining is not a necessary condition for the occurrence of earthquakes.

VII. HIGH FREQUENCY GROUND MOTION

Overview

A ten-station array of broad-band digital instrumentation (GEOS) was deployed by the U.S. Geological Survey to record the aftershock sequence of the moderate earthquake that occurred on January 31, 1986 (16:46:43 UTC). The occurrence of the event has raised questions concerning the character of earthquake-induced high-frequency ground motions in the area. This report provides interpretation of some of the data collected by the digital GEOS recording systems. Observations of ground motions generated by aftershocks suggests that vertical ground shaking at frequencies near 20 Hz are significantly higher at

a site near the Perry Nuclear Power Plant than are levels of shaking at 20 Hz for sites closer to the hypocenters. Spectra computed for the mainshock recorded at the power plant suggests similar exaggerated levels of vertical shaking near 20 Hz. Levels of shaking observed on the annulus of the containment structure during the mainshock are larger than those of the base of the reactor building foundation. This observation suggests that both the containment vessel and the near-surface soil layer may have contributed to observed levels of exaggerated vertical shaking near 20 Hz. Spectral amplifications computed from broad-band high-resolution recordings of the aftershock sequence near Painesville, Ohio, the aftershock sequence near Coalinga, California, and uphole–downhole recordings near Parkfield, California, suggest that local site conditions may significantly amplify high-frequency (10–80 Hz) ground motions. Such amplification effects are likely to be most significant in areas of low attenuation such as the eastern United States, and are important from an engineering point of view because of their potential influence on predicted peak acceleration values.

Introduction

Considerable scientific and engineering interest in the event resulted in a team of five seismologists being dispatched from Menlo Park, California on the evening of January 31 to install ten digital event recorders (GEOS) in the epicentral area [see Borcherdt *et al.*, 1985 and Borcherdt, 1986 for a detailed description of the recording equipment and configuration used to record this data set]. The seismograms and computed Fourier amplitude spectra collected from this deployment are presented in detail by Glassmoyer *et al.*[1986].

Recent improvements in recording system technology have permitted the extension of both bandwidth and dynamic range for recorded seismic signals. In the case of the data set recorded near Painesville, Ohio the digital recording systems (GEOS) were operated at 400 samples-per-second (sps) per-channel at high gain (42,48,54 dB). These instrument settings imply a Nyquist frequency of 200 Hz and a capability to record small-amplitude seismic signals near background noise levels at high resolution. The Fourier amplitude spectra computed for the recording of the larger aftershocks [Glassmoyer *et al.*, 1986] show that earthquake-generated ground motions in excess of 100 Hz were recorded for some of

the larger aftershocks. Such signals are generally not recorded on conventional seismic data acquisition systems. As a result, the collected data set provides an excellent opportunity to examine the influence of local site conditions on high-frequency ground motions.

Pioneering quantitative studies of the effects of local site conditions on ground motion recorded in the United States [Gutenberg, 1957; Borcherdt, 1968, 1970] confirmed the existence of amplified ground motions on certain types of geologic deposits, results that had initially been observed in Japan and the USSR [for a comprehensive bibliography of early observations see Duke, 1958]. The studies of the effects of local site conditions in the San Francisco Bay region [Borcherdt, 1970; Borcherdt and Gibbs, 1976] and those in the Los Angeles region [Gutenberg, 1957; Rogers *et al.*, 1984] established that it is possible to obtain estimates of the effects of local geological conditions from comparative ground motion measurements. They showed that simultaneous measurements of ground motion at appropriately selected recording sites can be utilized to isolate the effects of local geological conditions from those of the source, travel path and recording instruments. Although the measurements of the amplitude response of the local site conditions were shown to be an approximation, their work showed that the general characteristics of the response could be inferred and extrapolated over a wide range in amplitude to estimate the likely response of the local deposits during large earthquakes. These studies established the existence of predominant ground frequencies for certain types of deposits, however, other sites showed no single predominant ground frequency [Borcherdt, 1970; Borcherdt and Gibbs, 1976; Rogers *et al.*, 1984]. Where data were available, it was also shown that exaggerated levels of ground motion observed from small levels of ground shaking correlated well with areas of high intensity during damaging earthquakes [Borcherdt and Gibbs, 1976; Rogers *et al.*, 1984]. These observations on the amplitude response for local geologic deposits have been confined primarily for frequencies less than 5–10 Hz, because of the limited resolution characteristics of instrumentation (24–40 dB). Modern instrumentation with substantially improved signal resolution capabilities offers the opportunity to extend the bandwidth for observed responses to much higher frequencies.

Recent studies of the effects of local site conditions using modern recording capabilities suggests that the amplitude response characteristics of local deposits can be extended to

frequencies perhaps as high as 100 Hz for sites near the source. Borcherdt *et al.*[1983] observed that exaggerated ground shaking in the frequency range 10–25 Hz was apparent for sites located on thick sections of alluvium in the vicinity of Coalinga, California. They observed that local site resonances were consistently observed for events with similar azimuths and locations, but that significant changes in azimuth and/or locations for the events seemed to give rise to significant changes in the high-frequency amplitude response characteristics inferred from spectral ratios. Cranswick *et al.* [1985] also have observed exaggerated ground shaking at some sites in New Brunswick, Canada and near Goodnow, New York. These observations obtained with modern instrumentation (GEOS) confirm that local geologic conditions can play a significant role in modifying observed high-frequency (> 10 Hz) ground motions. In addition, these effects may also play a significant role in biasing estimates of small earthquake source parameters.

Recent studies of the response of near-surface deposits as observed on wide-dynamic-range instrumentation near Parkfield, California [Borcherdt *et al.*, 1985] show that near-surface deposits can consistently yield significant levels of amplified high-frequency (> 10 Hz) ground motions.

In this section, we document the nature of the high-frequency ground motion observed at the GEOS recording sites near Painesville, Ohio. In particular, the three sites selected along a linear array between the epicenters and the shore of Lake Erie are examined in detail. The high-frequency amplitude response of the lake shore sedimentary deposits are estimated and compared with those observed on the main shock records.

Recording Instrumentation

The GEOS recording system (Figure 30), deployed to record the aftershock sequence, was developed by the U.S. Geological Survey for use in a wide variety of active and passive seismic experiments. The digital data acquisition system operates under control of a central microcomputer which permits simple adaptation of the system in the field to a variety of experiments including near-source high-frequency studies of strong motion aftershock sequences, crustal structure, teleseismic earth structure, earth tidal strains, and free oscillations [see Borcherdt *et al.*, 1985, for detailed description].

The aftershock sequence was recorded on GEOS instruments configured as three-channel systems. The recorders were operated at 400 sps at gains of 42, 48, and 54 dB with no anti-aliasing filters [see Borcherdt, 1986, for variations on this configuration used at other sites]. This instrument configuration permitted broad-band high-resolution records to be obtained for the anticipated small magnitude events. Unit–impulse response for the recording system and two types of sensors (velocity transducer and force–balanced accelerometer) are shown in Figure 31.

Station and Aftershock Locations

Locations for the stations deployed in the 10–station array are shown in Figure 32 together with the location of the mainshock. Station locations, determined from 7.5–minute series topographic maps, were independently checked by a second interpreter and are believed to be accurate to within 60 meters. Station coordinates are listed in Table 1.

Objectives in the choice of the station locations included event location, source parameter determination, attenuation of high-frequency ground motion along a linear north–south array, and effects of local site conditions at stations GS01 and GS02. Due to the suspected low seismicity and expected small magnitudes for aftershocks, attempts were made to locate the stations at sites with anticipated low seismic background noise levels in areas (with the exception of station GS01) where the effects of local soil conditions were expected to be minimized. To reduce the effect of the adverse environmental conditions ($-15°$ C; snow and ice) on the recording equipment, each unit was located in an unheated shelter (small tool sheds or abandoned animal shelters some distance from local sources of cultural noise).

Six aftershocks were detected and recorded by three or more GEOS stations during the time period 1 February 19:45 to 10 February 20:07 GMT. The occurrence times of the six aftershocks, locations, and the number of stations detecting each one are listed in Table 7. Comparison of the events recorded on GEOS with those apparent on visible recorders (C. Langer and N. Seeber, personal communication, 1986) confirms that all events identified on visible recorders were detected and recorded on at least the three stations closest to the epicenters. Expansion of the digital traces on a graphics terminal permitted

picking of P and S arrival times to within 0.02 seconds by two independent observers. The automatic clock corrections provided every 12 hours and recorded on the GEOS tapes indicate the clock errors for the GEOS recordings are within $\pm$ 5 ms.

Four of the aftershocks (2 February 03:22, 3 February 19:47, 5 February 06:34, and 6 February 18:36) triggered four or more GEOS recorders with an appropriate station distribution to permit location of the events based only on P arrival times. The epicenters for these four events, located with the layered crustal model #1 (Table 2) and P arrival times only, are within 0.44 km of 41°38.85′N and 81°9.51′W, and at depths between 4.0 km to 6.5 km (essentially the locations shown in Figure 10).

Characteristics of High Frequency Ground Motions

Previous studies of seismic attenuation have established that seismic wave fields in the eastern United States, in general, attenuate less rapidly than those in the western United States [Nuttli, 1973]. As a result, high-frequency energy is generally more prevalent in seismograms recorded in the eastern United States. In addition, improvements in recording capabilities (bandwidth and dynamic range) also contribute to improvements in resolution of high-frequency energy. Consequently, it is of some interest to investigate the high-frequency character of ground motions recorded during the aftershock sequence and compare the results with those recorded during the mainshock at the Perry Nuclear Plant. The time histories and corresponding Fourier spectra for the recordings of the aftershocks are presented by Glassmoyer *et al.*[1986]. The strong-motion records and corresponding spectra as processed by Kinemetrics/Systems [1986] are presented in a strong-motion data report by Cleveland Electric Illuminating Company.

Strong–motion data

Two sets of three-component strong-motion time histories were recorded at the Perry Nuclear Plant during the m_b 4.9 main shock. One set was obtained at the base of the reactor building foundation (elevation 175 m or 575 ft) and the other on the containment vessel annulus at an elevation of 208 m (or 682 ft). The recordings were made with Kinemetrics model SMA–3 accelerograph systems with a nominal dynamic range of 40 dB,

natural frequencies between 50.6–53.7 Hz, and percent critical damping between 64 and 72 percent.

The acceleration, velocity, and displacement time histories obtained at the foundation of the reactor building are shown in Figure 33. The corresponding time histories obtained on the annulus of the containment vessel are shown in Figure 34. Relative velocity response and Fourier spectra corresponding to Figures 33 and 34 are shown in Figures 35 and 36, respectively. Maximum acceleration, velocity, and displacement values observed for each component and location are shown on the respective figures. A characteristic of special interest regarding the recorded strong ground motions is the preponderance of relatively high-frequency motions, especially apparent in the recordings made on the annulus of the containment structure (Figure 34). Inspection of the relative velocity response spectra and Fourier spectra computed for records from the annulus (Figure 36) shows well-defined peaks at about 4 Hz and 20 Hz for all three components of motions. The peak near 20 Hz is especially pronounced on the vertical and south-horizontal components. Comparison of the spectra computed on the annulus with that recorded at the foundation of the reactor structure shows that the peak relative response near 20 Hz on the annulus is 3–7 times as large as that at the base of the reactor structure. Comparison of the spectra near 4 Hz for the two locations shows the peak relative velocity responses are comparable on the vertical components and 2–3 times larger on the annulus. These data, without further analysis, would suggest that in general, vibratory motions at/or near 20 Hz were significantly larger (3–7 times) than those observed at the base of the reactor building. Increases in motion of the annulus near 4 Hz are smaller than those near 20 Hz and reach a maximum of about 2–3 times on the horizontal components.

Aftershock data

The seismograms and corresponding Fourier amplitude spectra obtained for the aftershocks recorded at the GEOS stations are presented by Borcherdt [1986]. For purposes of comparing the aftershock data with that of the mainshock, we shall restrict the discussion to the data recorded for the two larger aftershocks (events 19:47, $M \sim 2.2$; 18:36, $M \sim 2.5$ in Borcherdt, 1986). We shall also restrict the discussion to the data collected along the

north–south lineation of stations (GS01, GS02, and GS03). Station GS01 is about 400 m northeast of the Perry Nuclear Plant, station GS02 is located about 8 km further south, and station GS03 an additional 5 km further south and about 2 km NNW of the epicentral area.

Equiscaled plots of the time histories recorded at stations GS01 and GS02 are shown for the 19:47 event and the 18:36 event in Figures 37 and 38, respectively. The time histories have not been corrected for geometrical spreading. Comparison of the two plots shows that some of the amplitudes recorded at the station farthest from the epicenter (GS01) are larger than those recorded at station (GS02), which is about 8 km closer to the epicenter. The peak amplitudes for the 18:36 event slightly exceeded full-scale response at 54 dB gain at station GS02. As a result, comparison of peak amplitudes for the 18:36 event must be less conclusive than similar comparisons for the 19:47 event. Exceedence of full-scale response for the 18:36 event is expected to have only a minor influence on estimates of Fourier amplitude spectra.

Comparison of the vertical time histories at stations GS01 and GS02 for the 19:47 event (Figure 37) shows that the vertical peak amplitudes are as much as 4 times larger at station GS01 than at station GS02. The well-defined pulse of large vertical amplitude during the time interval for the arrival of the P wave at station GS01 is to be contrasted to the more gradual build-up in amplitude during the S wave arrival interval. The exaggerated vertical motions, with a modulated appearance during the S wave interval, might be interpreted as evidence for some type of resonance, either in the near-surface geologic layers or in some nearby man-made structure. It does not appear that the same phenomenon can account for the relatively large pulse near the onset of the initial P energy. Comparison of the vertical time histories for the 18:36 event (Figure 38) again shows larger motions at station GS01 during the S wave arrival interval with some suggestion of resonance. The peak amplitudes recorded during the arrival of the P wave are not larger than those observed at station GS02.

Comparing the horizontal amplitudes at station GS01 with those at station GS02 for the 19:47 event shows that only the initial S arrival on the radial (north–south) component is significantly larger at station GS01. Comparison of peak amplitudes for the 18:36 event

(Figure 38) is inconclusive as the peak amplitudes slightly exceeded full-scale response at 54 dB gain at station GS02.

A plot of peak acceleration amplitudes as observed for the 19:47 event at stations GS01, GS02, and GS03 is shown in Figure 39a. The plot shows that the maximum vertical amplitude at station GS01 which occurred near the onset of the seismogram is about 4 times larger than that at either stations GS02 or GS03 which are closer to the hypocenter at distances of 10.3 km and 6.9 km, respectively. Station GS01 is 18.7 km from the hypocenter. The plot (Figure 39) shows exaggerated peak amplitudes for the radial or north–south horizontal component at station GS01 but not for the east–west component.

A plot of peak amplitudes corrected for geometrical spreading is shown in Figure 39b. The amplitudes at stations GS01 and GS02 have been multiplied by the reciprocal of the ratio in hypocentral distance of the station to that of station GS03. (The geometrical attenuation factors are 2.8 and 1.7 for stations GS01 and GS02, respectively). The plot of peak amplitudes corrected for geometrical spreading (Figure 39b) provides strong evidence for exaggerated ground shaking at station GS01.

Fourier amplitude spectra for each of the recordings at the three stations have been computed [Glassmoyer *et al.*, 1986; see Figures B–6, 7, 8 and B–17, 18, 19]. The spectra show that the events 19:47 and 18:36 generated signals resolvable with the GEOS above background noise up to frequencies exceeding 100 Hz. The spectra show that the vertical motions detected at each of the sites show a rapid fall-off with increasing frequency only for frequencies exceeding about 70 or 80 Hz. The spectra for horizontal motions indicate an increased fall-off rate with increasing frequency for frequencies exceeding 30–40 Hz. The increased fall-off rate for the horizontal motions is consistent with intrinsic material absorption for shear waves being greater than that for compressional waves.

Spectral ratios for the frequency band 0–130 Hz are shown in Figure 40. Spectral ratios for the band 0–50 Hz are shown in Figure 41. The spectral ratios shown in Figures 40 and 41a, b, c have been computed from the ratio of the Fourier amplitude spectra for station GS01 to that of the corresponding component of motion recorded at station GS02. The ratios in Figures 40 and 41d, e, f, have been computed from corresponding spectra of stations GS01 and GS03. The spectral ratios are computed for only those frequencies for

which the spectral signal-to-noise ratios were greater than two. Spectral noise levels were determined from 1.25 seconds of noise prior to the onset of seismic energy. The spectra were computed from 10 seconds of time history sampled at 400 sps commencing about 1 second prior to the onset of the P wave. The spectra were smoothed with a 15-point triangular Hanning window which corresponds to a window width of 1.5 Hz. The scale factor to permit the ratios to be corrected for geometrical spreading is indicated in each of the figures.

The computed ratios (Figure 40) show that seismic energy was resolvable above instrument noise levels at the gain levels specified for the GEOS up to frequencies as high as 130 Hz. This upper limit represents a substantial extension in observable bandwidth over that previously observed from conventional strong-motion recorders with an upper limit of about 30–35 Hz. Interpretation of the significance of seismic signals in the 50–130 Hz band must await more detailed investigations.

Comparison of the spectral ratios shown for the 0–50 Hz band (Figure 41) for the 19:47 event with those for the 18:36 event show that the spectral ratios are similar in many respects with a few notable differences. The extent to which the ratios are similar argues that these spectral ratios provide an estimate of the amplitude response of station GS01 relative to that at station GS02 (Figures 41a, b, and c) and station GS03 (Figures 41d, e, and f). One notable difference in comparing the ratios for the two events is the reduction in the ratios computed for the vertical component of motion recorded from the 18:36 event. *In situ* relative instrument calibration characteristics computed prior to the 19:47 event and about 48 hours later, just prior to the 18:46 event, show that the computed calibration curves agree to within a percent over the entire band for which there is a good signal-to-noise ratio in the input signal. Variations near 100 Hz are due to seismic noise at the site during the second calibration interval. As a result, the apparent reduction in ratios for the 18:36 event does not seem to be associated with changes in instrument response.

Dominant features of the spectral ratios are the predominant peaks which occur for the vertical motion near 20 Hz. The occurrence of these peaks on each of the ratios computed from the vertical motions provides strong evidence for an exaggerated level of vertical shaking near 20 Hz at station GS01. Evidence for exaggerated level of shaking

near 20 Hz is also apparent in the spectra computed from the strong motion recordings (see Figures 35 and 36). The distance (~400 m) of station GS01 from the location of the strong-motion recorders would argue that the predominant peak in the aftershock ratios is associated with a resonance in the local soil layer. Consideration of the near-surface velocity log (Table 8) as compiled from cross-hole measurements shows an abrupt change in P velocity at an interface between glacial till and shale at a depth of about 20 meters below the surface. If we assume a simple one-dimensional model with vertically incident P waves, then the thickness corresponding to a 20 Hz resonance for an average P wave velocity of 1525 m/sec (5000 ft/sec) would be

$$H = \frac{V}{4f} \approx \frac{1525 \text{ m/s}}{4\,(20 \text{ Hz})} = 19 \text{ m}$$

The extent to which this estimated thickness agrees with that shown in drill hole logs (see Table 8) for the till–shale interface, provides additional evidence that the exaggerated levels of shaking near 20 Hz are due to amplification by the surface layer of soil of thickness about 20 meters. The exaggerated level of shaking observed on the annulus of the containment vessel argues that a resonance near 20 Hz might also exist in the plant structure. If both resonances do indeed coincide, then ground motions near these frequencies could be expected to be significantly larger on the structure than if only one or no such resonances existed.

VIII. CONCLUSIONS AND RECOMMENDATIONS

Absence of Obvious Structure

Analysis of the mainshock and aftershocks indicate no obvious structure or fault with which the January 31 earthquake can be associated. The hypocenter of the earthquake was located in the PreCambrian basement rocks. Two kilometers of Paleozoic and younger age rocks cover basement in this region. Although there is no evidence of any surface expression of the fault responsible for the earthquake, gravity and aeromagnetic field data display some relief, suggesting the presence of a basement structure; but no structure

has been currently defined which might be considered a capable fault in the sense used by the Nuclear Regulatory Commission. Locations of aftershocks obtained to date are permissive of the interpretation of a fault striking somewhat east of north, but as most of the aftershocks are tightly clustered in space, they provide only very weak evidence for the orientation of a fault.

Stress Regime

Analysis of available stress measurements as discussed above seems to indicate that the state of stress in northeastern Ohio is close to the theoretical threshold for small earthquakes as predicted by the Mohr–Coulomb failure criterion. This should not be surprising given the history of small to moderate earthquakes in the region.

Possible Role of Injection Wells

Although given the state of stress discussed above, triggering of small earthquakes by fluid injection would not be surprising, the distance of the January 31 earthquake and its aftershocks from the wells (with the exception of the very small earthquake on March 12), the lack of any small earthquakes detected near the bottom of the wells, the history of small to moderate earthquakes in the region prior to the initation of injection, and the attenuation of the pressure field with distance from the injection wells, all argue for a "natural" origin for the earthquake. Therefore, although triggering remains a possibility, the probability that the injection played a significant role in triggering the earthquake, based on the information currently available, must be regarded as low. The analysis of the possible relation between the injection wells and the January 31 earthquake has indicated nothing to suggest the occurrence of an earthquake larger than that expected for the broad region, or the activation of a major structure closer to the wells or near the power plant.

Value of Continued Earthquake Monitoring

Continued earthquake monitoring in the vicinity of the epicenter of the January 31 earthquake will be of considerable value for two reasons. First, as indicated above, the lack of many small earthquakes detected near the bottom of the injection wells is a very

important factor in concluding that the probability of an injection being the triggering mechanism is low. Although the single, small earthquake on March 12th may have been induced, no large numbers of small earthquakes, typical of induced earthquake sequences, have yet to be detected near the injection wells. Any more earthquakes closer to the bottom of the wells than the January 31 earthquake and its initial aftershocks could significantly alter the local seismic hazard assessment. Second, from the point of view of trying to understand the generic problem of eastern U.S. seismicity, the earthquake sequence near Hambden is invaluable and continued monitoring could prove of substantial importance in developing an understanding of the relationship between the January 31 earthquake and crustal structure, if any.

High Frequency Ground Motions

High-resolution (up to 96 dB), broadband (< 200 Hz) recordings of the aftershock sequence show that seismic signals as high as 130 Hz were resolvable above noise levels for the larger aftershocks (m_b 2.2; 2.5) at hypocentral distances up to 18 km. Fourier amplitude spectra of velocity show that amplitude spectra decrease most rapidly with increasing frequency only for frequencies exceeding 70–80 Hz for vertical motion and 30–40 Hz for horizontal motion.

Signals relatively rich in high frequencies were also observed on the strong-motion records of the mainshock for frequencies up to the upper bandwidth limit of the recorders (30 Hz). Based on the aftershock data, spectral ratios computed to estimate the amplitude response of local site conditions at a site near the Perry Nuclear Plant (site GS01) show exaggerated vertical ground shaking near 4–7 Hz and near 20 Hz. The peaks in the spectral ratios near these frequencies appear to be attributable to resonances in the near-surface soil layers. Smaller, but apparently significant, resonances are also indicated in the spectral ratios for horizontal motions.

Inspection of response spectra computed for strong-motion records of the mainshock on the annulus of the containment vessel and on the foundation of the reactor building also show amplified vibration of the containment structure near 20 Hz. These strong-motion data suggest that a 20 Hz resonance may also be associated with the containment structure.

At present insufficient data exists to conclusively determine if separate 20 Hz resonances exist in both the containment structure and the near-surface soil layers. If both resonances do exist then significantly exaggerated shaking near 20 Hz can be expected from future earthquakes.

Future studies to better describe the resonances suggested by the strong-motion data and the aftershock data would help in assessing the potential levels of exaggerated ground shaking and their significance for engineering purposes. Ambient vibration studies of pertinent structures, soil-structure interaction studies and comparative ground motion studies could contribute to an improved understanding of the significance of the observed motions. Additional investigations of local geologic and seismic site characteristics together with appropriate numerical models may also be warranted.

Evidence derived in this study and other recent studies using broadband instrumentation for levels of exaggerated ground shaking at high frequencies suggests that general studies pertinent to assessing the influence of possible high-frequency site resonances on peak accelerations in the band 10–40 Hz are warranted.

Need to Understand Basement Structure

Given the geologic setting and conditions in northeastern Ohio, the best chance to learn about the nature of the structure(s) responsible for the earthquakes will be through general geophysical investigations. Such studies might include seismic reflection, microgravity and/or detailed areomagnetic surveys. Seismic reflection profiles that penetrate to basement are likely to produce the highest resolution, and thus the greatest capability of identifying faults or other structures responsible for the seismicity, structures that may find little if any expression in the overlying rocks of Paleozoic age. Detailed gravity and magnetic surveys have already been commissioned, and hopefully they will also be revealing of significant local structure and/or basement topography.

Research–quality Measurements in Boreholes

As noted above, while the data from commercial hyrofractures has been valuable in estimating the regional state of stress, estimates could be made with considerably higher

confidence if research–quality measurements in boreholes were carried out. The resulting estimates of stress would be valuable from several points of view. First, measurements could confirm the inferences drawn from the commercial hydrofactures with regard to the magnitude of the least and maximum horizontal compressive stresses. In research–quality measurements, care would be taken to assure that hydrofactures were created in a previously unfractured part of the hole, and thus insure that pre-existing fractures do not bias the result. In addition, research–quality hydrofractures utilize only small volumes of fluid to minimize any pressure difference between the tip of the extending crack and the borehole, an effect which is suspected to have biased some of the values obtained from the Calhio wells. Observations could also be made to determine the orientation of the created fractures and thus determine the suspected orientation of the maximum compressive stress.

REFERENCES

Borcherdt, R. D. (1968), Spectral analysis of seismic measurements from nuclear explosions in Nevada recorded in the San Francisco Bay area, California, *Geol. Soc. Amer. Spec. Paper 121*, p. 486–487.

Borcherdt, R. D. (1970), Effects of local geology on ground motion near San Francisco Bay, *Bull. Seismol. Soc. Am.*, v. 60, p. 29–61.

Borcherdt, R. D., and Gibbs, J. F. (1976), Effects of local geological conditions in the San Francisco Bay region on ground motions and the intensities of the 1906 earthquake, *Bull. Seismol. Soc. Am.*, v. 66, p. 467–500.

Borcherdt, R. D., Fletcher, J. B., Jensen, E. G., Maxwell, G. L., VanSchaack, J. R., Warrick, R. E., Cranswick, E., Johnston, M. J. S., and McClearn, R. (1985), A General Earthquake Observation System (GEOS), *Bull. Seismol. Soc. Am.*, v. 75, p. 1783–1823.

Borcherdt, R. D., editor (1986), Preliminary report on aftershock sequence for the earthquake of January 31, 1986, near Painesville, Ohio, *U. S. Geol. Surv. Open-File Rep.* 86-181, 11 pp. with figures and maps.

Chaplin, M. P., Taylor, S. R., and Tokoz, M. N. (1980), Coda–length magnitude scale for New England, *Earthquake Notes* , v. 51, p. 15–22.

Cleveland Electric Illuminating Company (1982), The Perry Nuclear Power Plant Units I and II: *Final Safety Analysis Report*, Cleveland, Ohio.

Clifford, M. J. (1973), Silurian rock salt of Ohio, *Ohio Geol. Surv. Rep. of Investigations*, v. 9, 42 pp., Columbus, Ohio.

Clifford, M. J. (1975), Subsurface liquid-waste injection in Ohio, *Ohio Geol. Surv. Inform. Circular*, v. 43, 27 pp., Columbus, Ohio.

Cranswick, E., Wetmiller, R., and Boatwright J. (1985), High–frequency observations and source parameters of microearthquakes recorded at hard–rock sites, *Bull. Seismol. Soc. Am.*, v. 75, p. 1535–1568.

Davis, S. (1985), Investigations of natural and induced seismicity in the Texas Panhandle, *M. S. Thesis*, University of Texas, Austin, 230 pp.

Duke, C. M., compiler (1958), Bibliography of effects of soil conditions on earthquake damage, *Earthquake Eng. Inst.*, 47 pp.

Dunrud, C. R., and Nevins, B. B. (1981), Solution mining and subsidence in evaporite rocks in the United States, *U. S. Geol. Surv. Map I-1298.*

Fletcher, J. B., and Sykes, L. R. (1977), Earthquakes related to hyraulic mining and natural seismic activity in western New York State, *J. Geophys. Res.* , v. 82, p. 3767–3780.

Geauga County Disaster Service Agency (1986), Findings on damage associated with the January 31, 1986 earthquake, informal report, Chardon, Ohio.

Glassmoyer, G., Borcherdt, R., King, J., Dietal, C., Sembera, E., Roeloffs, E., Valdes, C., and Nicholson, C. (1986), Source and propagation characteristics for aftershock sequence near Painesville, Ohio (abstract), *Eos (Trans. Amer. Geophys. Un.)*, v. 67, p. 314.

Gutenberg, H. B. (1957), Effects of ground on earthquake motion, *Bull. Seismol. Soc. Am.*, v. 47, p. 221–250.

Haimson, B. C. (1978), Crsutal stress in the Michigan basin, *J. Geophys. Res.* , v. 83, p. 5857–5863.

Healy, J. H., Rubey, W. W., Griggs, D. T., and Raleigh, C. B. (1968), The Denver earthquakes, *Science* , v. 161, p. 1301–1309.

Herrmann, R. B. (1969), The structure of the Cincinnati Arch as determined by short period Rayleigh waves, *Bull. Seismol. Soc. Am.*, v. 59, p. 399–407.

Hickman, S. H., Healy, J. H., and Zoback M. D. (1985), In situ stress, natural fracture distribution, and borehole elongation in the Auburn geothermal well, Auburn, New York, *J. Geophys. Res.* , v. 90, p. 5497–5512.

Hsieh, P. A., and Bredehoeft, J. D. (1981), A reservoir analysis of the Denver earthquakes: A case of induced seismicity, *J. Geophys. Res.* , v. 86, p. 903–920.

Jaeger, J. C., and Cook, N. C. W. (1976), *Fundamentals of Rock Mechanics*, John Wiley and Sons, Inc., New York, 585 pp.

Kinemetrics/Systems (1986), M_L = 5.0 earthquake, January 31st, 1986: Strong-motion data from the Perry Nuclear Power Plant seismic instrumentation, Pasadena, Calif., 53 pp.

Lahr, J. C. (1985), HYPOELLIPSE/VAX: A computer program for determining local earthquake hypocentral paramters, magnitude and first-motion patterm, *U. S. Geol. Surv. Open-File Rep.* 84-519, 35 pp.

McGarr, A. (1980), Some constraints on levels of shear stress in the crust from observations and theory, *J. Geophys. Res.* , v. 85, p. 6231–6238.

Natural Resources Management Corp. (1971), Report on the drilling, testing and completion of the subsurface disposal well #1, Calhio Chemicals, Inc., Perry, Ohio, 81 pp. with maps, figures and graphs.

Nuttli, O. W., Stauder, W., and Kisslinger, C. (1969), Travel time tables for earthquakes in the central United States, *Earthquake Notes* , v. 40, p. 19–28.

Ohio UIC Permit Application for Class I Injection well (1985), Calhio Chemicals, Inc., Perry, Ohio, Injection Well #1, 22 pp.

Ohio UIC Permit Application for Class I Injection well (1985), Calhio Chemicals, Inc., Perry, Ohio, Injection Well #2, 22 pp.

Petro Evaluation Services, Inc. (1985), Well completion record, saltwater injection well, Painesville, Lake County, Ohio, 5 pp.

Press, F. (1966), Seismic velocities, *Handbook of Physical Constants*, edited by S. D. Clark, *Geol. Soc. Am. Memoir* , v. 97, p. 195–218.

Raleigh, C. B., Healy, J. H., and Bredehoeft, J. D. (1976), An experiment in earthquake control at Rangely, Colorado, *Science* , v. 191, p. 1230–1237.

Resources Services Inc. (1980), Report on the drilling, testing and completion of the subsurface disposal well, Injection Well #2, Calhio Chemicals, Inc., Perry, Ohio, 84 pp. with maps, figures, and graphs.

Rogers, A. M., Borcherdt, R. D., Covington, P. A., and Perkins, D. M. (1984), A comparative ground response study near Los Angeles using recordings of Nevada nuclear tests and the 1971 San Fernando earthquake, *Bull. Seismol. Soc. Am.,* v. 74, p. 1925–1950.

Simpson, D. W. (1986), Triggerred earthquakes, *Ann. Rev. Earth Planet. Sci.*, v. 14, p. 21–42.

Stover, C. W., Reagor, B. G., and Algermissen, S. T. (1979), Seismicity map of the state of Ohio, *U. S. Geol. Surv. Map MF-1142.*

TABLE 1. LOCATIONS OF STATIONS DEPLOYED TO MONITOR AFTERSHOCKS.

STATION ABBREV.	LATITUDE Deg Min	LONGITUDE Deg Min	AFFILIATION ABBREV.	DATES OF OCCUPATION
CON	41N42.06	081W12.55	LAMONT	
GAR	41N47.30	081W10.64	LAMONT	
HLH	41N41.20	081W07.01	LAMONT	
HPV	41N44.41	081W03.08	LAMONT	
HSE	41N33.77	081W06.76	LAMONT	
POP	41N37.23	081W07.05	LAMONT	
TTR	41N35.25	081W11.69	LAMONT	
HSOH	41N35.66	081W07.84	MICHIGAN	FEB. 01 - FEB. 02
MTOH	41N36.68	081W03.07	MICHIGAN	FEB. 01 - FEB. 02
CHOH	41N35.56	081W11.84	SLU	JAN. 31 - FEB. 03
HAOH	41N36.46	081W08.51	SLU	JAN. 31 - FEB. 03
PAOH	41N45.41	081W11.95	SLU	JAN. 31 - FEB. 03
CALM	41N34.1	081W10.3	TEIC	
ELFM	41N36.8	081W10.9	TEIC	
FARM	41N38.3	081W10.4	TEIC	
HOWM	41N35.0	081W07.9	TEIC	
MONM	41N36.7	081W02.9	TEIC	
BUR	41N39.24	081W04.94	U.S.G.S	FEB. 02 - FEB. 11
CAL	41N41.21	081W08.89	DENVER	FEB. 02 - FEB. 11
COT	41N34.73	081W05.93	"	FEB. 02 - FEB. 11
CUY	41N33.56	081W10.15	"	FEB. 03 - FEB. 11
ERJ	41N39.44	081W05.00	"	FEB. 06 - FEB. 11
FOT	41N38.90	080W59.69	"	FEB. 04 - FEB. 11
HAM	41N36.18	081W08.48	"	FEB. 02 - FEB. 11
HAR	41N36.67	080W59.62	"	FEB. 02 - FEB. 04
HWK	41N41.83	080W59.03	"	FEB. 02 - FEB. 11
LOX	41N44.58	081W02.60	"	FEB. 02 - FEB. 11
MON	41N35.52	081W02.39	"	FEB. 02 - FEB. 11
WSH	41N37.61	081W13.30	"	FEB. 02 - FEB. 11
GS01	41N48.27	081W08.52	U.S.G.S.	FEB. 01 - APR. 03
GS02	41N43.75	081W09.47	MENLO PARK	FEB. 01 - APR. 03
GS03	41N39.45	081W10.07	"	FEB. 01 - APR. 03
GS04	41N36.85	081W17.55	"	FEB. 01 - FEB. 11
GS05	41N35.64	081W08.19	"	FEB. 01 - FEB. 04
GS06	41N37.75	081W03.77	"	FEB. 01 - APR. 03
GS07	41N32.40	081W04.26	"	FEB. 01 - FEB. 11
GS08	41N32.38	081W12.93	"	FEB. 02 - FEB. 10
GS09	41N24.81	081W11.91	"	FEB. 02 - FEB. 10
GS11	41N09.20	081W04.42	"	FEB. 02 - FEB. 10
GS55	41N37.10	081W07.18	"	FEB. 04 - FEB. 10

STATION ABBREV.	LATITUDE Deg Min	LONGITUDE Deg Min	AFFILIATION ABBREV.	DATES OF OCCUPATION
CFD	41N40.45	081W13.41	WESTON	
CLD	41N31.44	081W20.19	WESTON	
HTG	41N37.17	080W57.27	WESTON	
KEL	41N32.82	081W06.12	WESTON	
MFD	41N27.77	081W04.41	WESTON	
MIN	41N33.56	081W15.41	WESTON	
PAT	41N33.63	081W21.91	WESTON	
PER	41N48.06	081W08.61	WESTON	
TOM	41N41.29	081W03.09	WESTON	
WEL	41N45.00	081W09.31	WESTON	
WKR	41N36.06	081W03.13	WESTON	
WC01	41N36.90	081W18.08	WOODWARD-CLYDE	
WC02	41N40.05	081W09.53	"	
WC03	41N43.87	081W04.46	"	
WC04	41N35.10	081W09.36	"	
WC06	41N32.40	081W01.75	"	
WC07	41N48.00	081W08.58	"	
WC08	41N40.24	081W14.48	"	
WC09	41N35.45	081W09.36	"	

Table 2. Models used to locate events listed in Table 3

Depth (km)	Thickness (km)	P Velocity (km/s)	S Velocity (km/s)	Vp/Vs	Description*
0.0	2.00	4.25	2.53	1.68	Paleozoic section
2.00	99.00	6.50	3.87	1.68	Granitic basement
0.0	1.00	3.70	2.06	1.80	Upper Sedimentary
1.00	1.00	5.60	3.20	1.75	Lower Sedimentary
2.00	35.00	6.33	3.66	1.73	Granitic crust
37.00	99.00	8.10	4.68	1.73	Mantle
0.0	0.05	1.80	0.60	3.00	Glacial till
0.05	0.45	3.00	1.58	1.90	Devonian shale
0.50	0.50	4.20	2.33	1.80	Silurian dolomite
1.00	0.75	4.50	2.53	1.78	Ordovician limestone and dolomite
1.75	0.35	4.75	2.70	1.76	Cambrian sandstone and dolomite
2.10	17.90	6.15	3.54	1.74	Precambrian granite
20.00	25.00	6.70	3.87	1.73	Lower crust
40.00	99.00	8.15	4.63	1.75	Mantle

* Weston Geophysical, Herrmann [1969], Cleveland Electric Illuminating Co. [1982]

TABLE 3. LOCATIONS OF RECENT EARTHQUAKES AND BLASTS IN NORTHEASTERN OHIO.

DATE	ORIGIN		LATITUDE	LONGITUDE	DEPTH	MAG	NO.	RMS	ERH	ERZ	AZI
YrMoDy	Hr:Mn	Sec	Deg Min	Deg Min	km		PHA	sec	km	km	GAP
MAINSHOCK AND PRIOR EVENTS											
430309	03:25	25.00	41N37.80	81W18.60	8.00	4.7	**(NEIS,Dewey,1986)**				
830122	07:46	59.30	41N48.00	81W10.00	6.00	2.7					
860131	16:46	42.30	41N39.00	81W09.72	8.00	4.9					
AFTERSHOCKS (MODEL #3)											
860201	18:54	49.20	41N38.82	81W 9.42	4.97	1.4	21	0.13	0.45	0.80	100
860202	3:22	48.53	41N38.75	81W 9.53	4.99	0.8	24	0.06	0.25	0.23	72
860203	19:47	19.56	41N38.90	81W 9.61	6.93	1.8	35	0.08	0.26	0.36	74
860205	6:34	2.40	41N38.94	81W 9.64	2.07	−.3	20	0.21	0.83	0.66	49
860206	18:36	22.24	41N38.57	81W 9.64	5.89	2.4	42	0.12	0.28	0.41	48
860207	15:20	20.20	41N39.06	81W 9.25	4.64	1.0	27	0.07	0.29	0.22	42
860210	20: 6	13.49	41N39.16	81W 9.27	4.97	0.9	26	0.09	0.29	0.42	69
860223	3:29	48.46	41N39.06	81W 9.44	4.77	−.3	16	0.08	0.47	0.43	96
860224	16:55	6.37	41N38.96	81W 9.81	3.72	0.1	10	0.09	0.56	0.71	126
860228	1:39	34.07	41N39.11	81W 9.59	4.31	0.1	12	0.08	0.49	0.69	92
860308	20:42	49.49	41N38.72	81W 9.36	4.42	−.5	12	0.10	0.66	0.61	102
860312	8:55	26.59	41N43.63	81W10.24	2.01	−.2	10	0.06	1.35	0.44	216
860324	13:42	41.20	41N38.05	81W 9.97	4.92	1.3	12	0.06	0.45	0.40	97
AFTERSHOCKS (MODEL #2)											
860201	18:54	49.35	41N38.77	81W 9.38	5.16		21	0.10	0.37	0.64	100
860202	3.22	48.69	41N38.69	81W 9.41	5.37		24	0.09	0.34	0.38	70
860203	19:47	19.82	41N38.97	81W 9.57	5.89		44	0.12	0.44	0.30	71
860205	6:34	2.51	41N38.87	81W 9.47	1.62		20	0.22	0.94	1.05	51
860206	18:36	22.48	41N38.70	81W 9.66	5.46		43	0.13	0.46	0.31	48
860207	15:20	20.44	41N38.96	81W 9.26	3.63		27	0.09	0.35	0.27	43
860210	20: 6	13.68	41N38.90	81W 9.44	4.39		26	0.10	0.33	0.48	71
860223	3:29	48.59	41N39.14	81W 9.39	4.76		16	0.05	0.33	0.30	96
860224	16:55	6.45	41N38.92	81W 9.61	4.52		10	0.06	0.45	0.56	122
860228	1:39	34.15	41N39.19	81W 9.38	4.73		12	0.05	0.31	0.44	97
860308	20:42	49.67	41N38.76	81W 9.42	3.99		12	0.11	0.76	0.71	102
860324	13:42	41.38	41N38.07	81W10.05	4.47		12	0.06	0.47	0.42	96
AFTERSHOCKS (MODEL #1)											
SEE TABLE 7											
BLASTS											
860205	15:39	06.45	41N40.08	81W02.28	0.90	0.6	13	0.09	0.65	0.62	74
860205	17:57	03.85	41N40.02	81W02.46	0.01	0.4	12	0.07	0.23	0.37	75

Table 4. Stress estimates (bars)

Measurement Site	Principal Stresses S_v	S_h	S_H	Formation Pore Pressure Maynardsville	Mt. Simon	Injection Pressure
Regional (Evans)	459	275-321				
Michigan (Haimson)	464	344	503			
W. New York (Hickman et al)	441	370	570			
Calhio#1 inital		302	457	197	210	291
Calhio#1 final		336	559			
Calhio#2 initial		268	357	199	198	291
Calhio#2 final		343	582			
Brine well initial		262				267
Brine well final		295				
Accepted value	460	300	460-560	200		290

Table 5. Measured pore pressures from drill stem tests

Formation	Calhio #1 April 11, 1971	Calhio #2 August 20, 1979
Maynardsville	2821 psi	2930 psi
Mt. Simon	3096 psi	2906 psi

Table 6. Physical properties of reservoir rocks into which waste is being injected

	Maynardville	Rome	Mt. Simon
Permeability, darcies	4.2E–3	?	5.5E–3
Hydraulic conductivity, m/s	4.2E–8	?	5.5E–8
Thickness, meters	52.7	22.3	37.8
Transmissivity, m^2/s	2.2E–6	?	2.1E–6
Porosity	0.08	?	0.085
Minimum storativity	1.25E–5	?	9.54E–6

Other values assumed are fluid density = 1.2 g/cm^3, fluid compressibility = 3.03E–11 cm^2/dyne

Table 7. Origin time and locations for seismic events by GEOS
for time period 2/1/86 through 2/10/86

Aftershocks										
Yr	Mo	Da	Origin	Lat. N	Lon. W	Depth	RMS	ERH	ERZ	GAP	M (Max. disp
86	2	2	322 48.57	41 38.76	81 9.50	5.12	0.01	1.16	0.78	150	1.1
86	2	3	1947 19.65	41 38.92	81 9.43	5.81	0.03	0.88	0.76	116	2.2
86	2	5	634 2.40	41 38.96	81 9.68	4.05	0.02	0.88	1.31	134	0.9
86	2	6	1836 22.26	41 38.68	81 9.33	6.06	0.03	0.82	0.80	121	2.5
86	2	7	1520 20.19	41 38.97	81 9.42	4.66	0.03	0.92	5.21	115	1.9
86	2	10	20 6 13.59	41 39.07	81 9.31	3.38	0.04	0.81	6.31	115	1.5

Table 8. Near-surface velocity measurements*

Elevation (feet)	V_p (ft/s)	V_s (ft/s)	Description
620			Lacustrine Sediments:
612	1200	600	(unsaturated)
605	5000	700	(saturated)
595	5000	1200	(saturated)
583	5900	1900	Glacial till: (upper)
560	7800	2600	(lower)
510	10400	4900	Shale
410	9000	4000	Shale

*Safety Analysis Report, Perry Nuclear Plant

FIGURE CAPTIONS

Figure 1. Seismicity map of Ohio.

Figure 2. Intensities resulting from the January 31, 1986 earthquake in northeastern Ohio as compiled by the U.S. Geological Survey.

Figure 3. Intensites compiled by Weston Geophysical.

Figure 4. Example smoked paper recordings of aftershocks

Figure 5. Seismograph stations deployed by all cooperating institutions to record aftershocks. Shaded areas on this and subsequent maps represent areas of dense population.

Figure 6. Smoked paper recordings of two local quarry blasts.

Figure 7. Composite Wadati diagram for four aftershocks as recorded by U.S. Geological Survey stations.

Figure 8. Map of U.S. Geological Survey seismograph stations.

Figure 9. Map showing mainshock epicenter (solid star), locations of six aftershocks (open circles) and two blasts (filled circles). Numbers correspond to relative position in time.

Figure 10. Map showing distribution of aftershock and blast epicenters with associated 94% confidence ellipses. Other symbols as in Figure 9.

Figure 11. Vertical cross sections of aftershock hypocenters with associated error estimates. Orientations of cross sections are shown on map at left.

Figure 12. Enlarged map showing all seismograph stations in immediate epicentral area.

Figure 13. Map and vertical cross sections of aftershock locations obtained using all available data as of April 15, 1986. Cross sections show projections onto planes parallel and perpendicular to N20° E.

Figure 14. Lower hemisphere, equal area, single event focal mechanisms for two largest aftershocks, February 6 18:36, and February 3 19:47. Solid circles are

compressions; open triangles are dilatations. Legend indicates origin time, location and focal depth.

Figure 15. Focal mechanisms for aftershocks February 10 20:06 and February 5 06:34. Notice relatively large component of normal faulting for these two events.

Figure 16. Focal mechanisms for aftershocks February 2 03:22 and Febraury 7 15:20. Notice that these two events show nearly diametrically opposite solutions.

Figure 17. Focal mechanisms for aftershocks February 23 03:29 and February 1 18:54. Nodal planes are not well constrained.

Figure 18. Composite of first motions for all smaller aftershocks with nodal planes determined for largest aftershock, February 6 18:36.

Figure 19. Volume of fluid injected into Calhio wells through time.

Figure 20. Location of deep injection wells in Lake County and epicenters of earthquakes. Large uncertainties in location are associated with both the 1943 and 1983 earthquake epicenters.

Figure 21. Seismogram of small event near station GS02 within 3 km of the Calhio injection wells.

Figure 22. Mohr circle diagrams showing state of stress a) at bottom of injection well; b) at hypocenter.

Figure 23. Pressure produced by waste injection into infinite reservoir. Each curve is labeled with the elapsed number of years since the beginning of injection. Injection at steady rate of 6.7 million liters/month.

Figure 24. Pressure versus time at the wellhead for the three reservoir models. See text for explanation.

Figure 25. Pressure produced by waste injection into strip reservoir 7.5 km wide with same transmissivity as infinite reservoir.

Figure 26. Pressure produced by waste injection into strip reservoir 1 km wide.

Figure 27. Spatial pressure distribution for the scenario of ceasing injection after injection at steady rate of 6.7 million liters/month for 15 years, a) infinite reservoir, b) infinite strip reservoir with width of 7.5 km, c) infinite strip reservoir with width of 1 km.

Figure 28. Pressure at well head for the scenarios of ceasing injection after 15 years.

Figure 29. a) Distribution of Silurian salt [from Dunrud and Nevins, 1981] and b) major injection wells, solution mines and historical earthquakes in northeastern Ohio. Filled circles are major injection wells for disposal or solution mining.

Figure 30. Side and front panel view of the General Earthquake Observation System (GEOS) together with a WWVB antenna and two sets of three-component sensors commonly used to provide more than 180 dB of linear, dynamic range. Full capability to reconfigure system in the field is facilitated by simple operator response to English language prompts via keyboard.

Figure 31. Unit-impulse response of GEOS recorder, spectra for typical earth noise, and complete system response with two types of sensors (force–balance accelerometer and velocity transducer).

Figure 32. Locations of sites occupied by GEOS recorders and location of mainshock on January 31, 1986 (J. Dewey, pers. comm., 1986). Major highways, city and community boundaries, and lake boundaries also are shown.

Figure 33. Acceleration, velocity and displacement time histories obtained at foundation of reactor building for the mainshock for a) vertical b) north-south and c) east–west components [Kinemetrics/Systems, 1986].

Figure 34. Acceleration, velocity and displacement time histories obtained on the annulus of the containment vessel for the main shock for a) vertical b) north-south and c) east–west components [Kinemetrics/Systems, 1986].

Figure 35. Relative velocity response and Fourier spectra for mainshock as recorded at foundation of reactor building a) vertical, b) north–south and c) east–west component [Kinemetrics/Systems, 1986].

Figure 36. Relative velocity response and Fourier spectra for mainshock as recorded on annulus of containment vessel a) vertical, b) north–south and c) east–west component [Kinemetrics/Systems, 1986].

Figure 37. Equiscaled plots of ground velocity aas recorded at station GS01 (traces 1, 2, 3) and at station GS02 (traces 4, 5, 6) for aftershock on February 3 at 19:47 (Magnitude 2.2). Comparison of amplitudes shows that vertical amplitudes of velocity are up to four times larger at station GS01, which is about 8 km more distant from the hypocenter.

Figure 38. Equiscaled plots of ground velocity as recorded at station GS01 (traces 1, 2, 3) and at station GS02 (traces 4, 5, 6) for aftershock on February 6 at 18:36.

Figure 39. Plot of peak acceleration amplitudes as a function distance observed for aftershock of February 3 19:47 a) with and b) without correction for geometric spreading.

Figure 40. Spectral ratios computed to characterize amplitude response at station GS01 relative to station GS02 (a, b, c) and relative to station GS03 (d, e, f). Spectral ratios shown cover the band from 0.1 to 130 Hz, the frequency band for which the signal-to-noise ratio exceeds 2. Note that the spectral ratios computed from broadband digital data allow recognition of site response characteristics at frequencies much higher than previously observed with conventional recording equipment!

Figure 41. Spectral ratios of vertical component computed to characterize amplitude response at station GS01 relative to station GS02 (a, b, c) and relative to station GS03 (d, e, f) as shown in Figure 40 for frequency band 0.1 to 50 Hz. Amplitude response as computed for station GS01 with respect to station GS02 and station GS03 and for both events (19:47 and 18:36) suggests exaggerated levels of ground motion between 5 and 10 Hz and near 20 Hz. Smaller, but still significant levels of exaggerated shaking are also apparent for horizontal components.

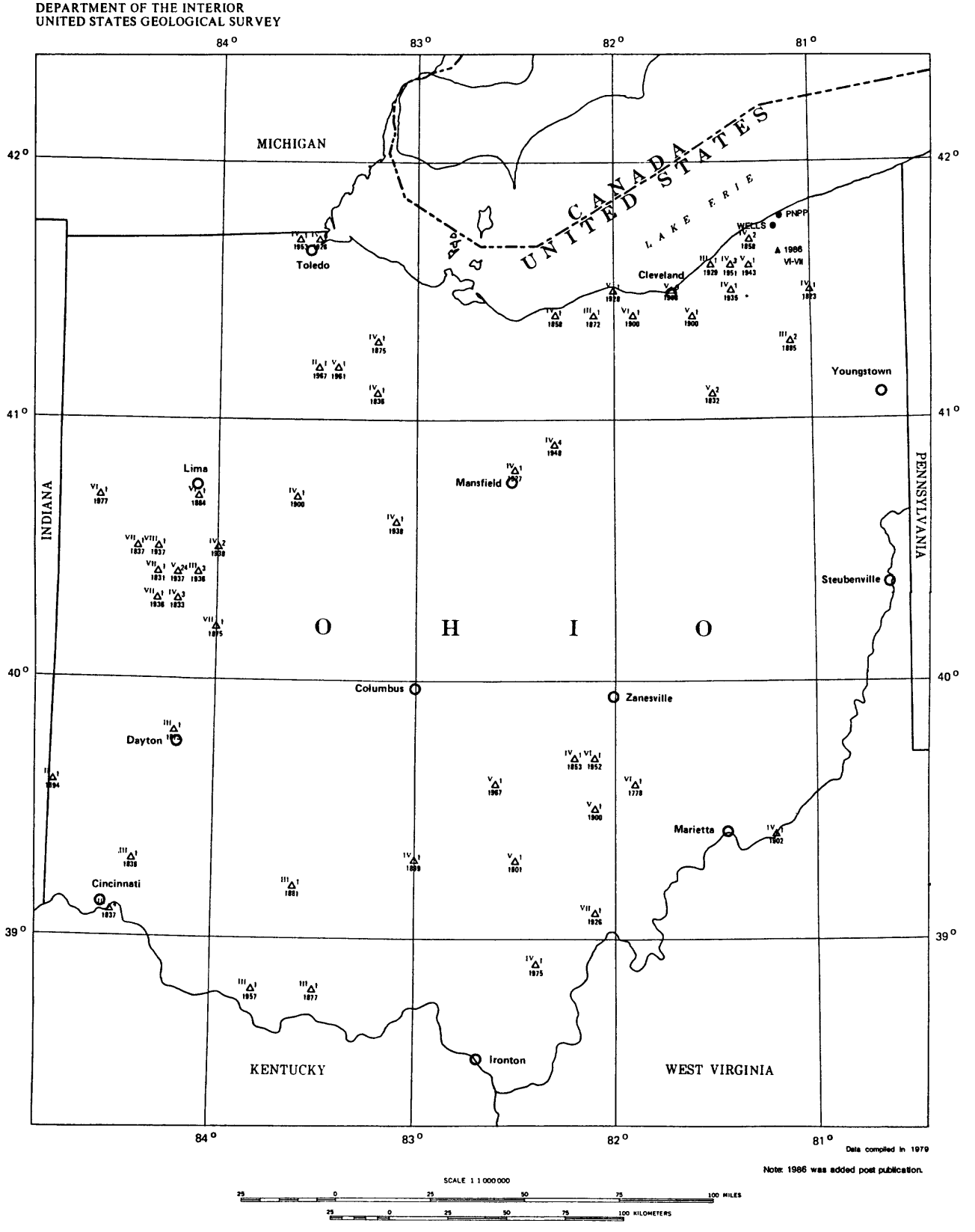

SEISMICITY MAP OF THE STATE OF OHIO

By

C. W. Stover, B. G. Reagor, and S. T. Algermissen

1979

Figure 1

Figure 2

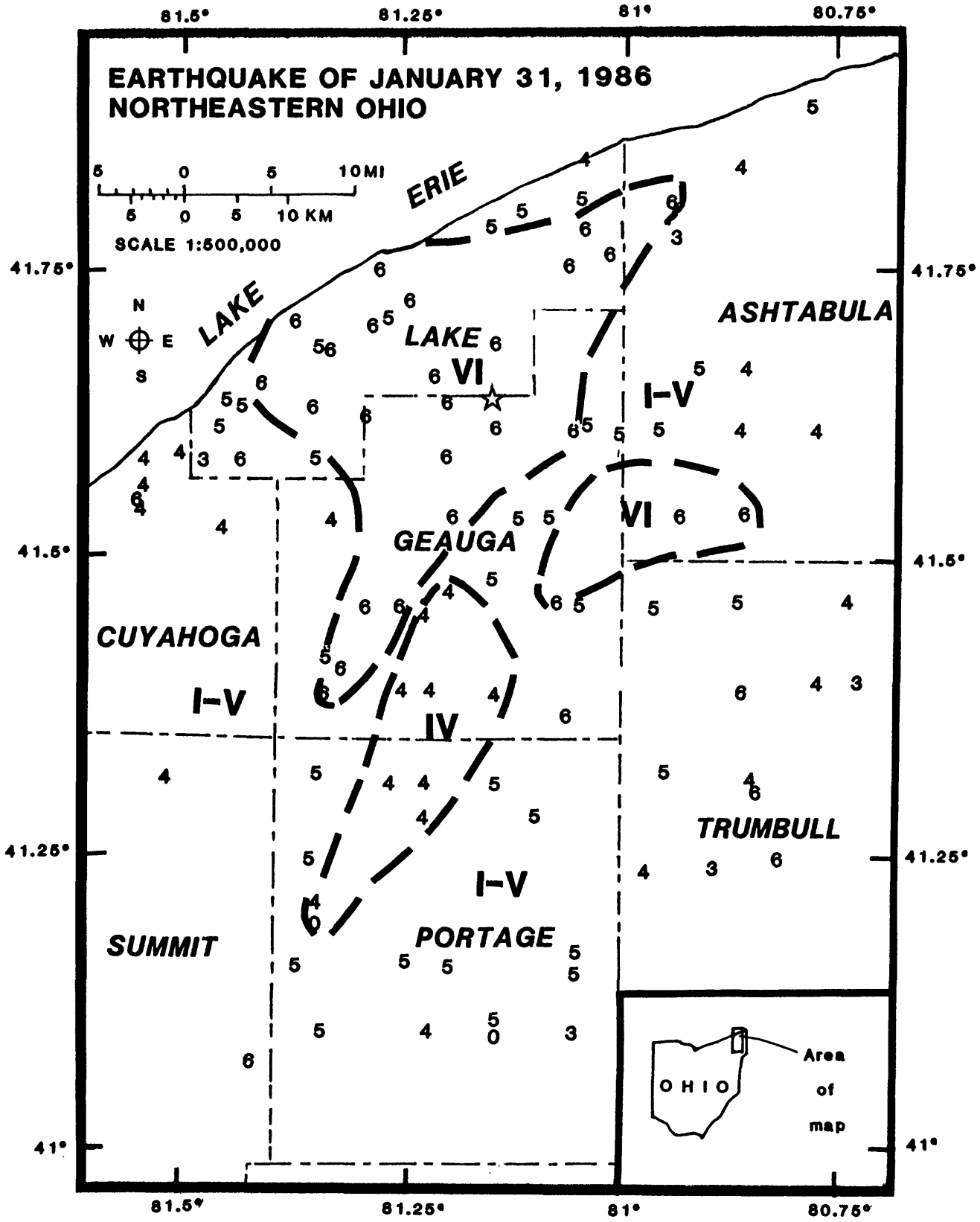

Preliminary interior MM isoseismals for the earthquake of January 31, 1986, northeastern Ohio. Site intensities are shown by Arabic numerals. Isoseismal intensities are denoted by Roman numerals. Star shows the location of the main shock epicenter. The isoseismal lines are shown as dashed because all the data are not yet in. When the data set is complete the lines will be finalized.

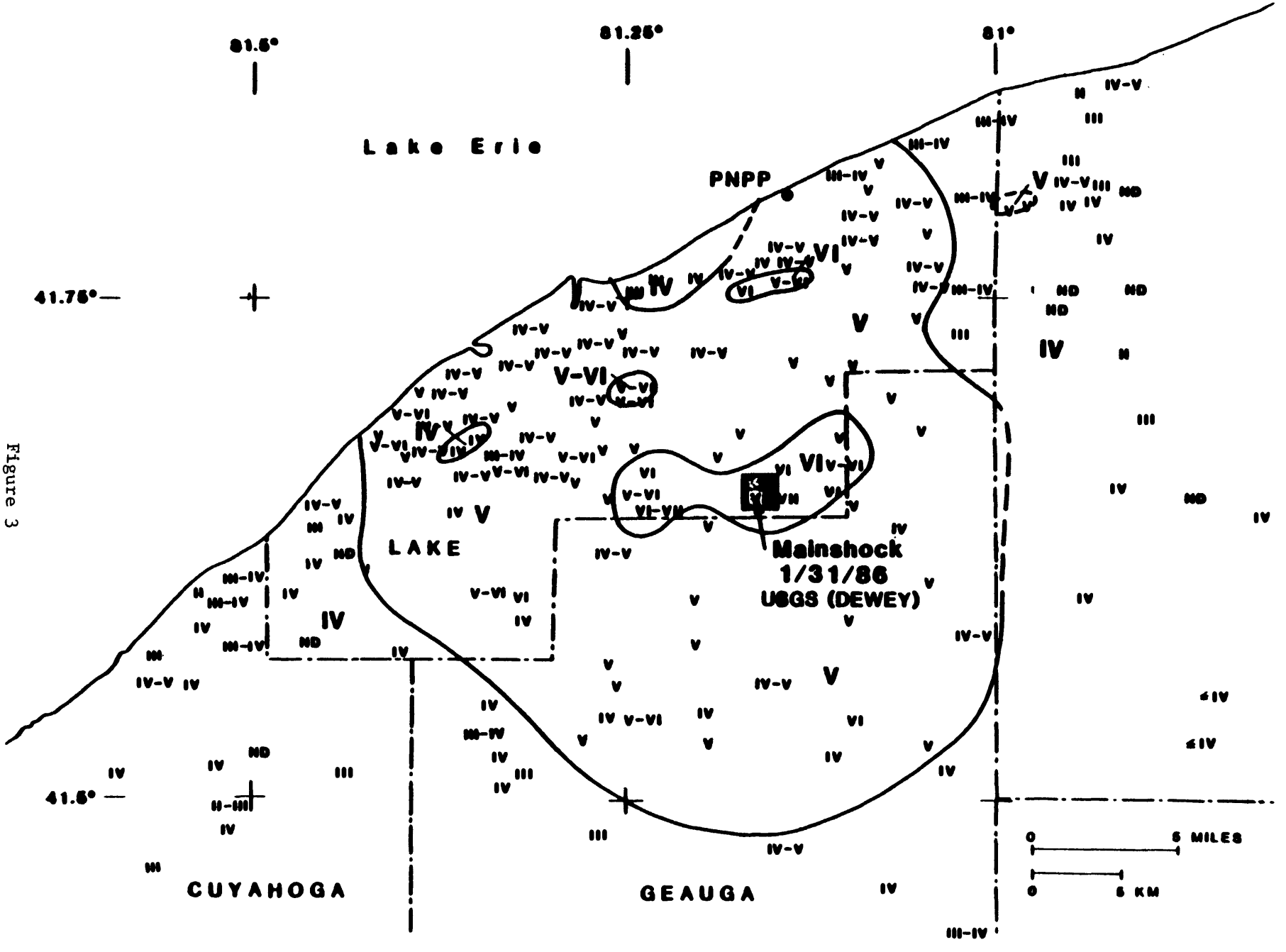
81.5°
81.25°
81°
Lake Erie
PNPP
41.75°
41.5°
LAKE
Mainshock
1/31/86
USGS (DEWEY)
CUYAHOGA
GEAUGA
0 5 MILES
0 5 KM

Figure 3
58

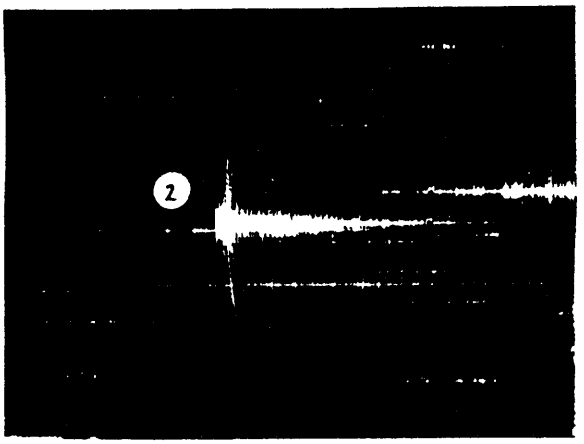

2-3-86 19:47 HAR

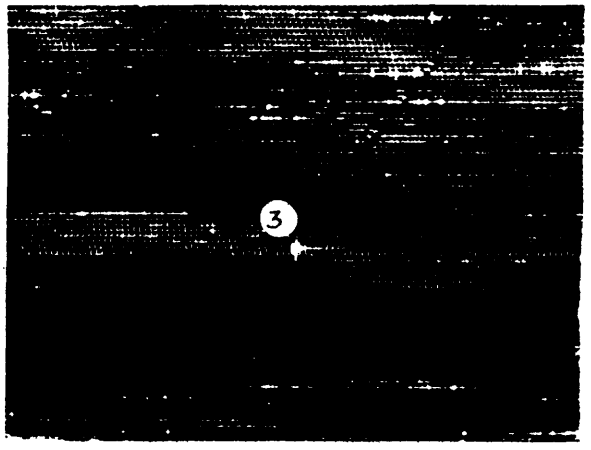

2-5-86 6:34 HAM

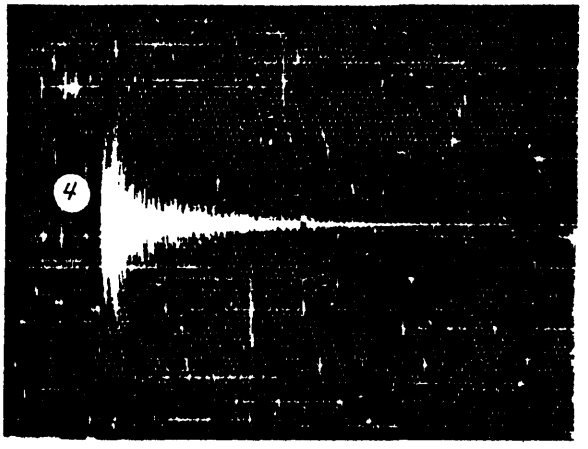

2-6-86 18:36 CUY

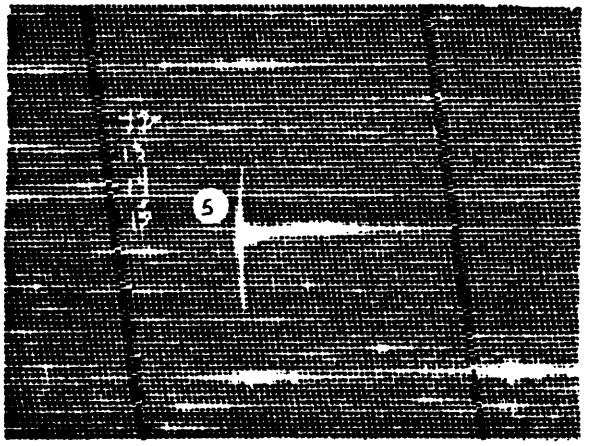

2-7-86 15:20 CAL

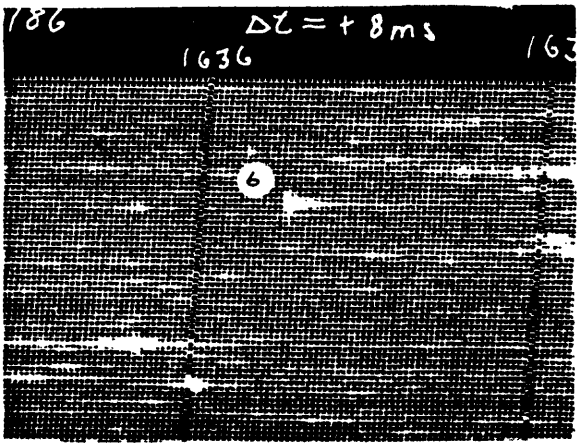

2-10-86 20:06 CAL

Figure 4

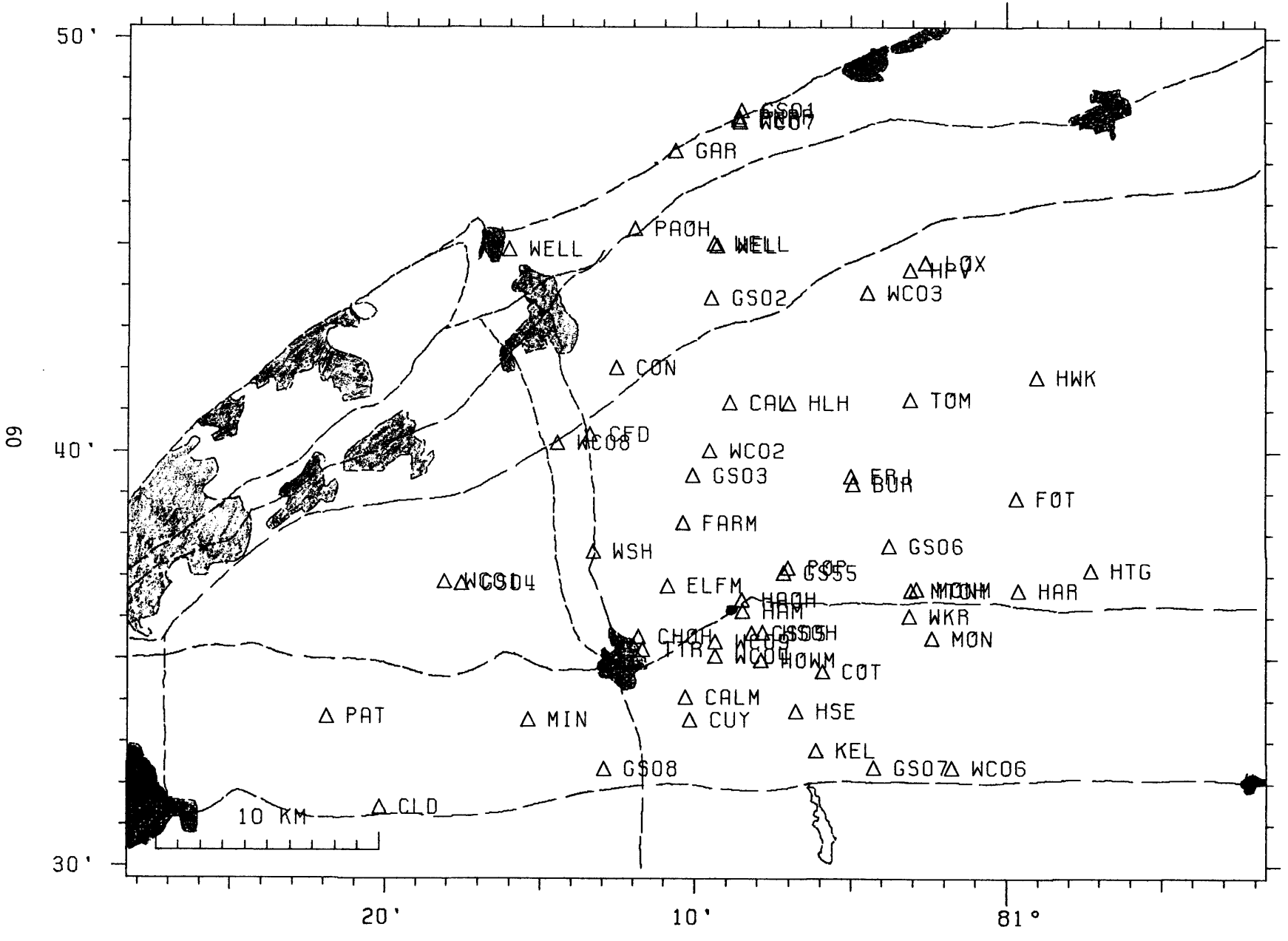
50'
40'
30'
20'
10'
81°
60
GAR
WELL
PAOH
GSO2
WCO3
CON
HWK
CAL
HLH
TOM
CFD
WCO8
WCO2
GSO3
BUR
FOT
FARM
WSH
GSO6
ELFM
GS55
HTG
HAR
HAM
WKR
MON
COT
CALM
PAT
MIN
CUY
HSE
KEL
GSO8
GSO7
WCO6
CLD
10 KM

Figure 5

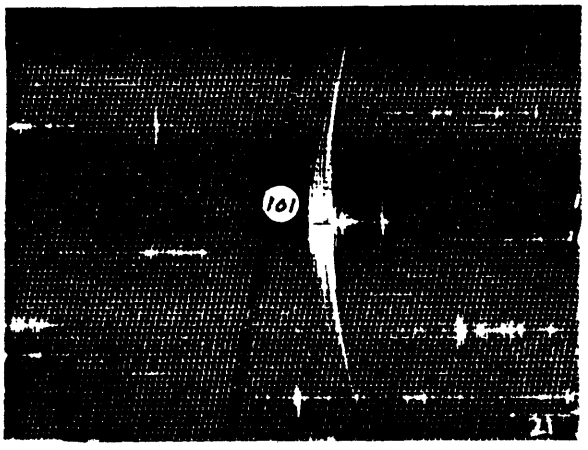

2-5-86 15:39 FOT

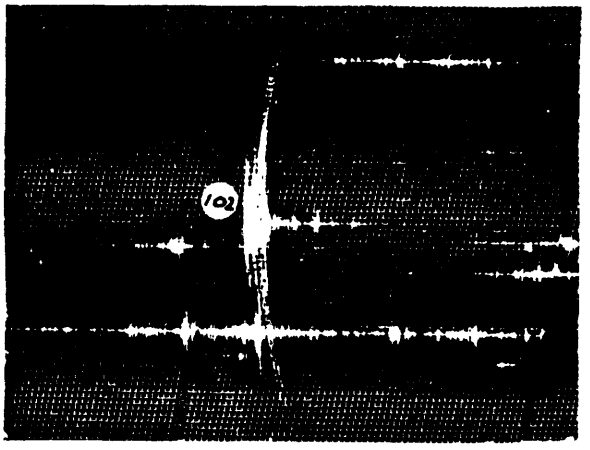

2-5-86 17:57 FOT

Figure 6

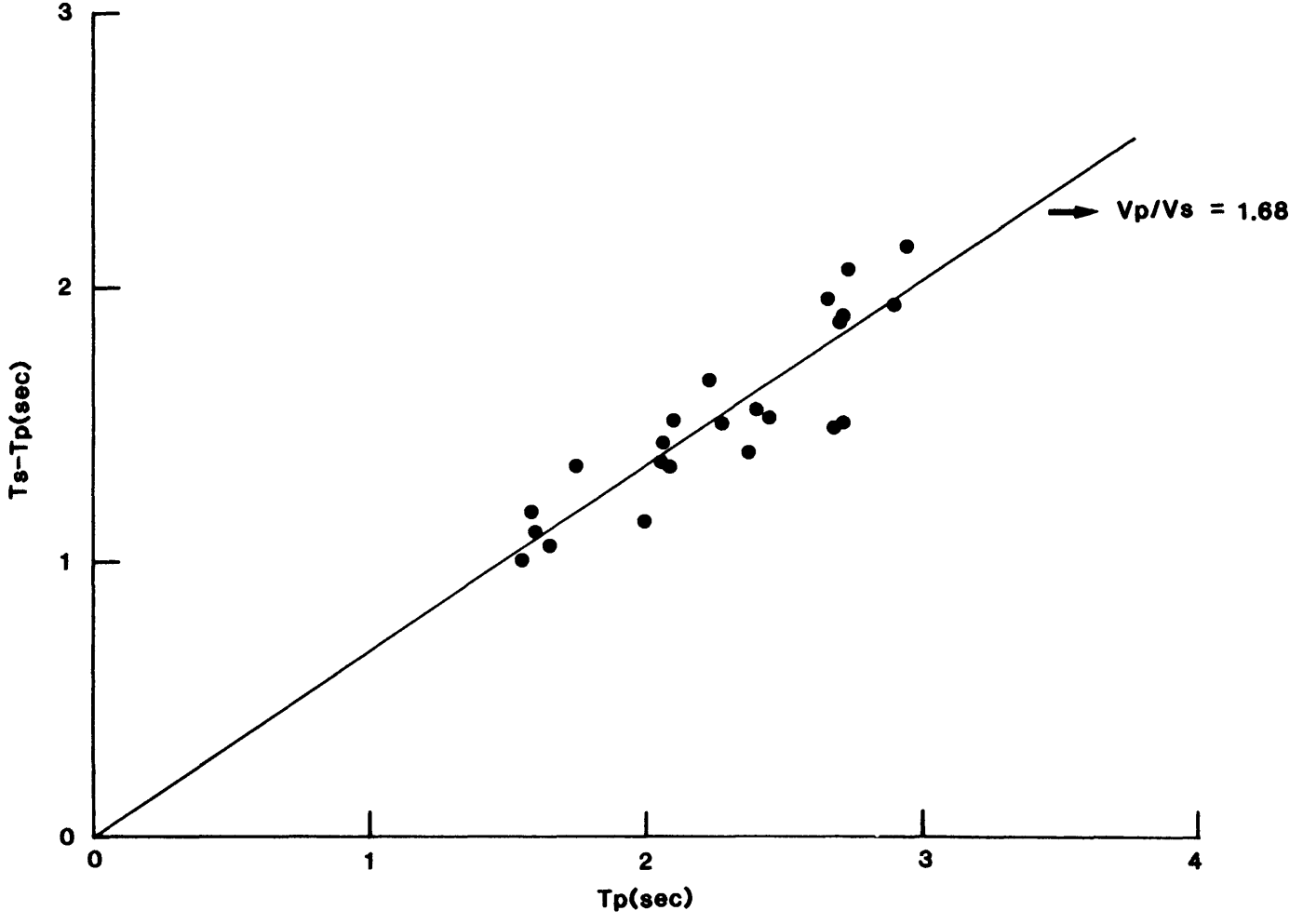

Figure 7

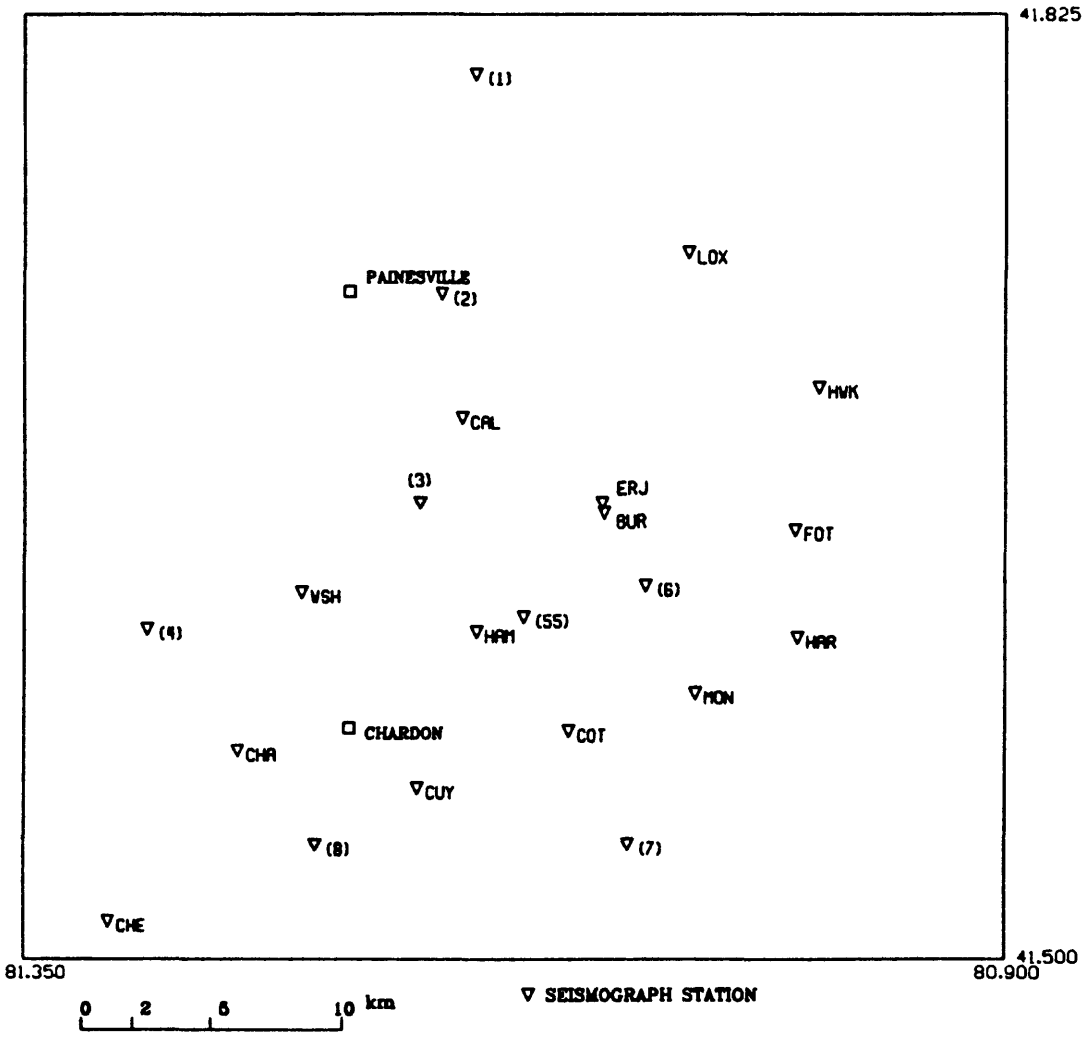
41.825
(1)
LOX
PAINESVILLE
(2)
HWK
CAL
(3)
ERJ
BUR
FOT
VSH
(6)
(4)
(55)
HRM
HAR
MON
CHARDON
COT
CHR
CUY
(8)
(7)
CHE
41.500
81.350
80.900
0 2 5 10 km
SEISMOGRAPH STATION

Figure 8

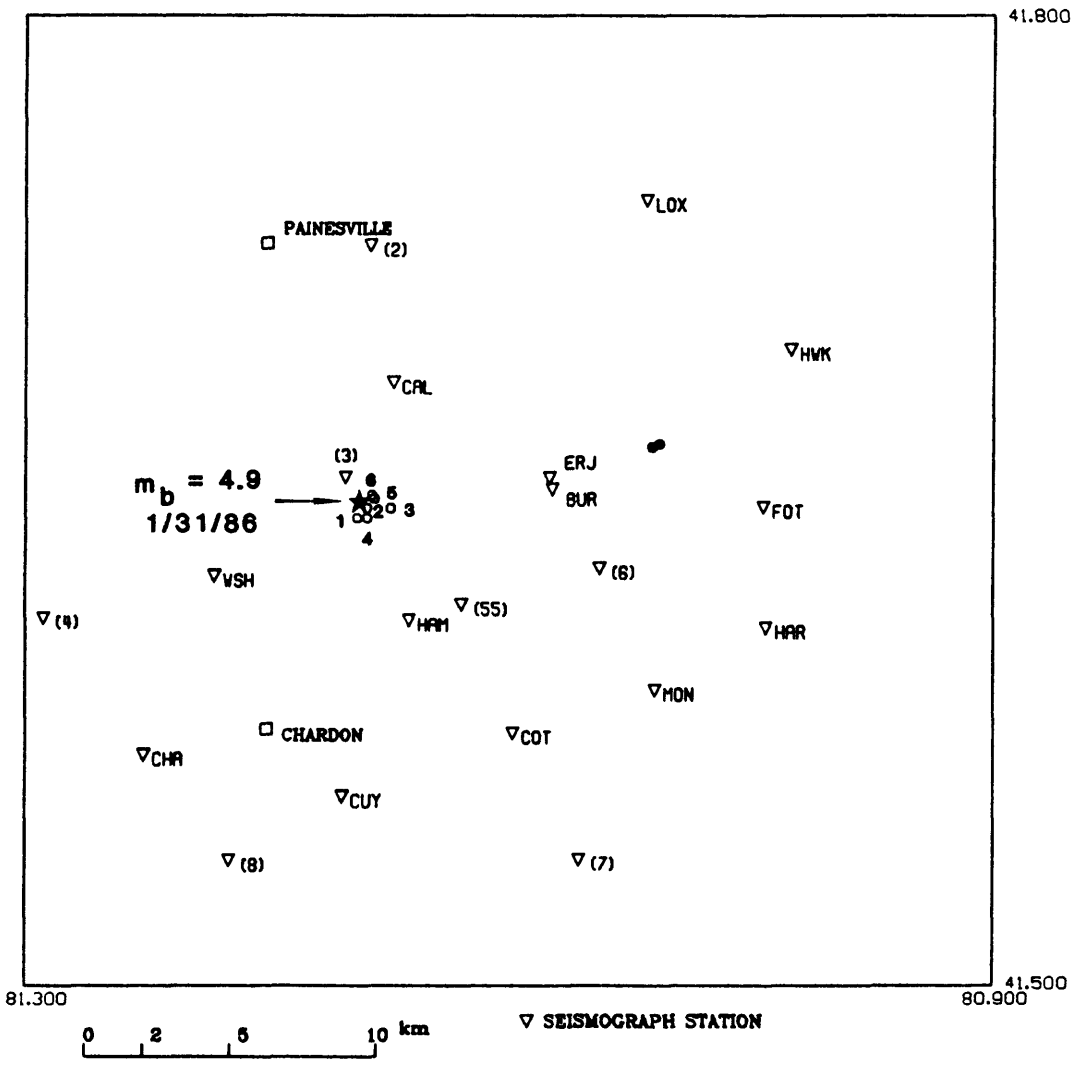
41.800
LOX
PAINESVILLE
(2)
HWK
CAL
(3)
ERJ
m_b = 4.9
1/31/86
BUR
FOT
1
2
3
4
5
6
VSH
(6)
(4)
HAM
(55)
HAR
MON
CHARDON
COT
CHA
CUY
(8)
(7)
41.500
81.300
80.900
0
2
5
10
km
SEISMOGRAPH STATION

Figure 9

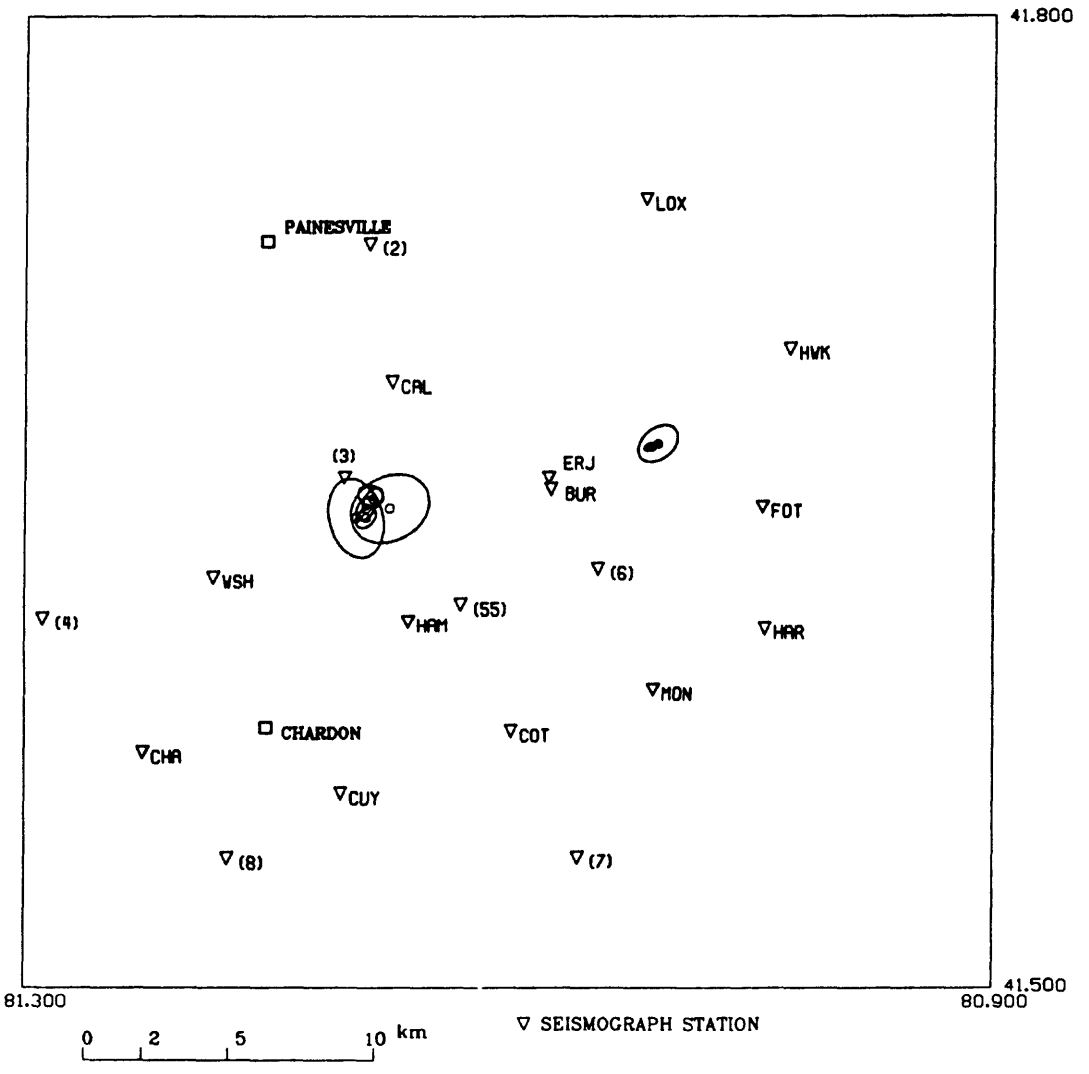
41.800
LOX
PAINESVILLE
(2)
HWK
CAL
(3)
ERJ
BUR
FOT
WSH
(6)
(4)
(55)
HAM
HAR
MON
CHARDON
COT
CHR
CUY
(8)
(7)
41.500
81.300
80.900
0 2 5 10 km
SEISMOGRAPH STATION

Figure 10

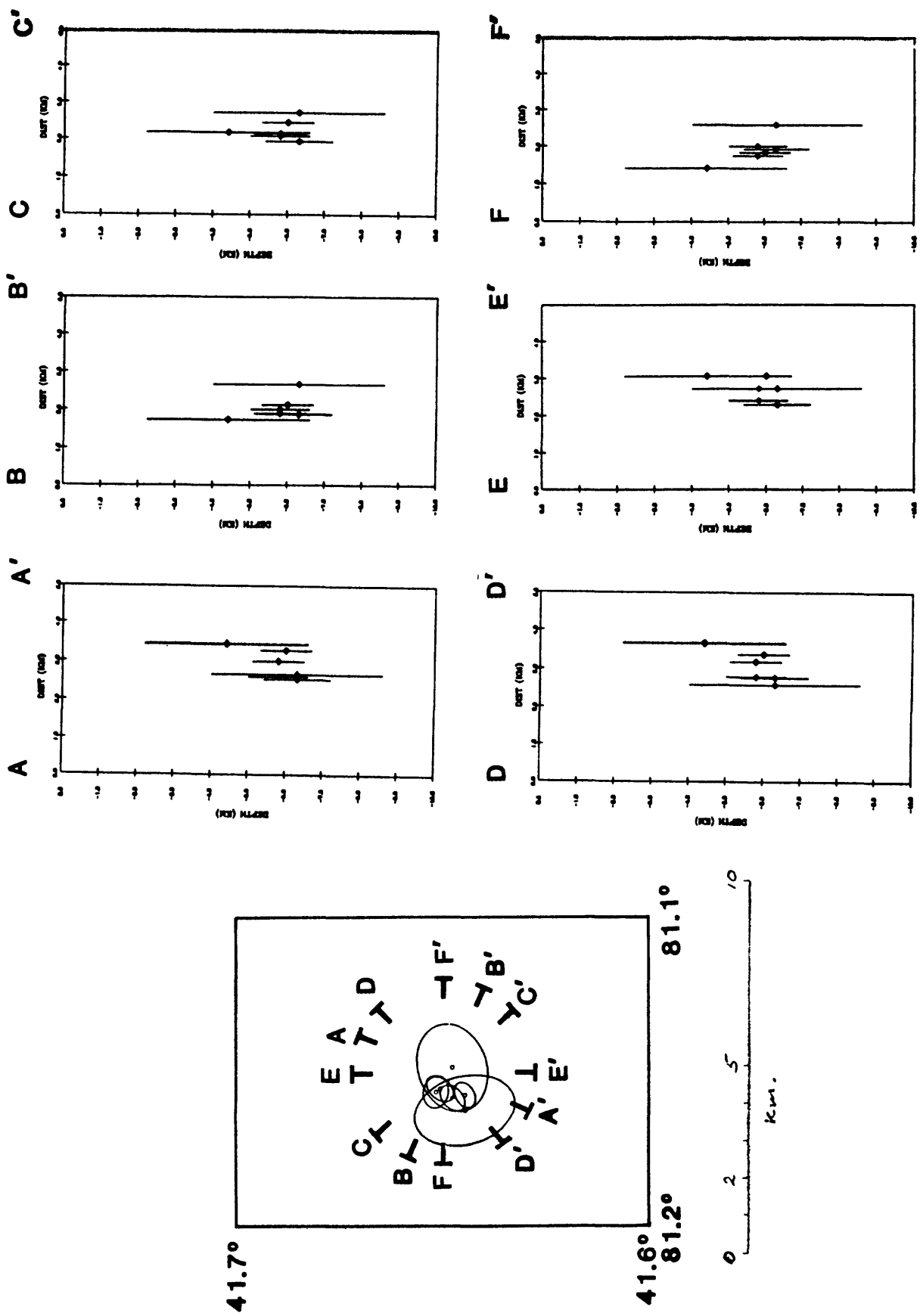

Figure 11

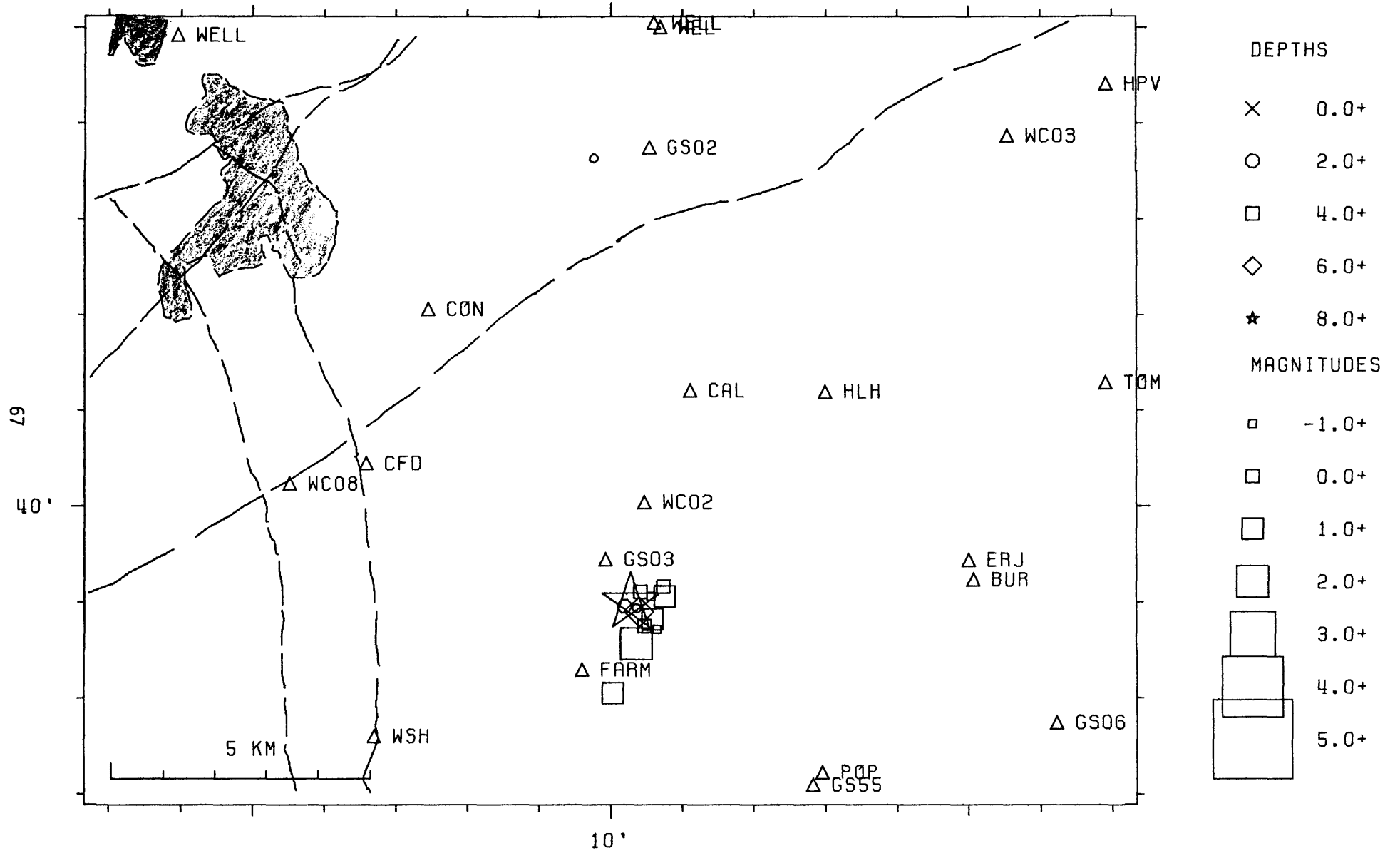
WELL
WELL
HPV
GS02
WC03
CON
CAL
HLH
TOM
CFD
WC08
WC02
GS03
ERJ
BUR
FARM
GS06
WSH
5 KM
POP
GS55
67
40'
10'
DEPTHS
0.0+
2.0+
4.0+
6.0+
8.0+
MAGNITUDES
-1.0+
0.0+
1.0+
2.0+
3.0+
4.0+
5.0+

Figure 12

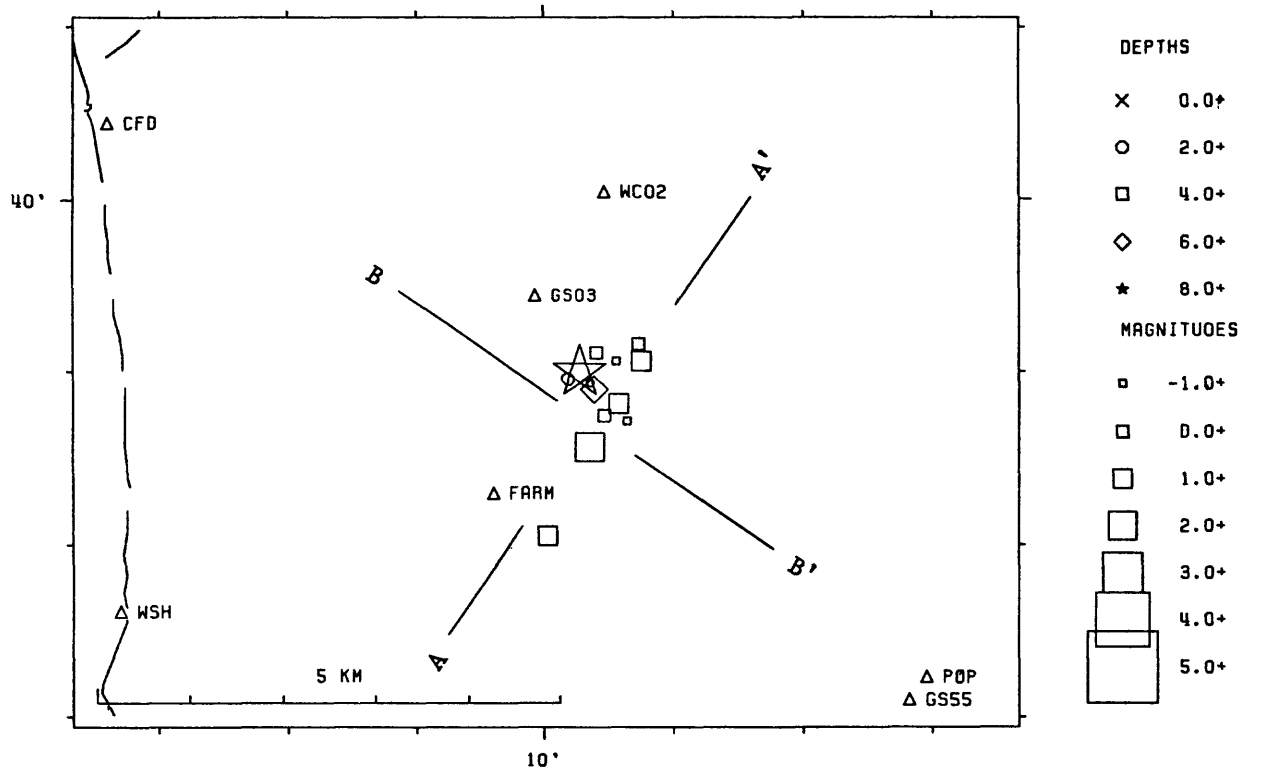
CFD
WCO2
GSO3
FARM
WSH
POP
GSS5
A
A'
B
B'
5 KM
40'
10'
DEPTHS
0.0+
2.0+
4.0+
6.0+
8.0+
MAGNITUOES
-1.0+
0.0+
1.0+
2.0+
3.0+
4.0+
5.0+

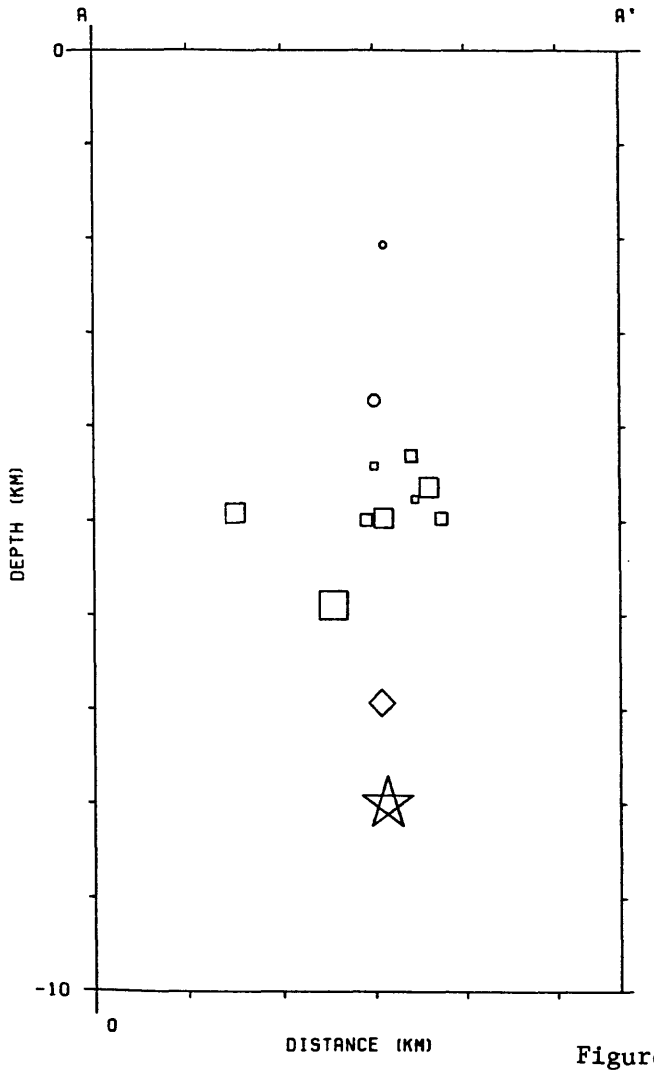
A
A'
0
-10
0
DEPTH (KM)
DISTANCE (KM)

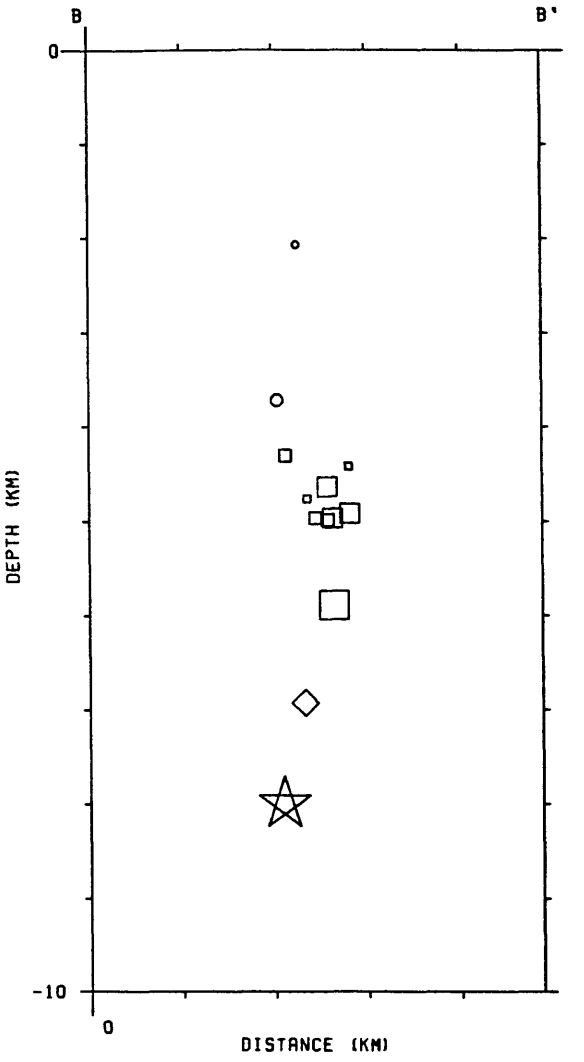
B
B'
0
-10
0
DEPTH (KM)
DISTANCE (KM)

Figure 13

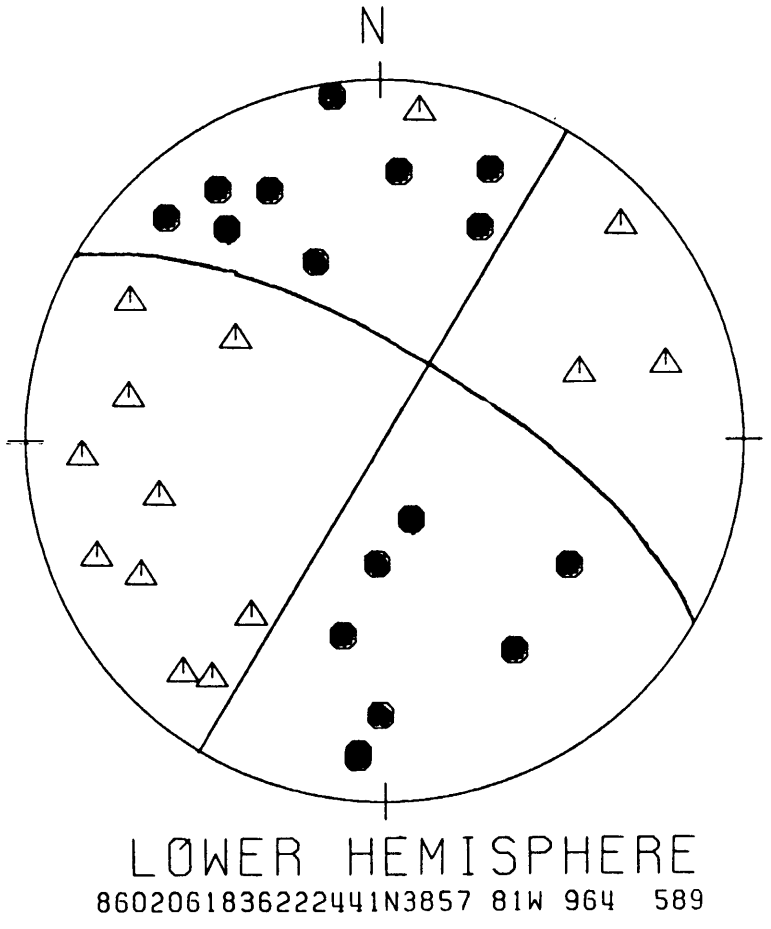
N
LOWER HEMISPHERE
860206183622244 1N3857 81W 964 589

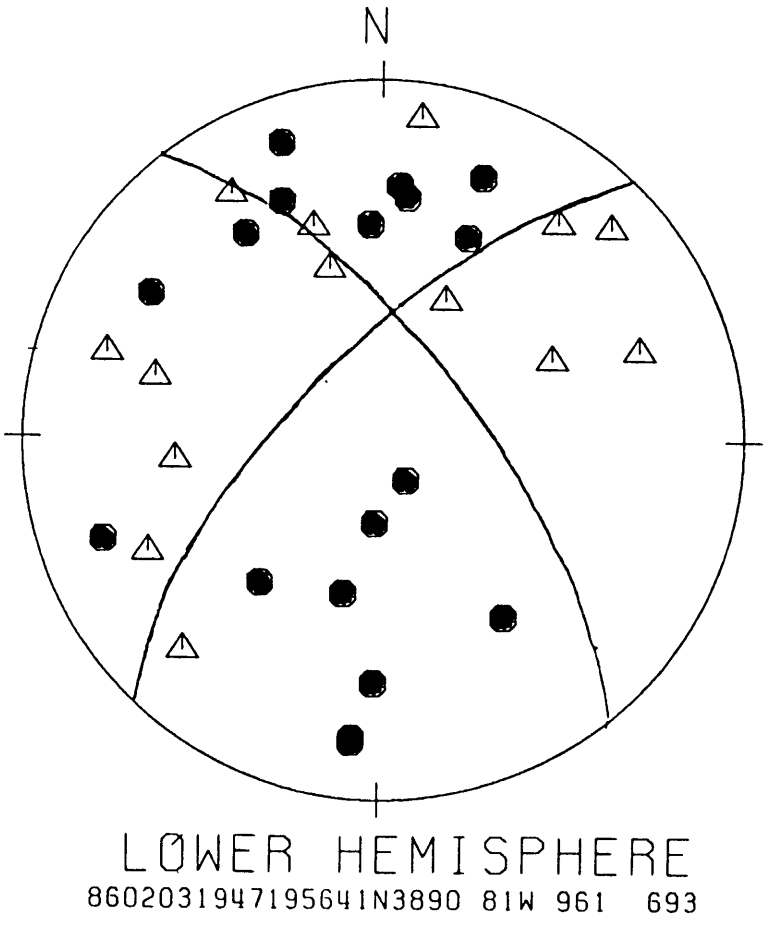
N
LOWER HEMISPHERE
860203194719564 1N3890 81W 961 693

Figure 14

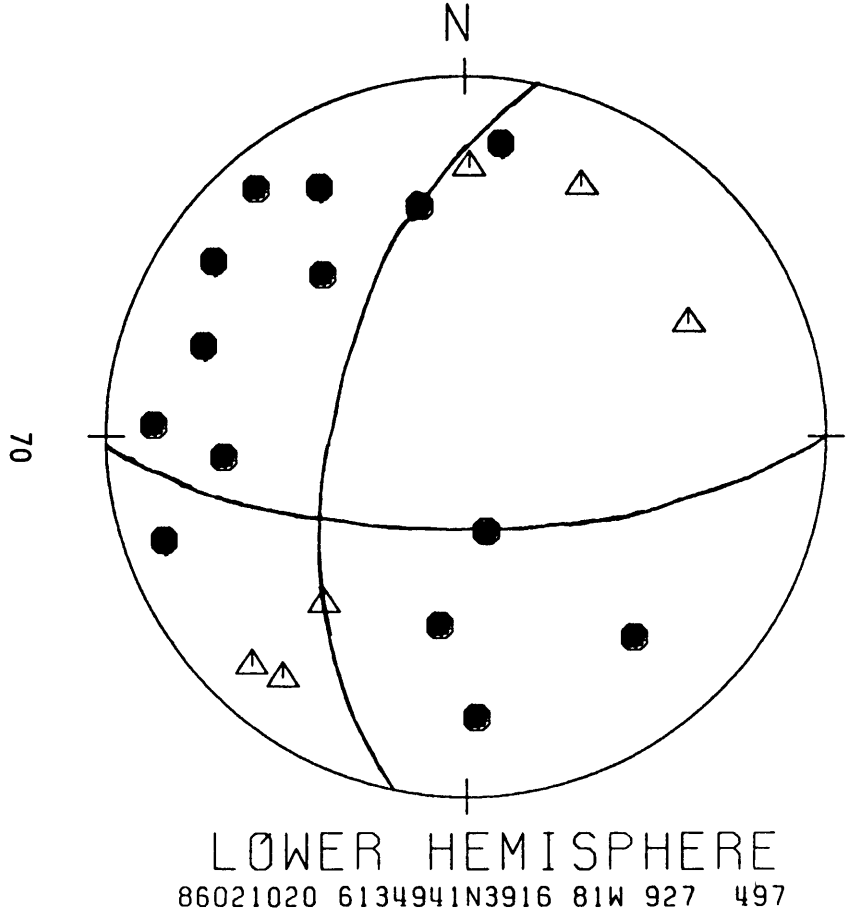
N
70
LOWER HEMISPHERE
86021020 6134941N3916 81W 927 497

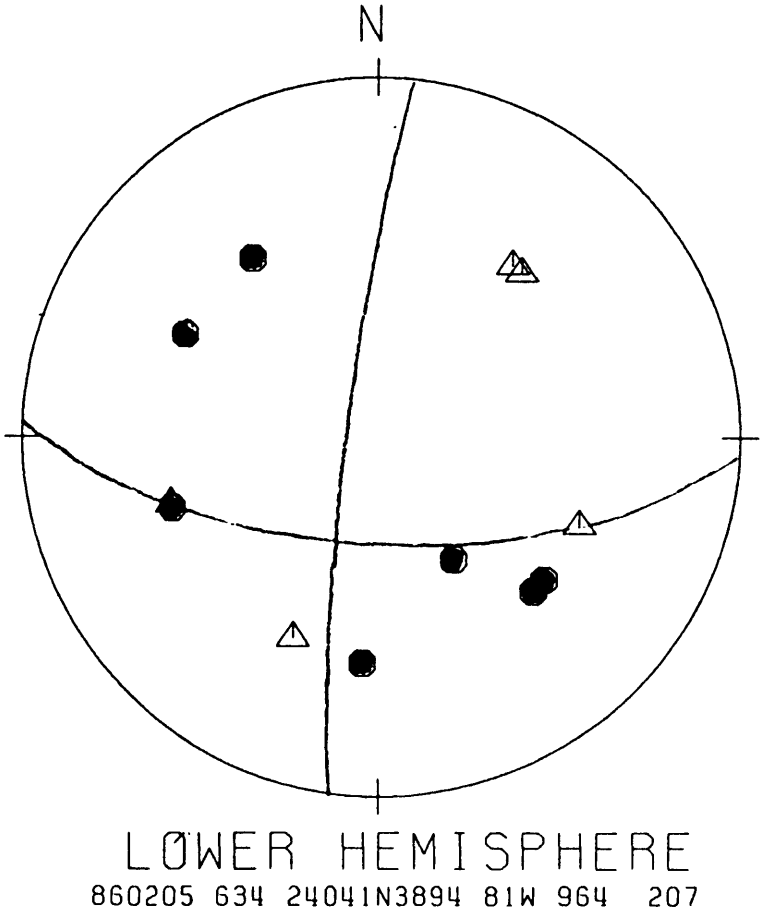
N
LOWER HEMISPHERE
860205 634 24041N3894 81W 964 207

Figure 15

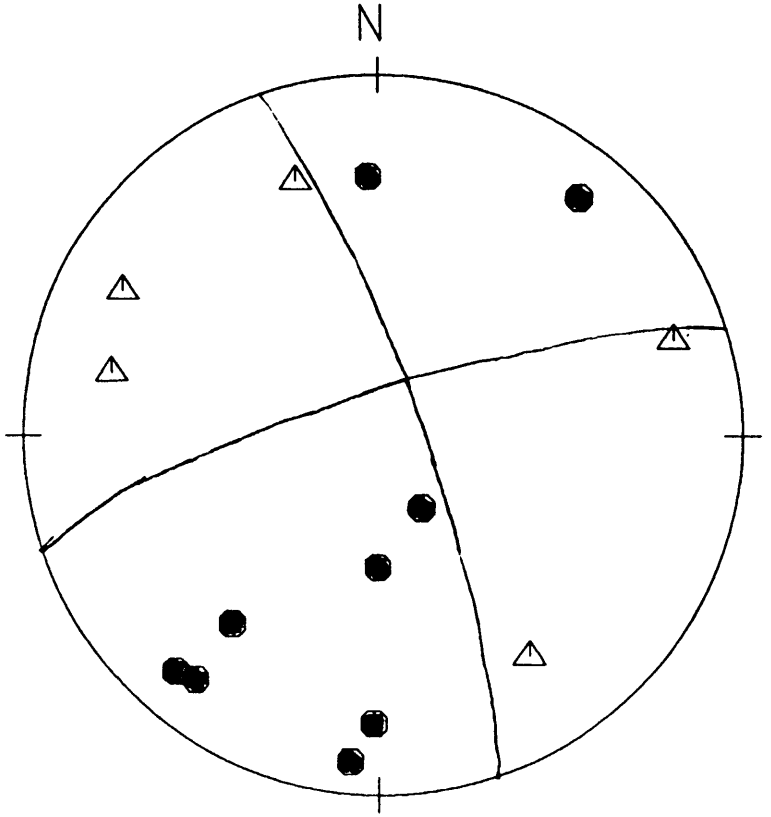
N
LOWER HEMISPHERE
860202 322485341N3875 81W 953 499

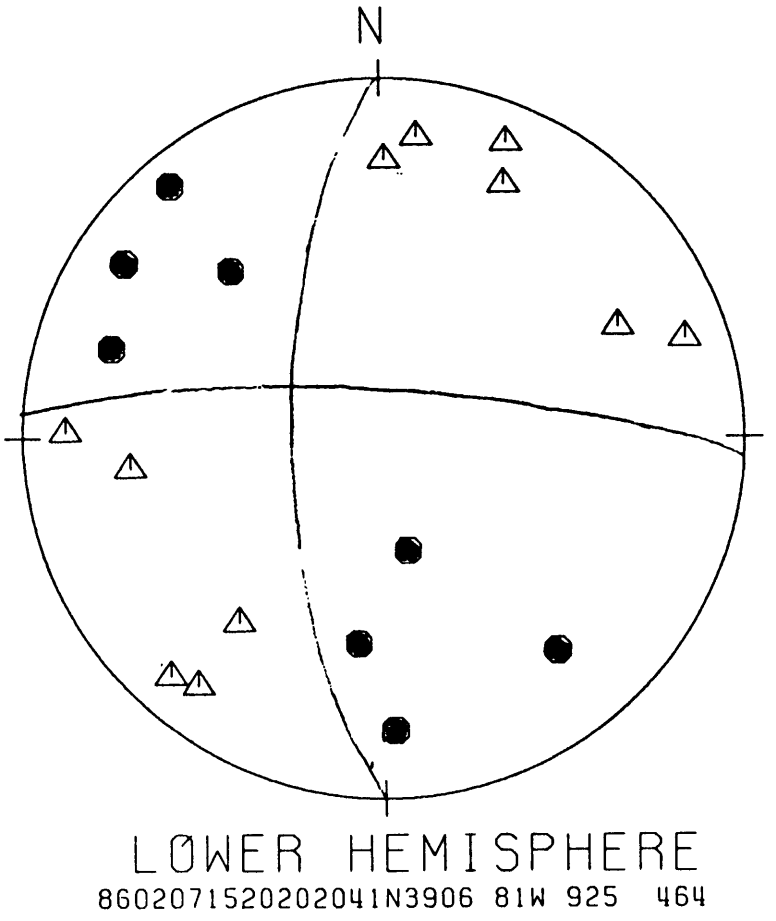
N
LOWER HEMISPHERE
860207152020241N3906 81W 925 464

Figure 16

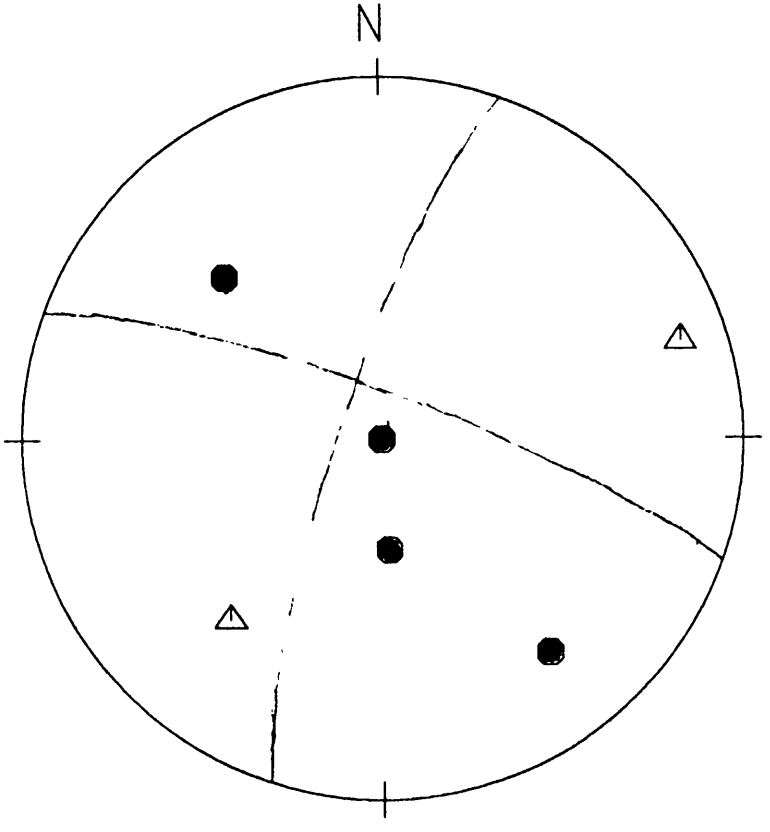
N
LOWER HEMISPHERE
860223 329484641N3906 81W 944 477

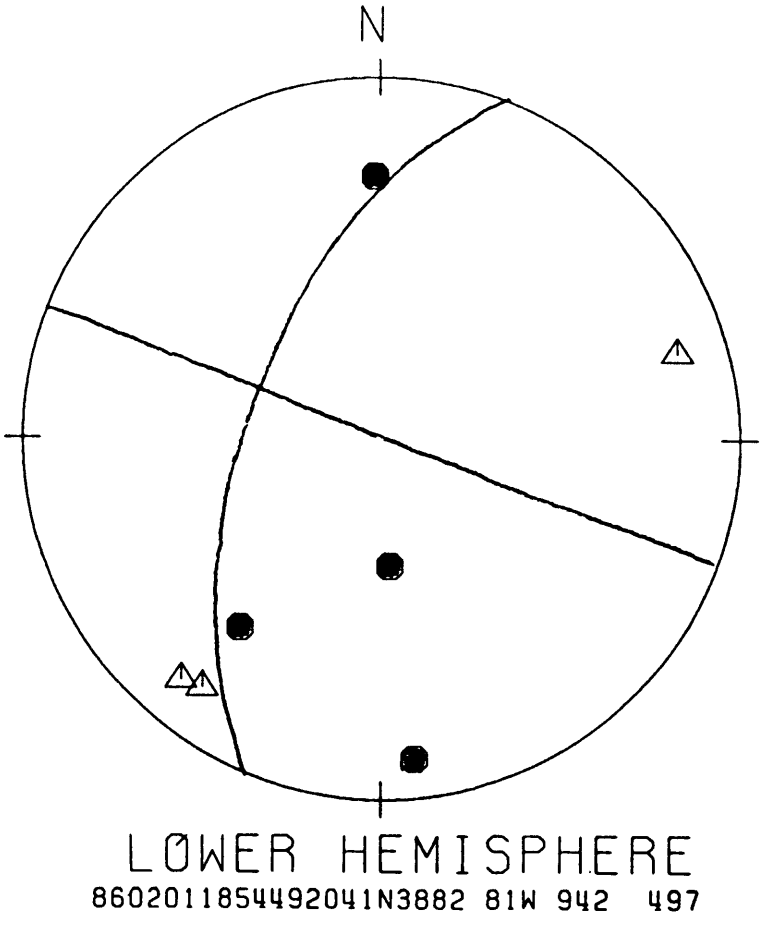
N
LOWER HEMISPHERE
860201185449204 1N3882 81W 942 497

Figure 17

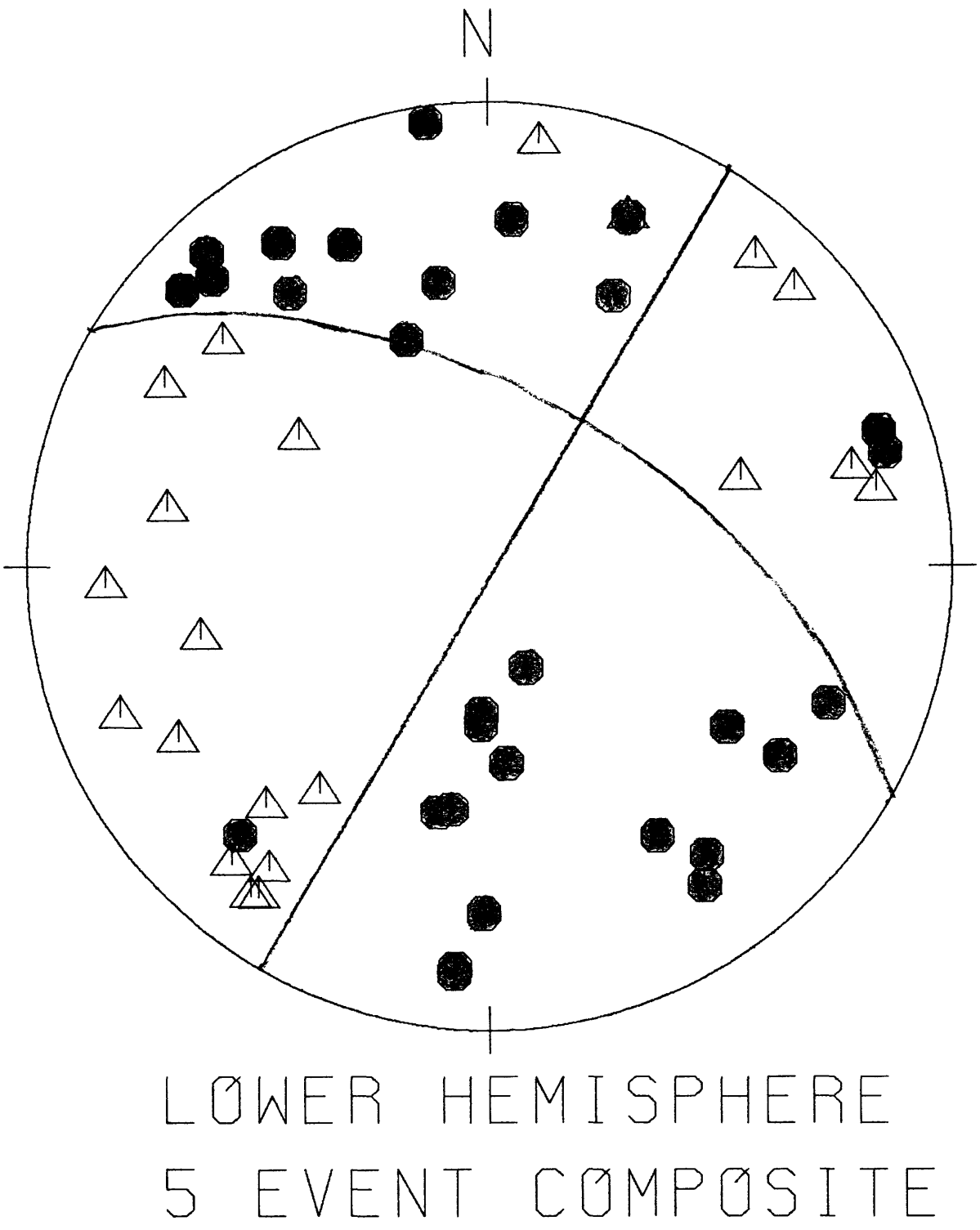

Figure 18

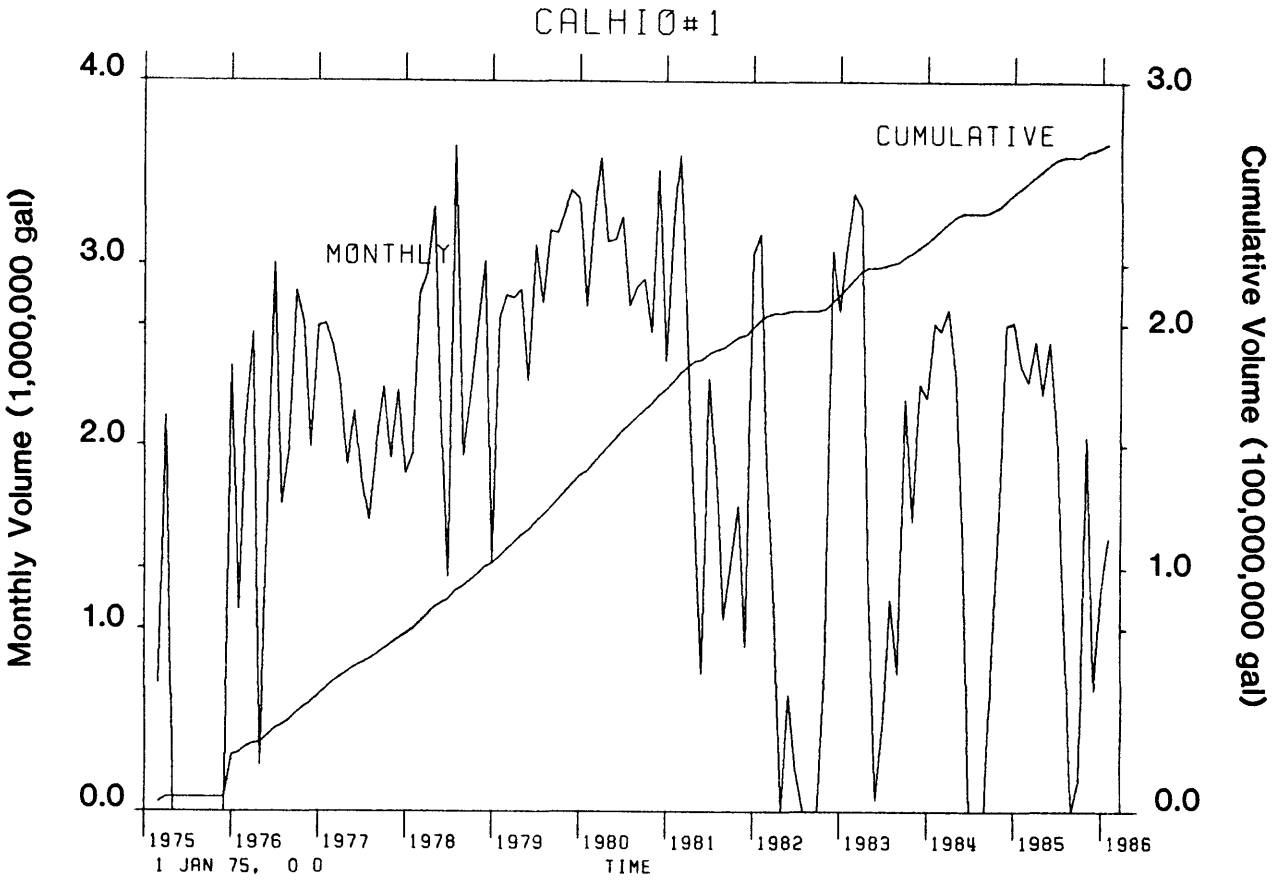
CALHI0#1
CUMULATIVE
MONTHLY
Monthly Volume (1,000,000 gal)
Cumulative Volume (100,000,000 gal)
4.0
3.0
2.0
1.0
0.0
3.0
2.0
1.0
0.0
1975
1976
1977
1978
1979
1980
1981
1982
1983
1984
1985
1986
1 JAN 75, 0 0
TIME

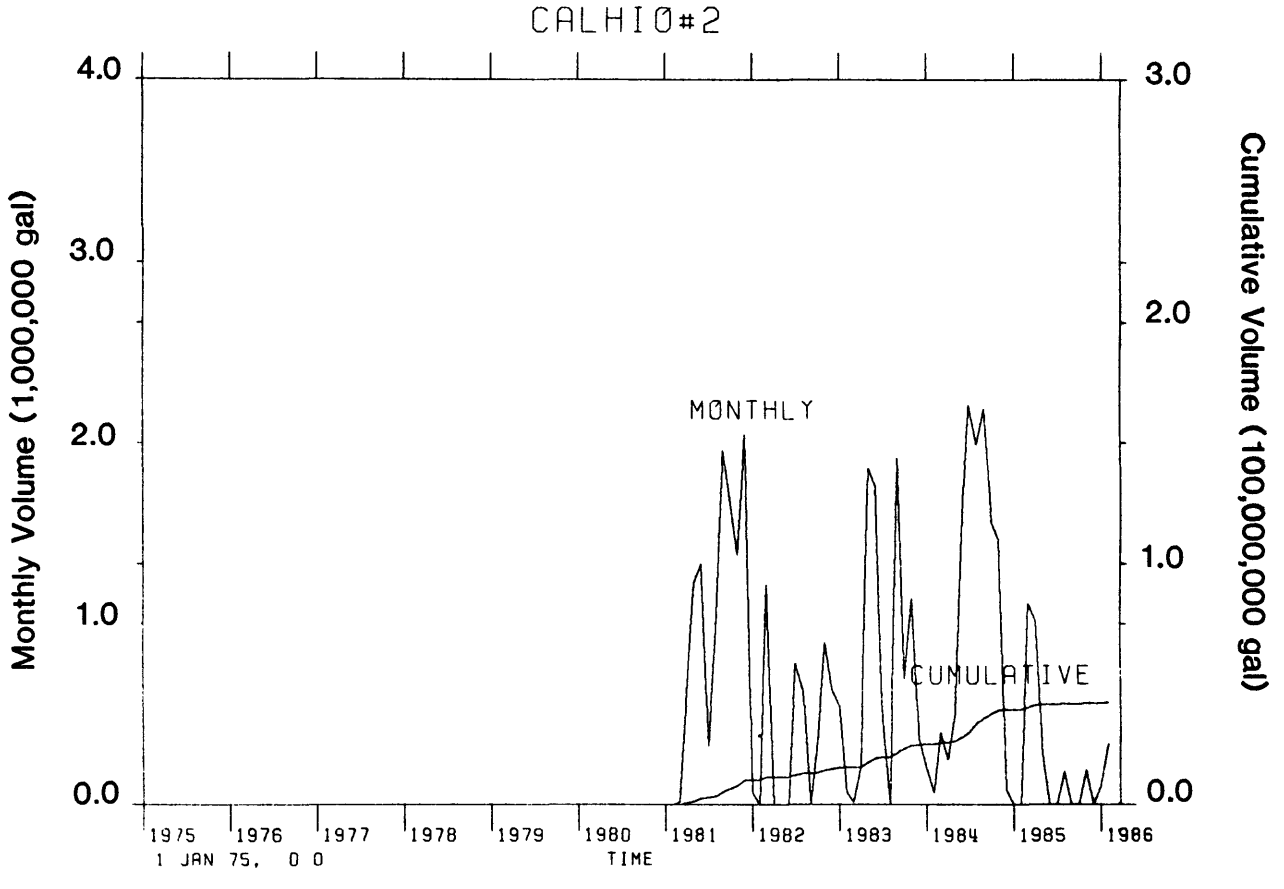
CALHI0#2
MONTHLY
CUMULATIVE
Monthly Volume (1,000,000 gal)
Cumulative Volume (100,000,000 gal)
4.0
3.0
2.0
1.0
0.0
3.0
2.0
1.0
0.0
1975
1976
1977
1978
1979
1980
1981
1982
1983
1984
1985
1986
1 JAN 75, 0 0
TIME

Figure 19

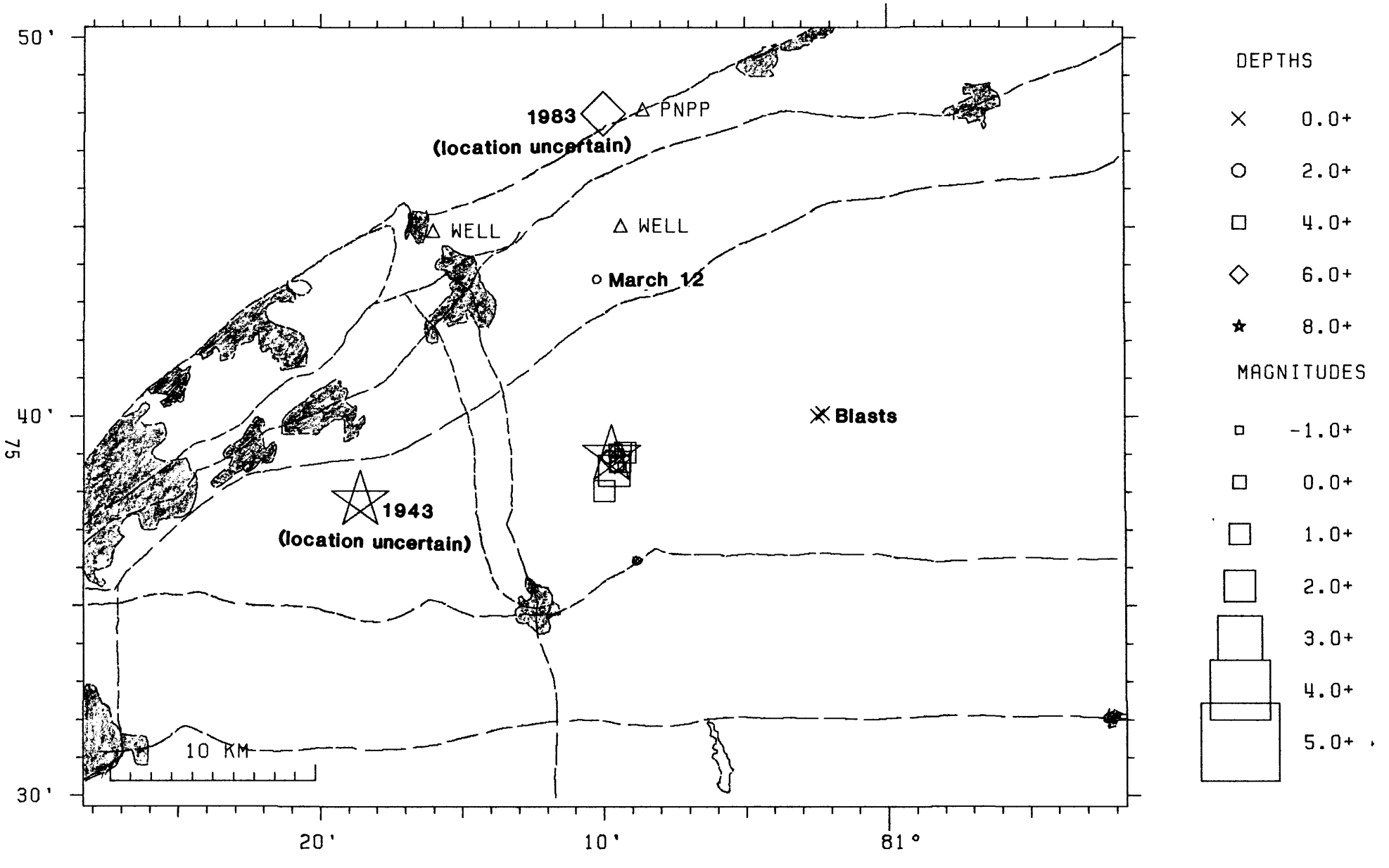
50'
40'
30'
75
20'
10'
81°
1983
(location uncertain)
PNPP
WELL
WELL
March 12
Blasts
1943
(location uncertain)
10 KM
DEPTHS
0.0+
2.0+
4.0+
6.0+
8.0+
MAGNITUDES
-1.0+
0.0+
1.0+
2.0+
3.0+
4.0+
5.0+

Figure 20

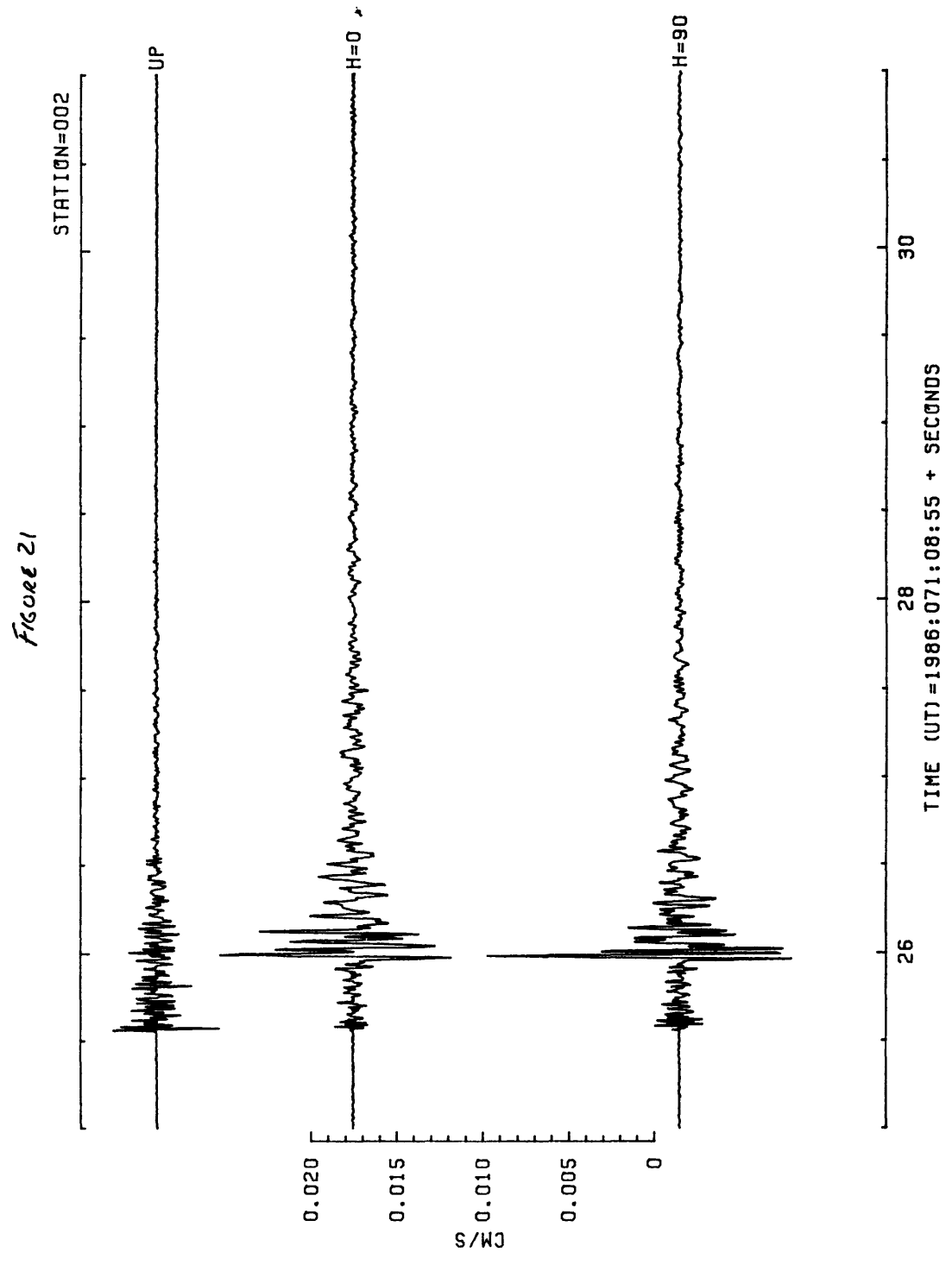
FIGURE 21
STATION=002
UP
H=0
H=90
0.020
0.015
0.010
0.005
0
CM/S
26
28
30
TIME (UT)=1986:071:08:55 + SECONDS

Figure 21

* *

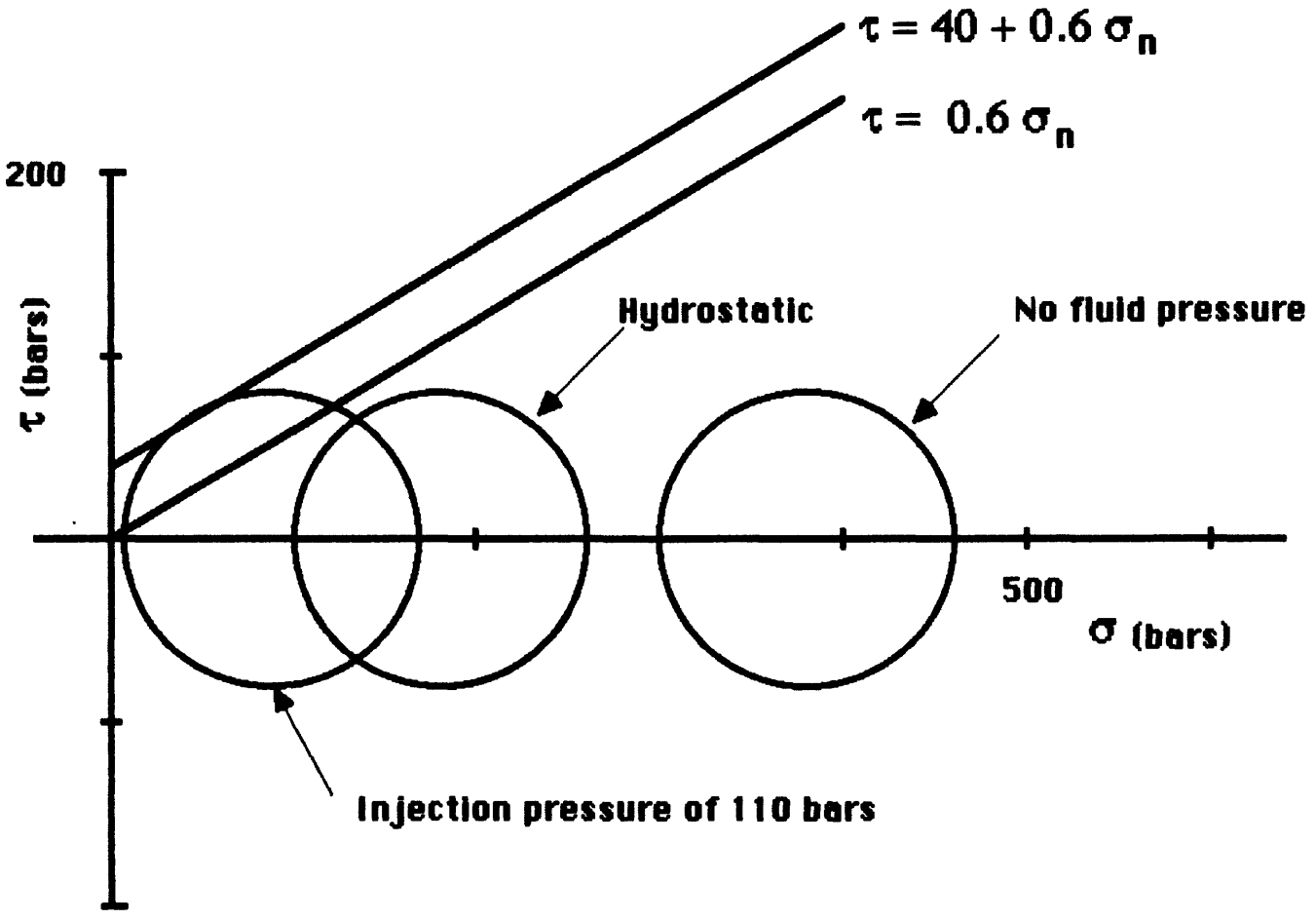
τ = 40 + 0.6 σn
τ = 0.6 σn
200
τ (bars)
Hydrostatic
No fluid pressure
500
σ (bars)
Injection pressure of 110 bars

Figure 22 A

Figure 22 B

IN SITU STRESS STATE

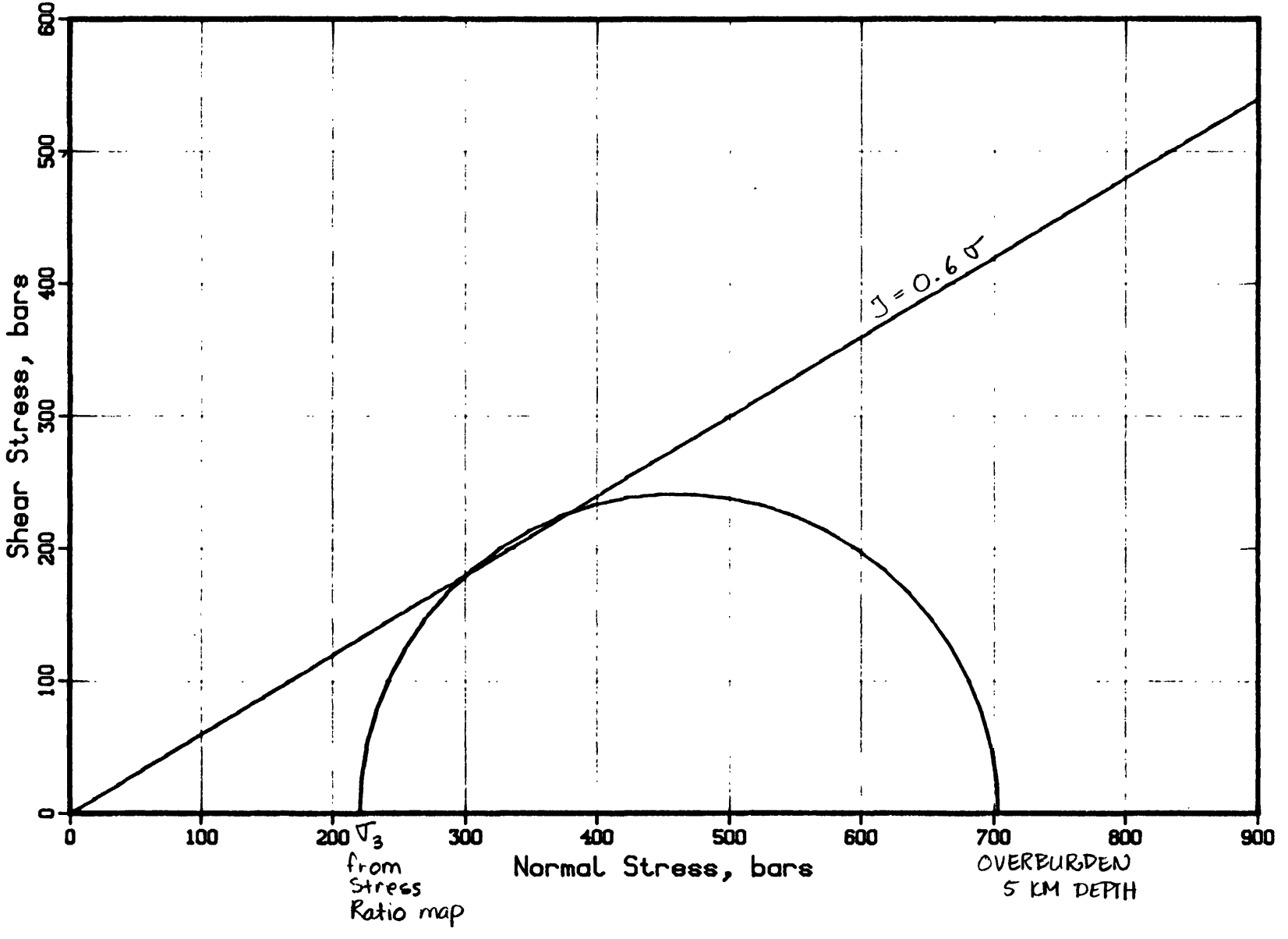

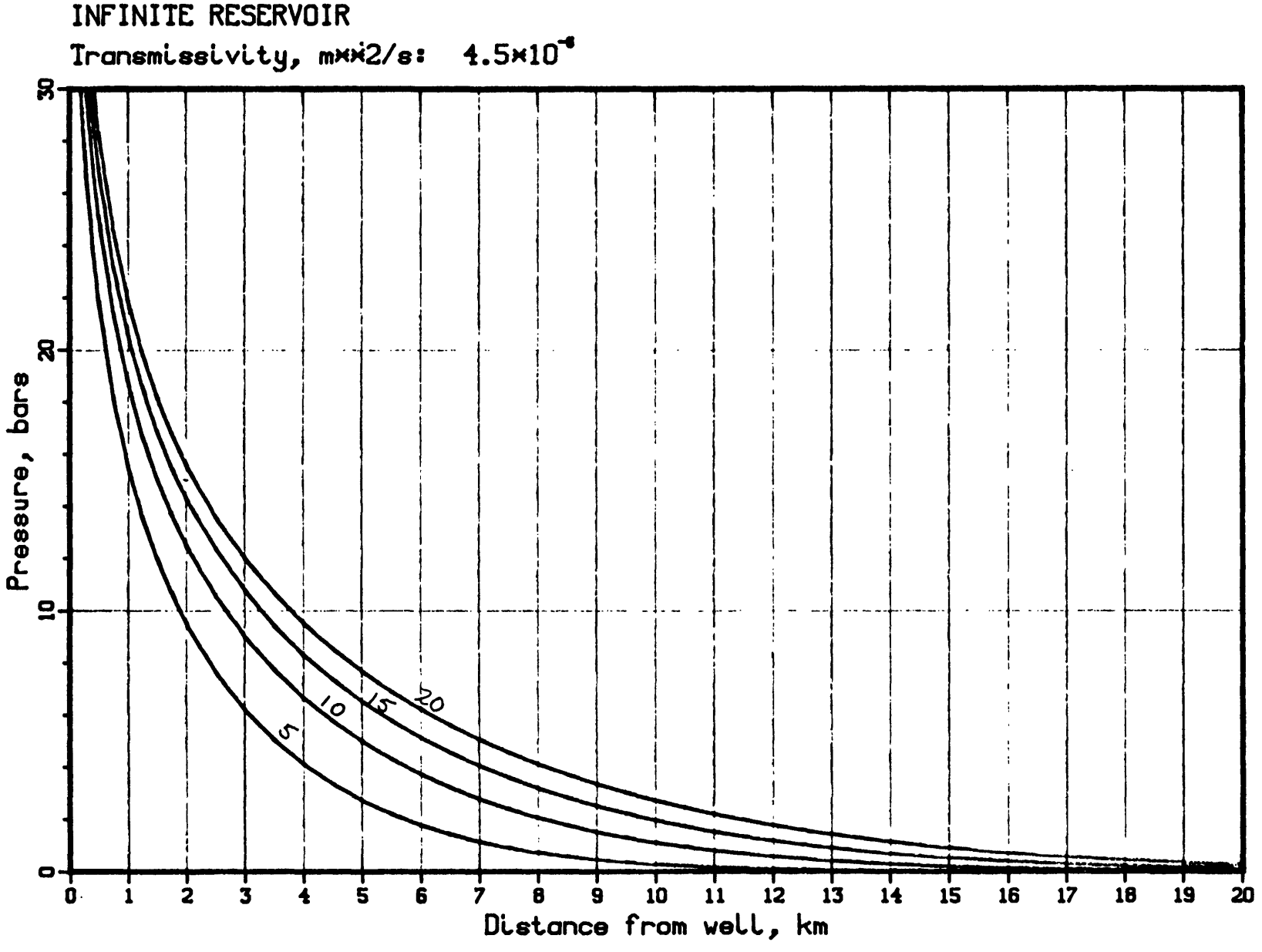
INFINITE RESERVOIR
Transmissivity, m**2/s: 4.5*10**-4
Pressure, bars
0
10
20
30
0 1 2 3 4 5 6 7 8 9 10 11 12 13 14 15 16 17 18 19 20
Distance from well, km
5
10
15
20

Figure 23

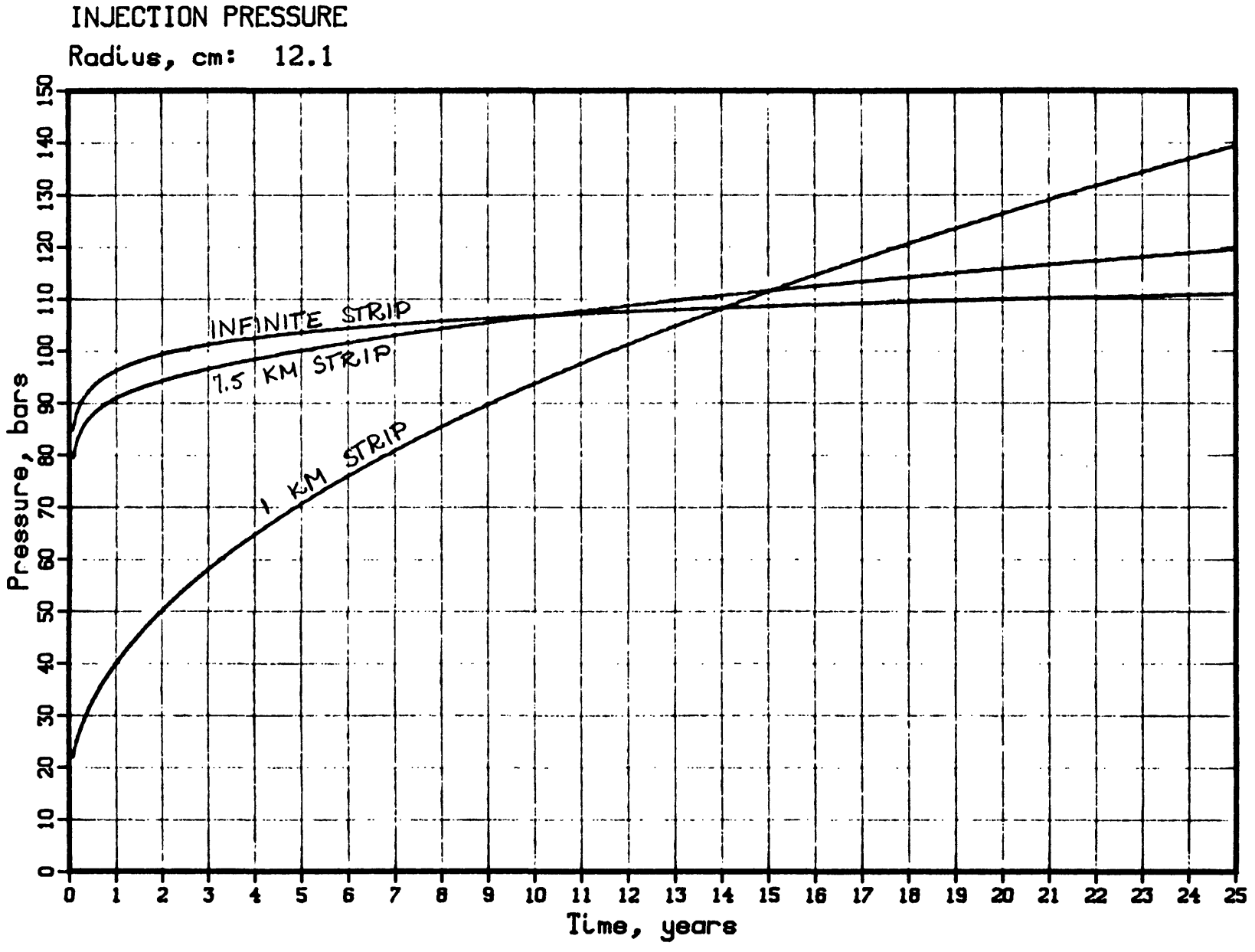
INJECTION PRESSURE
Radius, cm: 12.1
INFINITE STRIP
7.5 KM STRIP
1 KM STRIP
Pressure, bars
Time, years
0
10
20
30
40
50
60
70
80
90
100
110
120
130
140
150
0 1 2 3 4 5 6 7 8 9 10 11 12 13 14 15 16 17 18 19 20 21 22 23 24 25

Figure 24

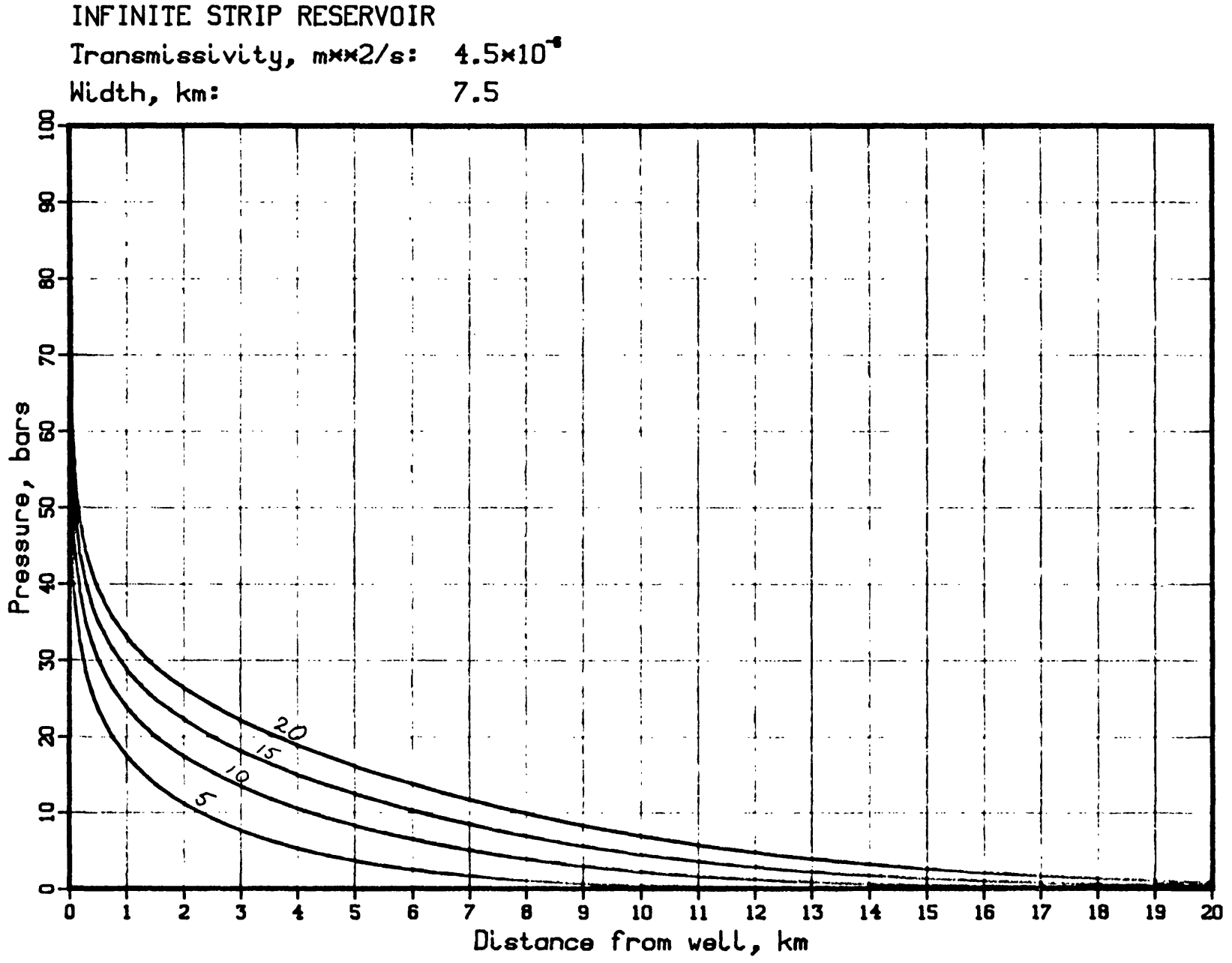
INFINITE STRIP RESERVOIR
Transmissivity, m**2/s: 4.5*10**-6
Width, km: 7.5
Pressure, bars
Distance from well, km
20
15
10
5

Figure 25

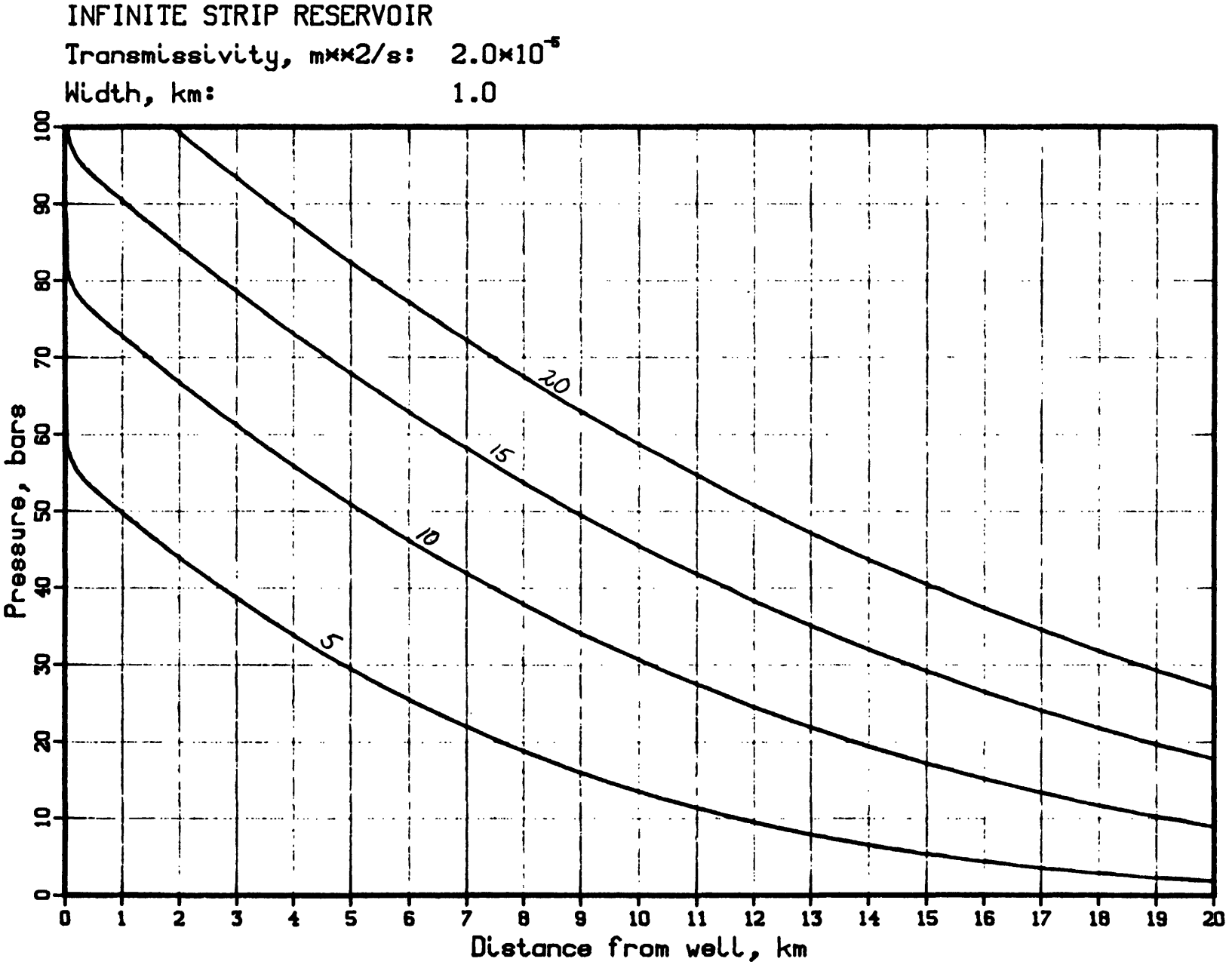
INFINITE STRIP RESERVOIR
Transmissivity, m**2/s: 2.0*10**-5
Width, km: 1.0
Pressure, bars
Distance from well, km
0
10
20
30
40
50
60
70
80
90
100
0
1
2
3
4
5
6
7
8
9
10
11
12
13
14
15
16
17
18
19
20
20
15
10
5

Figure 26

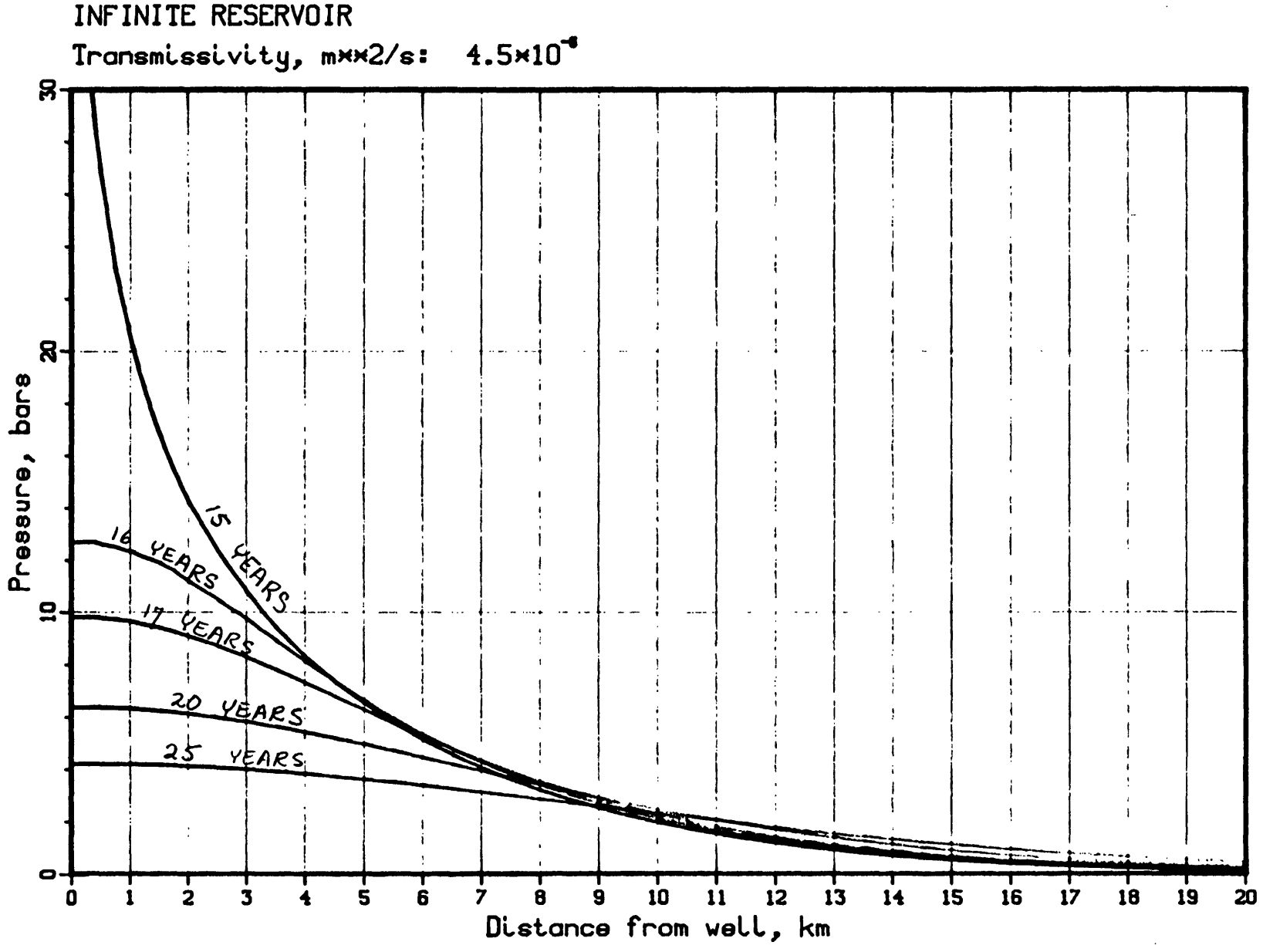
INFINITE RESERVOIR
Transmissivity, m**2/s: 4.5*10**-6
Pressure, bars
Distance from well, km
15 YEARS
16 YEARS
17 YEARS
20 YEARS
25 YEARS
0
10
20
30
0 1 2 3 4 5 6 7 8 9 10 11 12 13 14 15 16 17 18 19 20

Figure 27 A

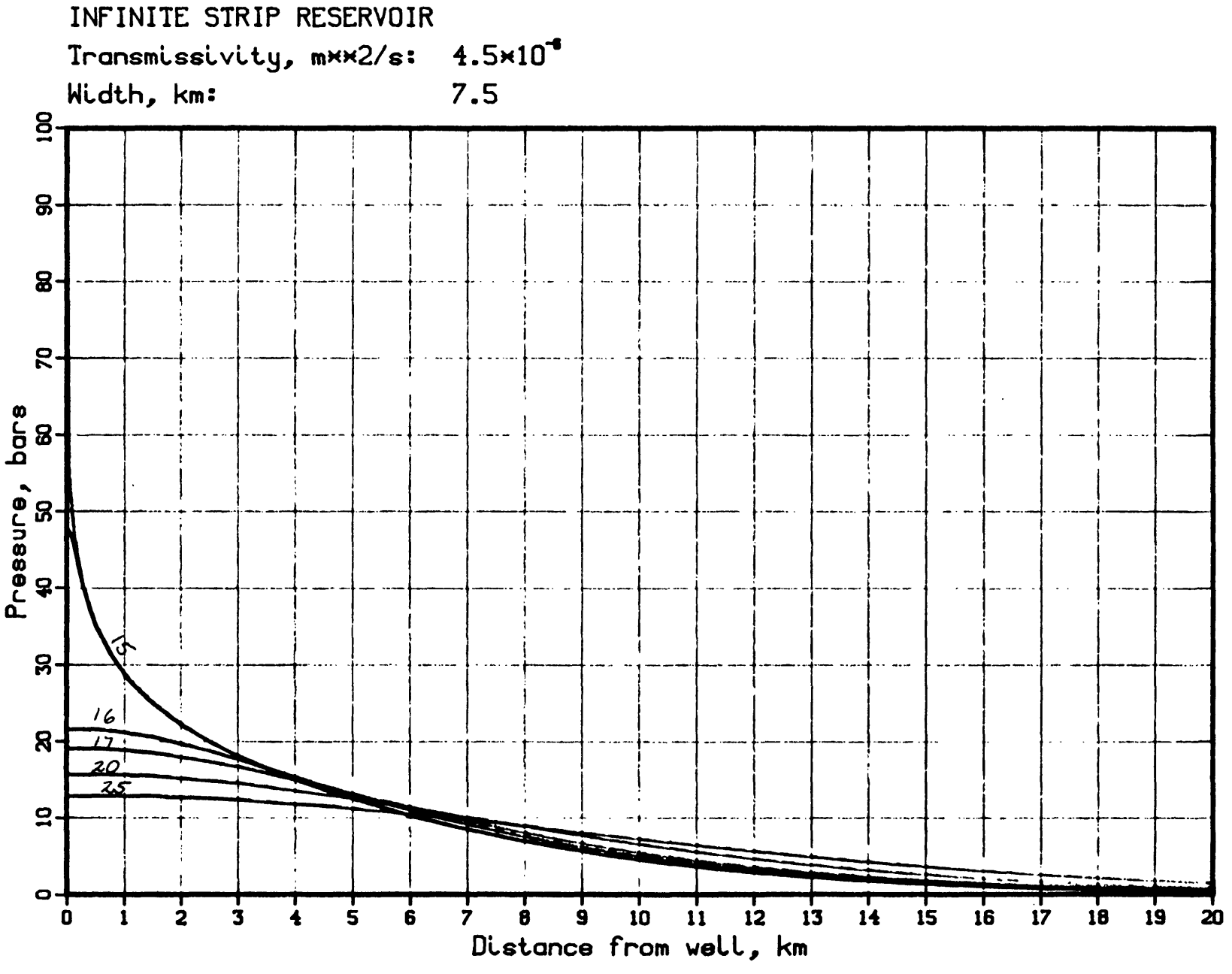
INFINITE STRIP RESERVOIR
Transmissivity, m**2/s: 4.5*10**-6
Width, km: 7.5
Pressure, bars
Distance from well, km
15
16
17
20
25

Figure 27 B

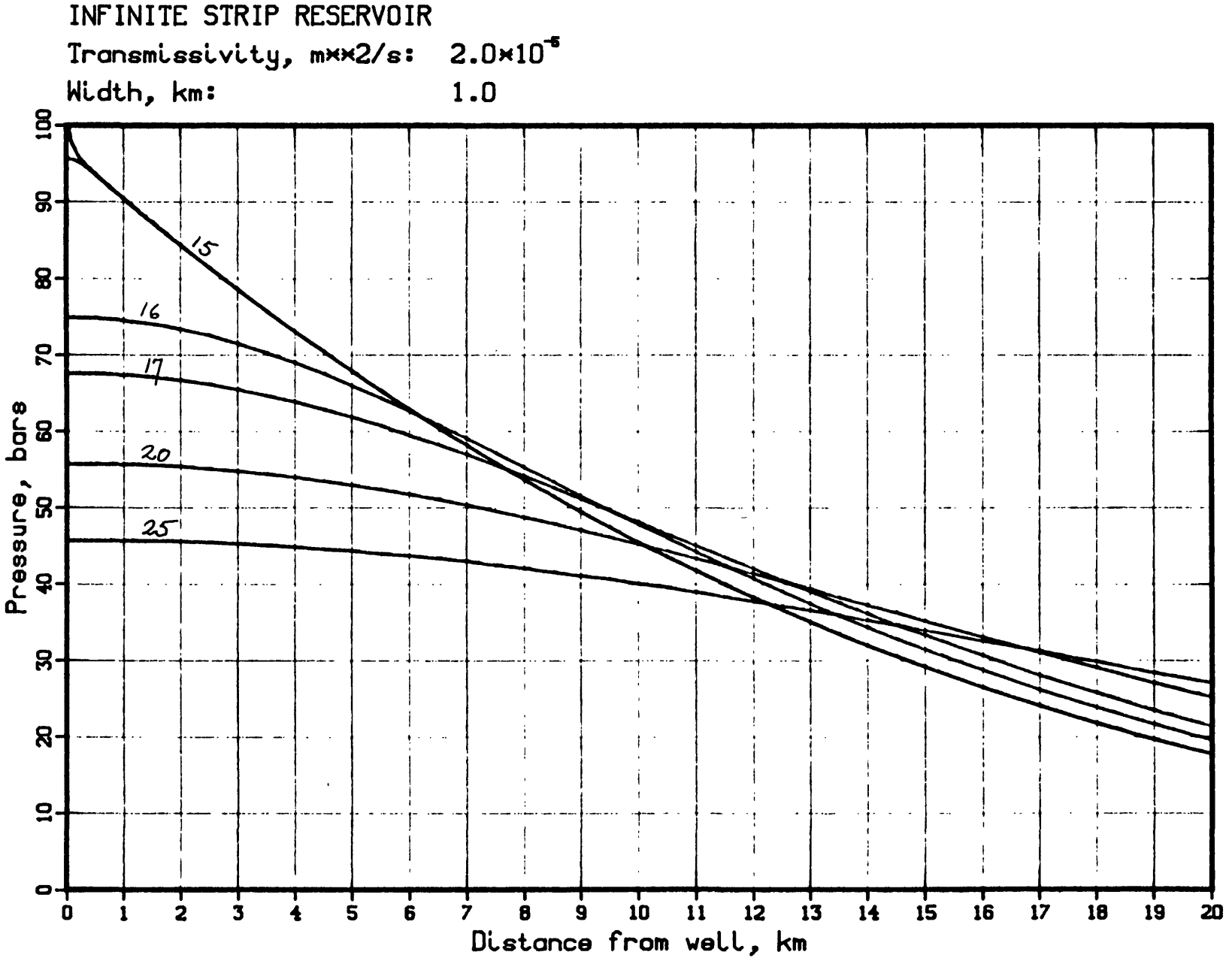
INFINITE STRIP RESERVOIR
Transmissivity, m**2/s: 2.0x10**-5
Width, km: 1.0
Pressure, bars
Distance from well, km
15
16
17
20
25
0
10
20
30
40
50
60
70
80
90
100
0
1
2
3
4
5
6
7
8
9
10
11
12
13
14
15
16
17
18
19
20

Figure 27 C

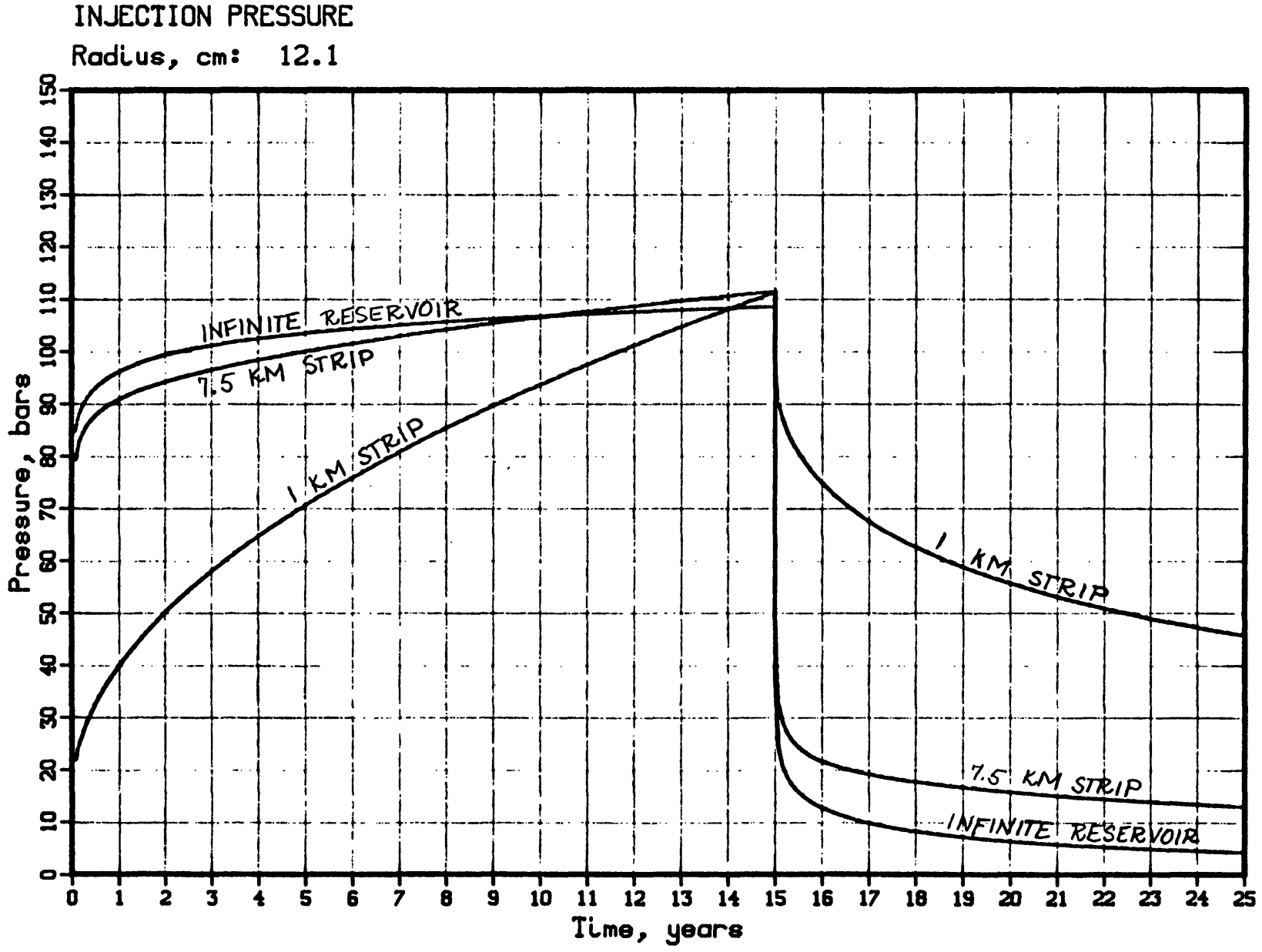
INJECTION PRESSURE
Radius, cm: 12.1
Pressure, bars
Time, years
INFINITE RESERVOIR
7.5 KM STRIP
1 KM STRIP
1 KM STRIP
7.5 KM STRIP
INFINITE RESERVOIR

Figure 28

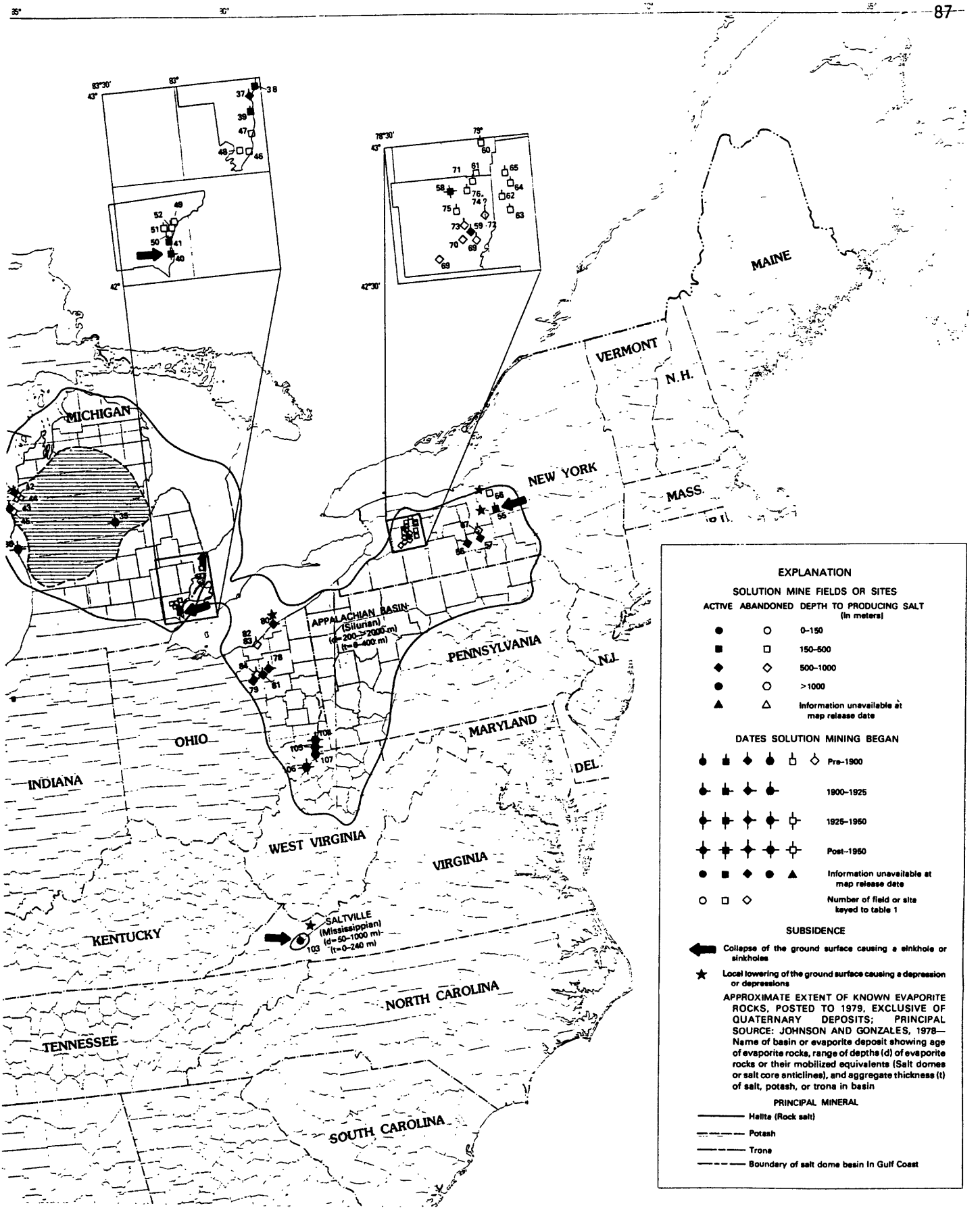
MAINE
VERMONT
N.H.
MASS.
NEW YORK
MICHIGAN
PENNSYLVANIA
N.J.
MARYLAND
DEL.
OHIO
INDIANA
WEST VIRGINIA
VIRGINIA
KENTUCKY
TENNESSEE
NORTH CAROLINA
SOUTH CAROLINA
APPALACHIAN BASIN
(Silurian)
(d=200->2000 m)
(t=0-400 m)
SALTVILLE
(Mississippian)
(d=50-1000 m)
(t=0-240 m)
EXPLANATION
SOLUTION MINE FIELDS OR SITES
ACTIVE ABANDONED DEPTH TO PRODUCING SALT (in meters)
0-150
150-500
500-1000
>1000
Information unavailable at map release date
DATES SOLUTION MINING BEGAN
Pre-1900
1900-1925
1925-1950
Post-1950
Information unavailable at map release date
Number of field or site keyed to table 1
SUBSIDENCE
Collapse of the ground surface causing a sinkhole or sinkholes
Local lowering of the ground surface causing a depression or depressions
APPROXIMATE EXTENT OF KNOWN EVAPORITE ROCKS, POSTED TO 1979, EXCLUSIVE OF QUATERNARY DEPOSITS; PRINCIPAL SOURCE: JOHNSON AND GONZALES, 1978—Name of basin or evaporite deposit showing age of evaporite rocks, range of depths (d) of evaporite rocks or their mobilized equivalents (Salt domes or salt core anticlines), and aggregate thickness (t) of salt, potash, or trona in basin
PRINCIPAL MINERAL
Halite (Rock salt)
Potash
Trona
Boundary of salt dome basin in Gulf Coast

Figure 29 B

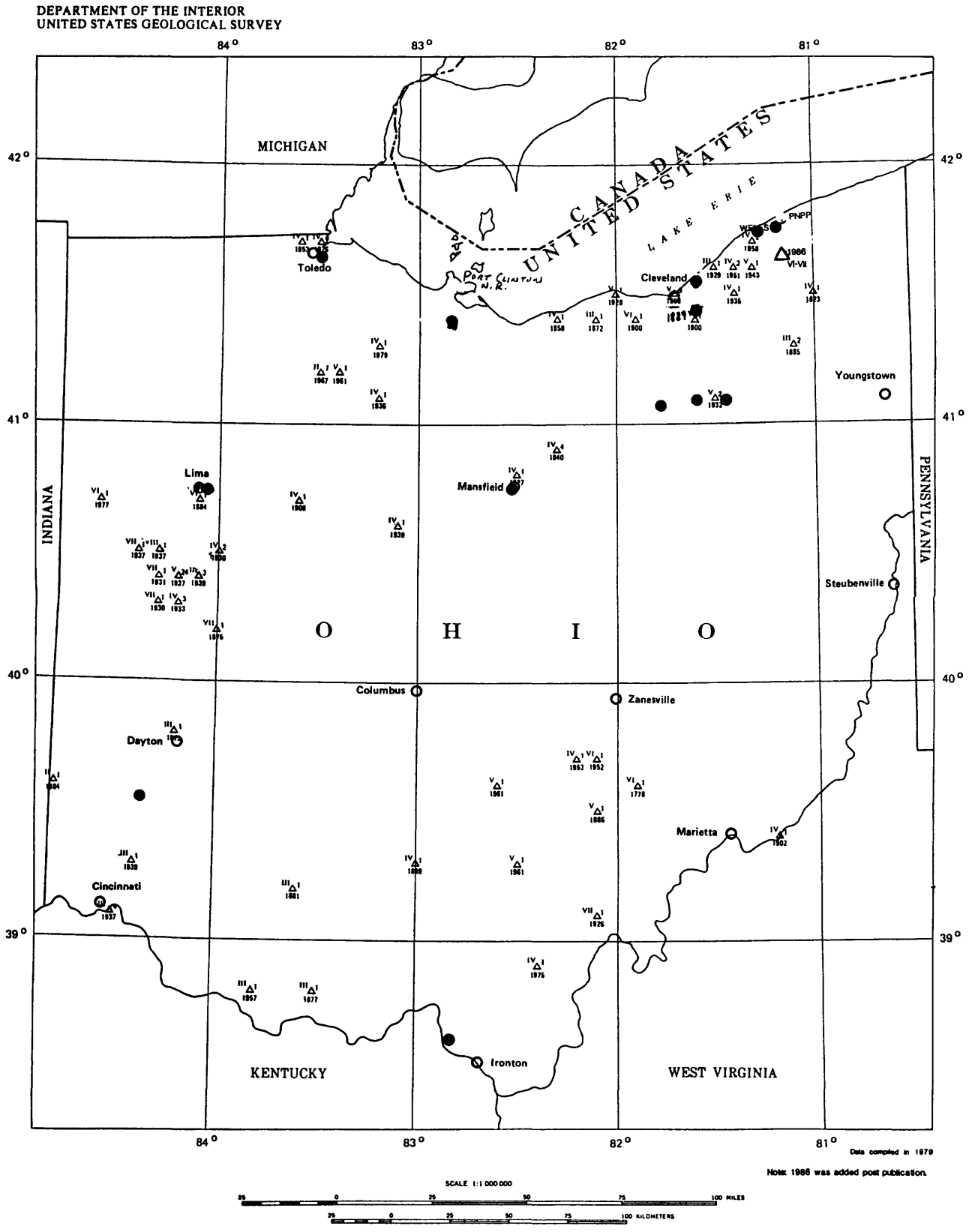

SEISMICITY MAP OF THE STATE OF OHIO

By

C. W. Stover, B. G. Reagor, and S. T. Algermissen

1979

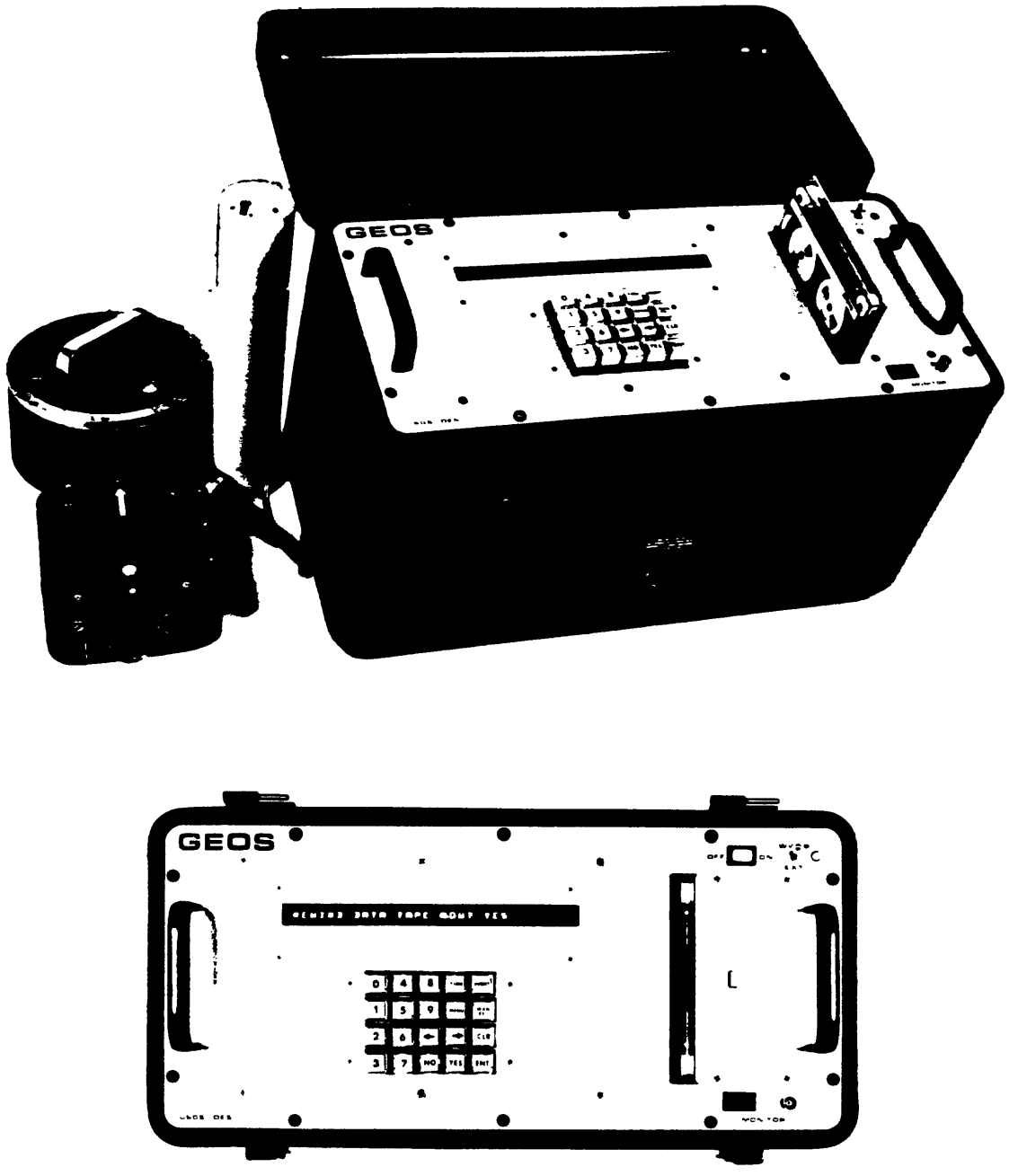

Figure 1. Side and front panel view of the General Earthquake Observation System (GEOS) together with a WWVB antenna and two sets of three-component sensors commonly used to provide more than 180 dB of linear, dynamic range. System operation for routine applications requires only initiation of power. Full capability to reconfigure system in the field is facilitated by simple operator response to english language prompts via keyboard.

Figure 30

Figure 31

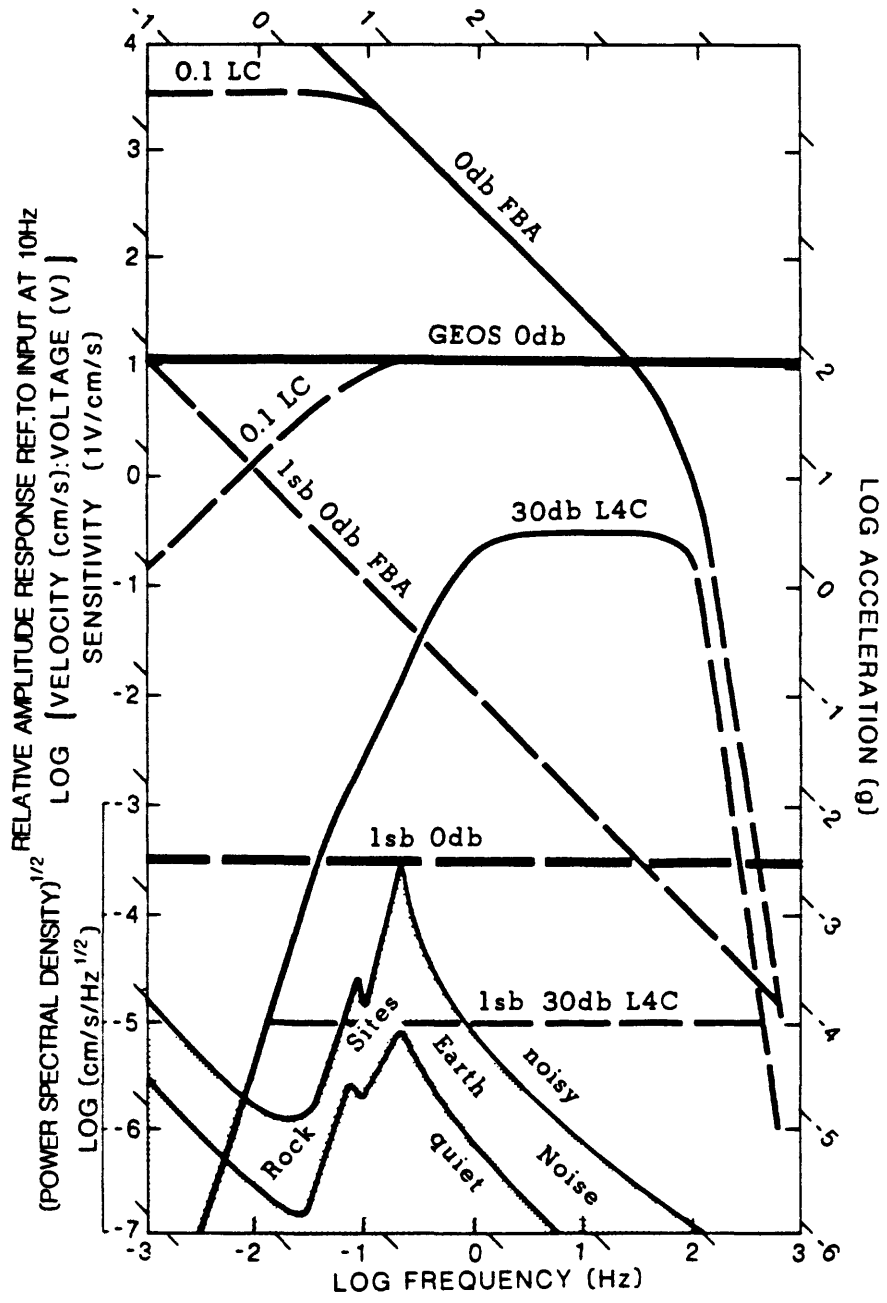

The unit-impulse response designed for the GEOS recorder, spectra for Earth noise (Aki and Richards, 1980), and complete system response with two types of sensors (force-balance accelerometer at 0 dB gain and L4–C velocity transducer at 30 dB gain). Two sets of sensors and linear dynamic range of 96 dB (16-bit) offers the capability to record without gain change 10 Hz signals on scale with amplitudes ranging from 20 angstroms in displacements to 2 g in acceleration.

Figure 32

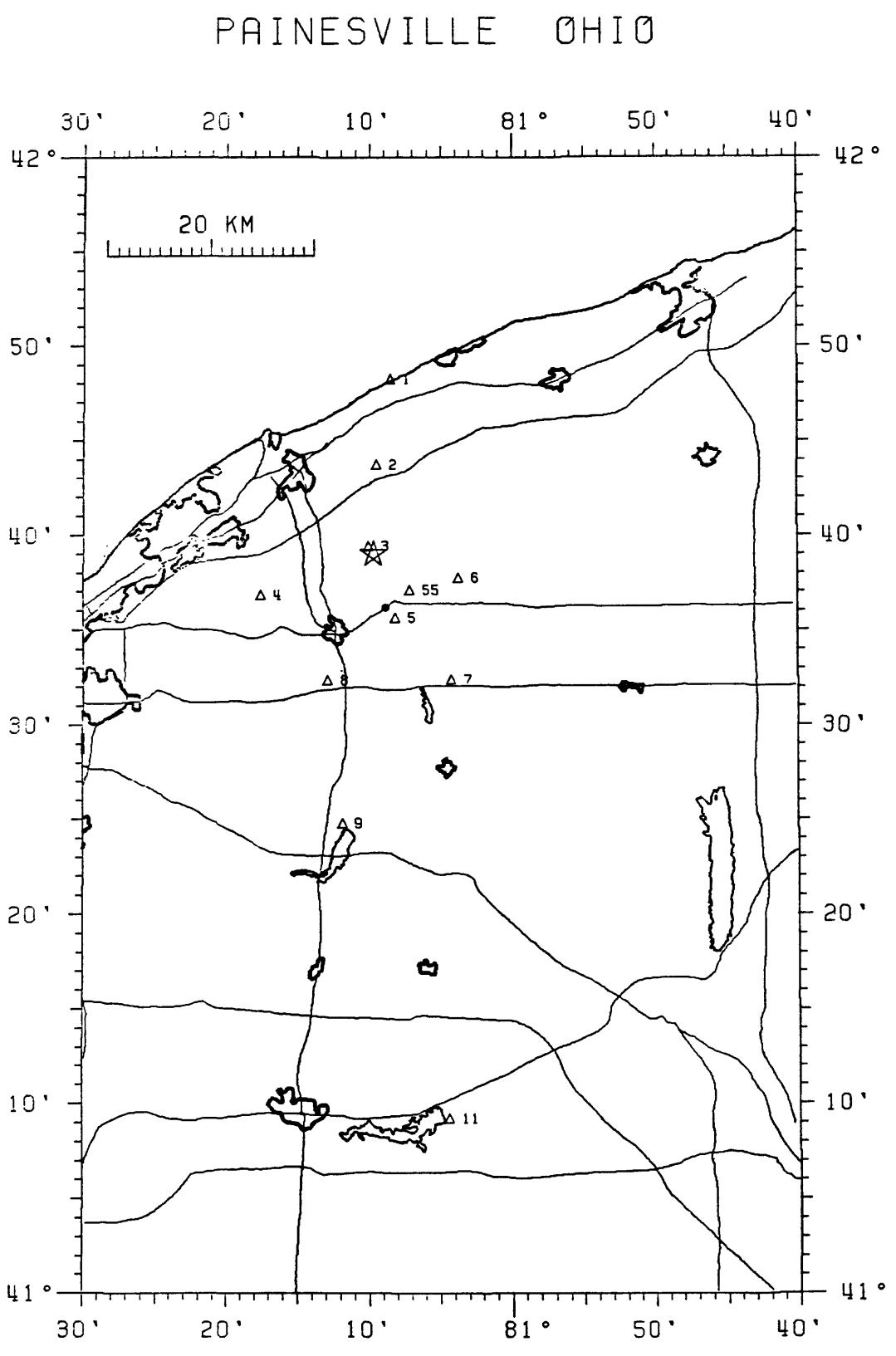

Locations of sites occupied by GEOS recorders and location of main shock on January 31, 1986 (J. Dewey, pers. comm., 1986). Major highways, city and community boundaries, and lake boundaries also are shown.

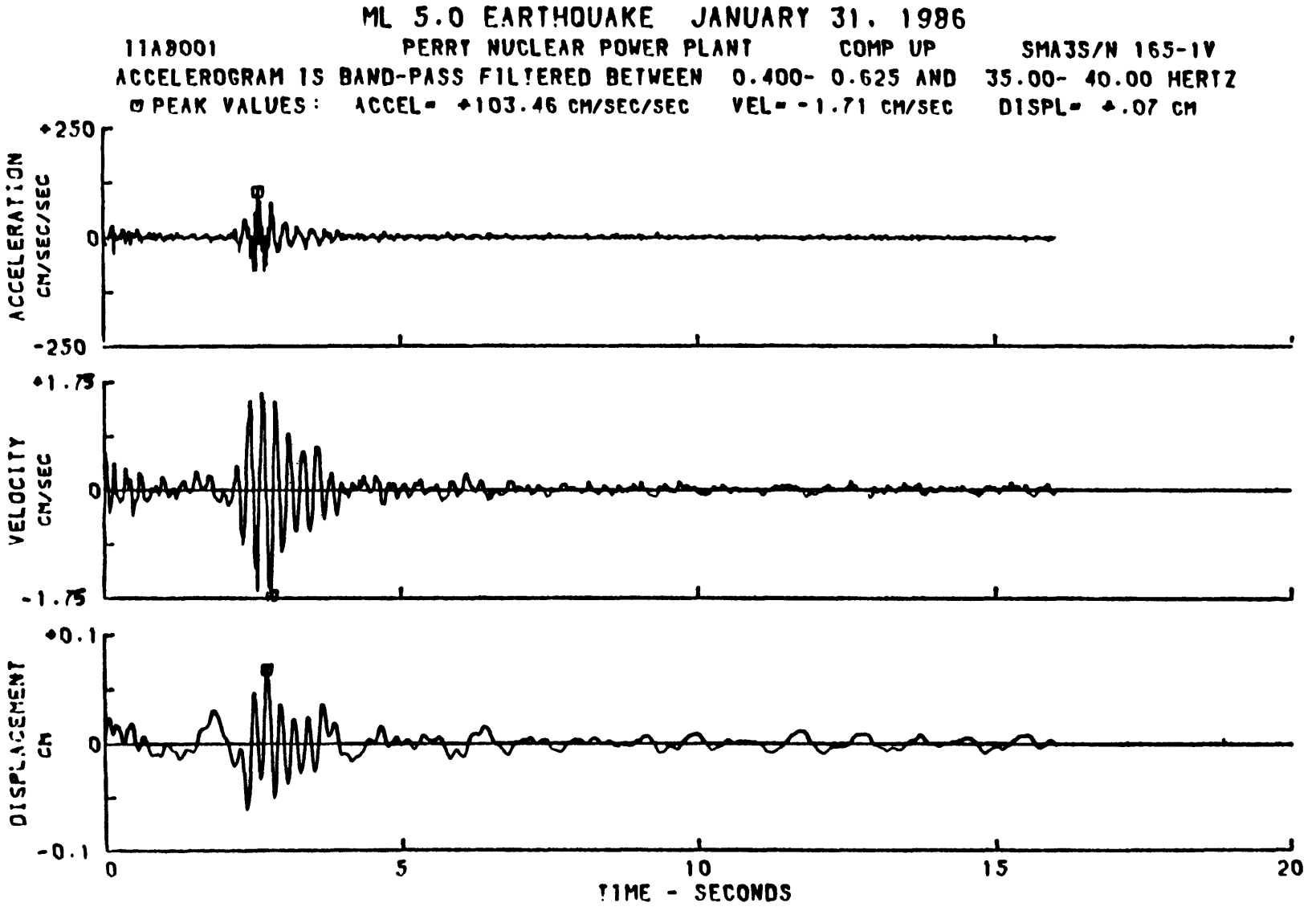
ML 5.0 EARTHQUAKE JANUARY 31, 1986
11A8001 PERRY NUCLEAR POWER PLANT COMP UP SMA3S/N 165-1V
ACCELEROGRAM IS BAND-PASS FILTERED BETWEEN 0.400- 0.625 AND 35.00- 40.00 HERTZ
PEAK VALUES: ACCEL= +103.46 CM/SEC/SEC VEL= -1.71 CM/SEC DISPL= +.07 CM
ACCELERATION CM/SEC/SEC
+250
0
-250
VELOCITY CM/SEC
+1.75
0
-1.75
DISPLACEMENT CM
+0.1
0
-0.1
0
5
10
15
20
TIME - SECONDS

Figure 33 A

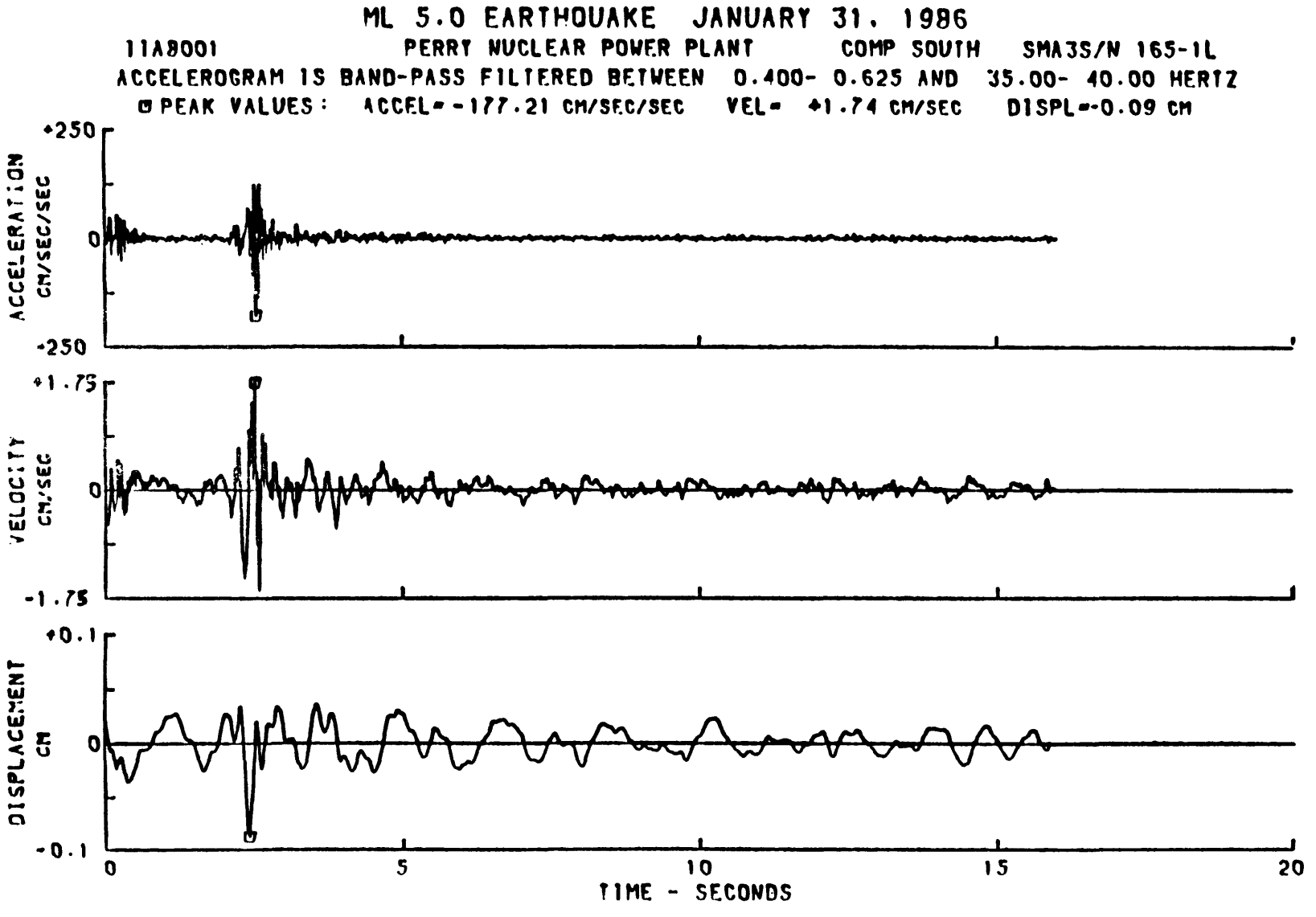
ML 5.0 EARTHQUAKE JANUARY 31, 1986
11A8001 PERRY NUCLEAR POWER PLANT COMP SOUTH SMA3S/N 165-1L
ACCELEROGRAM IS BAND-PASS FILTERED BETWEEN 0.400- 0.625 AND 35.00- 40.00 HERTZ
PEAK VALUES: ACCEL=-177.21 CM/SEC/SEC VEL= +1.74 CM/SEC DISPL=-0.09 CM
ACCELERATION CM/SEC/SEC
+250
0
-250
VELOCITY CM/SEC
+1.75
0
-1.75
DISPLACEMENT CM
+0.1
0
-0.1
0
5
10
15
20
TIME - SECONDS

Figure 33 B

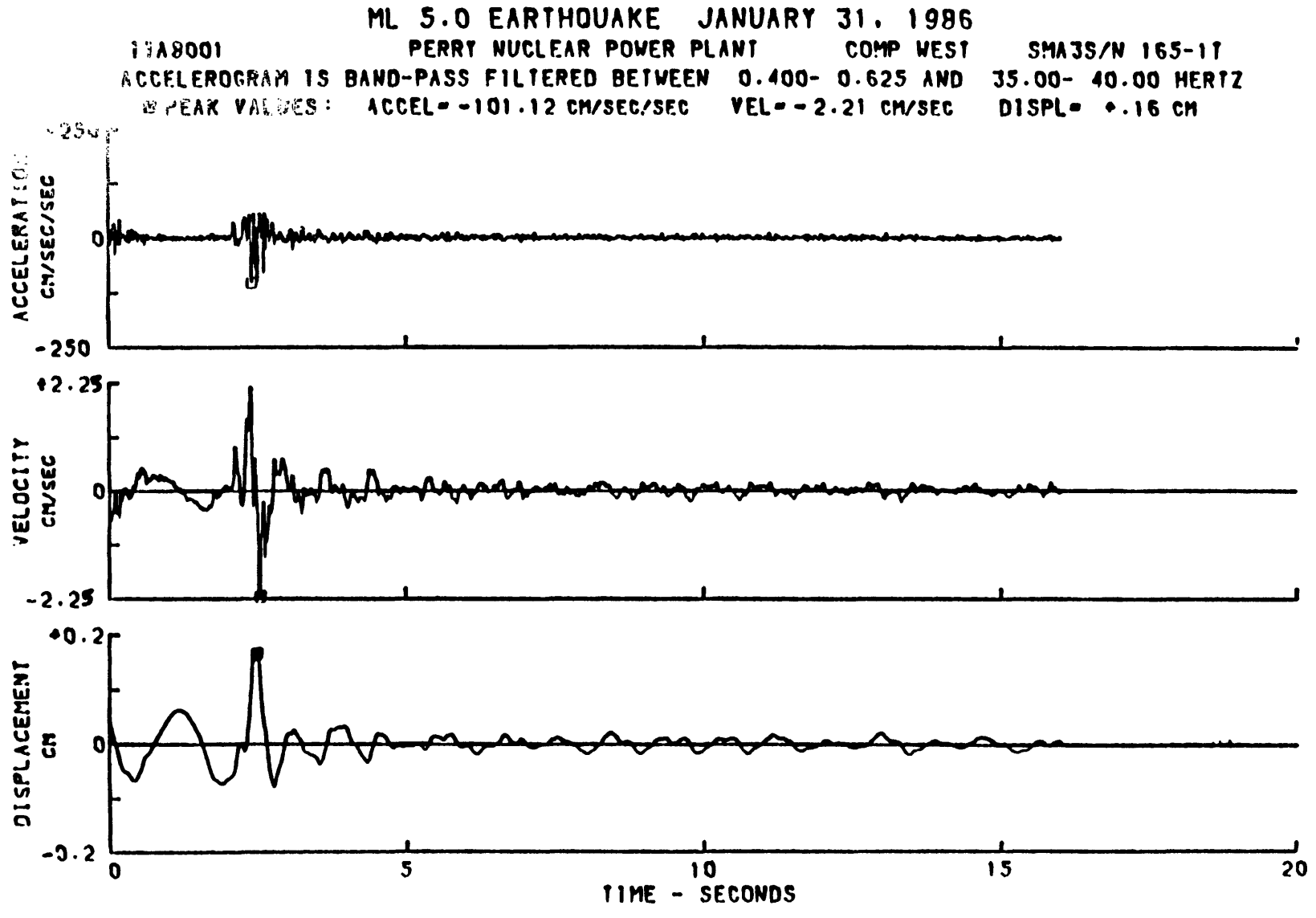
ML 5.0 EARTHQUAKE JANUARY 31, 1986
PERRY NUCLEAR POWER PLANT
COMP WEST
SMA3S/N 165-11
ACCELEROGRAM IS BAND-PASS FILTERED BETWEEN 0.400- 0.625 AND 35.00- 40.00 HERTZ
PEAK VALUES: ACCEL= -101.12 CM/SEC/SEC VEL= -2.21 CM/SEC DISPL= +.16 CM
ACCELERATION CM/SEC/SEC
+250
0
-250
VELOCITY CM/SEC
+2.25
0
-2.25
DISPLACEMENT CM
+0.2
0
-0.2
0
5
10
15
20
TIME - SECONDS

Figure 33 C

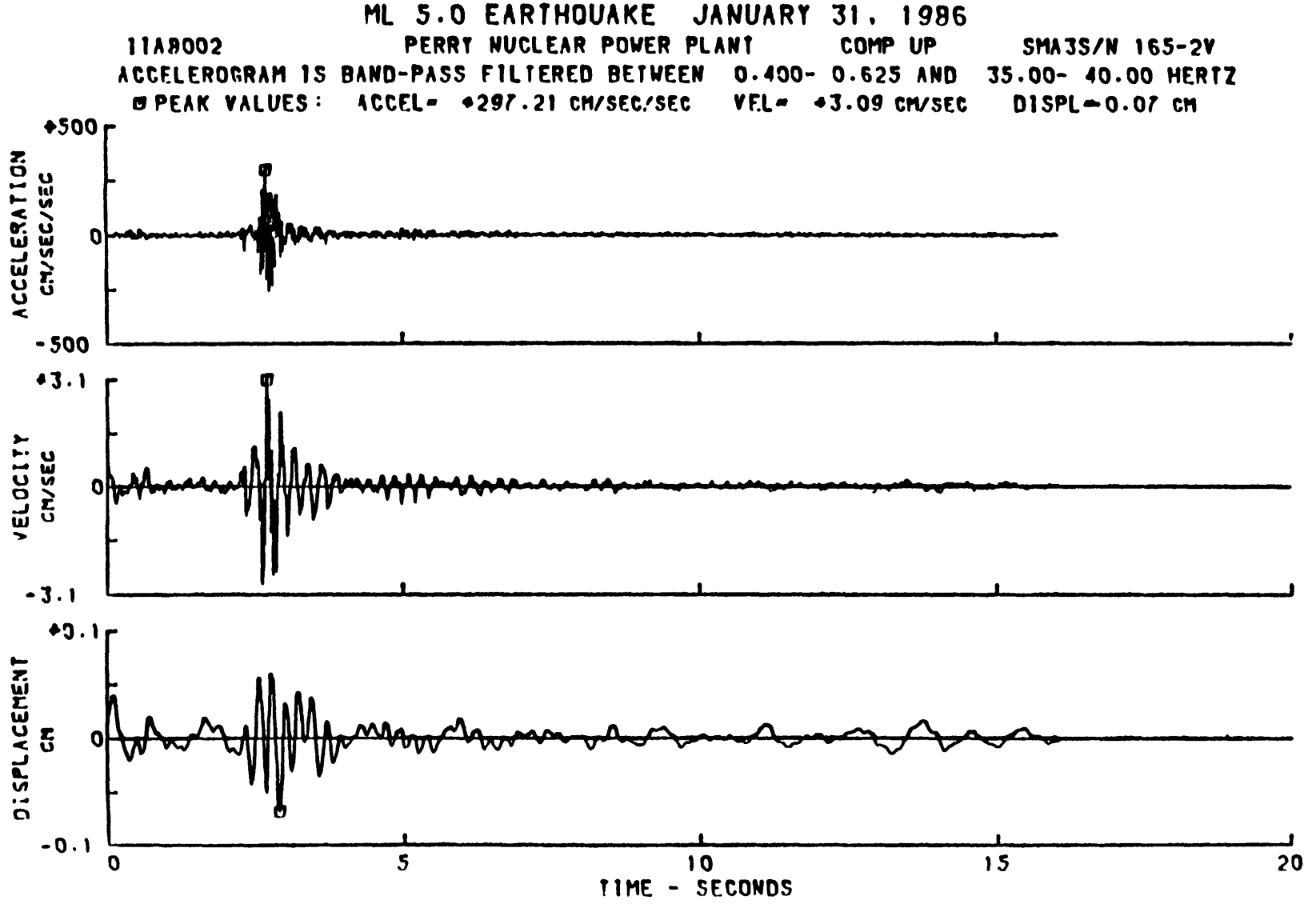
ML 5.0 EARTHQUAKE JANUARY 31, 1986
11A8002 PERRY NUCLEAR POWER PLANT COMP UP SMA3S/N 165-2V
ACCELEROGRAM IS BAND-PASS FILTERED BETWEEN 0.400- 0.625 AND 35.00- 40.00 HERTZ
PEAK VALUES: ACCEL= ±297.21 CM/SEC/SEC VEL= ±3.09 CM/SEC DISPL=0.07 CM
ACCELERATION CM/SEC/SEC
+500
0
-500
VELOCITY CM/SEC
+3.1
0
-3.1
DISPLACEMENT CM
+0.1
0
-0.1
0
5
10
15
20
TIME - SECONDS

Figure 34 A

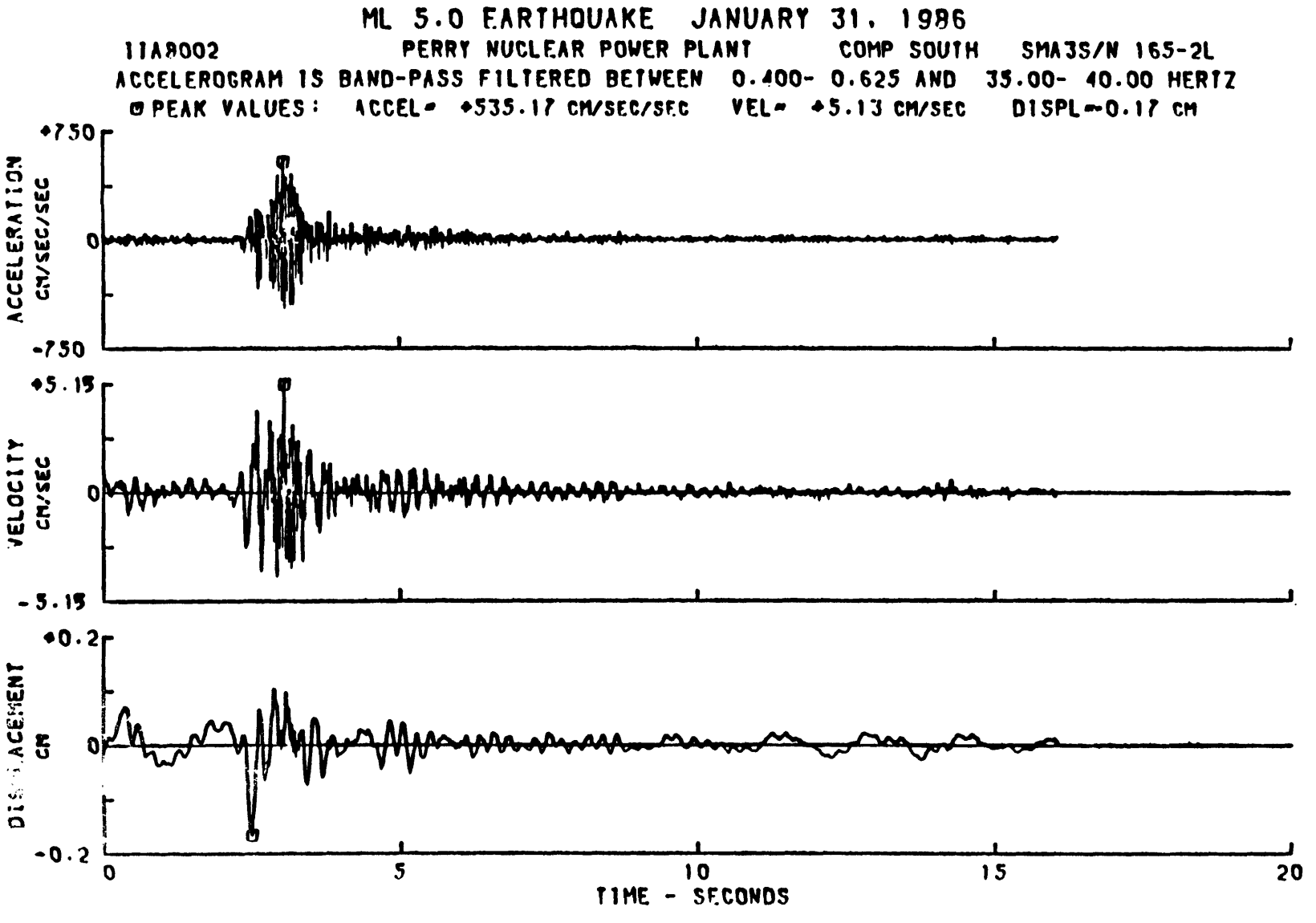
ML 5.0 EARTHQUAKE JANUARY 31, 1986
11A8002 PERRY NUCLEAR POWER PLANT COMP SOUTH SMA3S/N 165-2L
ACCELEROGRAM IS BAND-PASS FILTERED BETWEEN 0.400- 0.625 AND 35.00- 40.00 HERTZ
@PEAK VALUES: ACCEL= +535.17 CM/SEC/SEC VEL= +5.13 CM/SEC DISPL=0.17 CM
+750
ACCELERATION CM/SEC/SEC
0
-750
+5.13
VELOCITY CM/SEC
0
-5.13
+0.2
DISPLACEMENT CM
0
-0.2
0
5
10
15
20
TIME - SECONDS

Figure 34 B

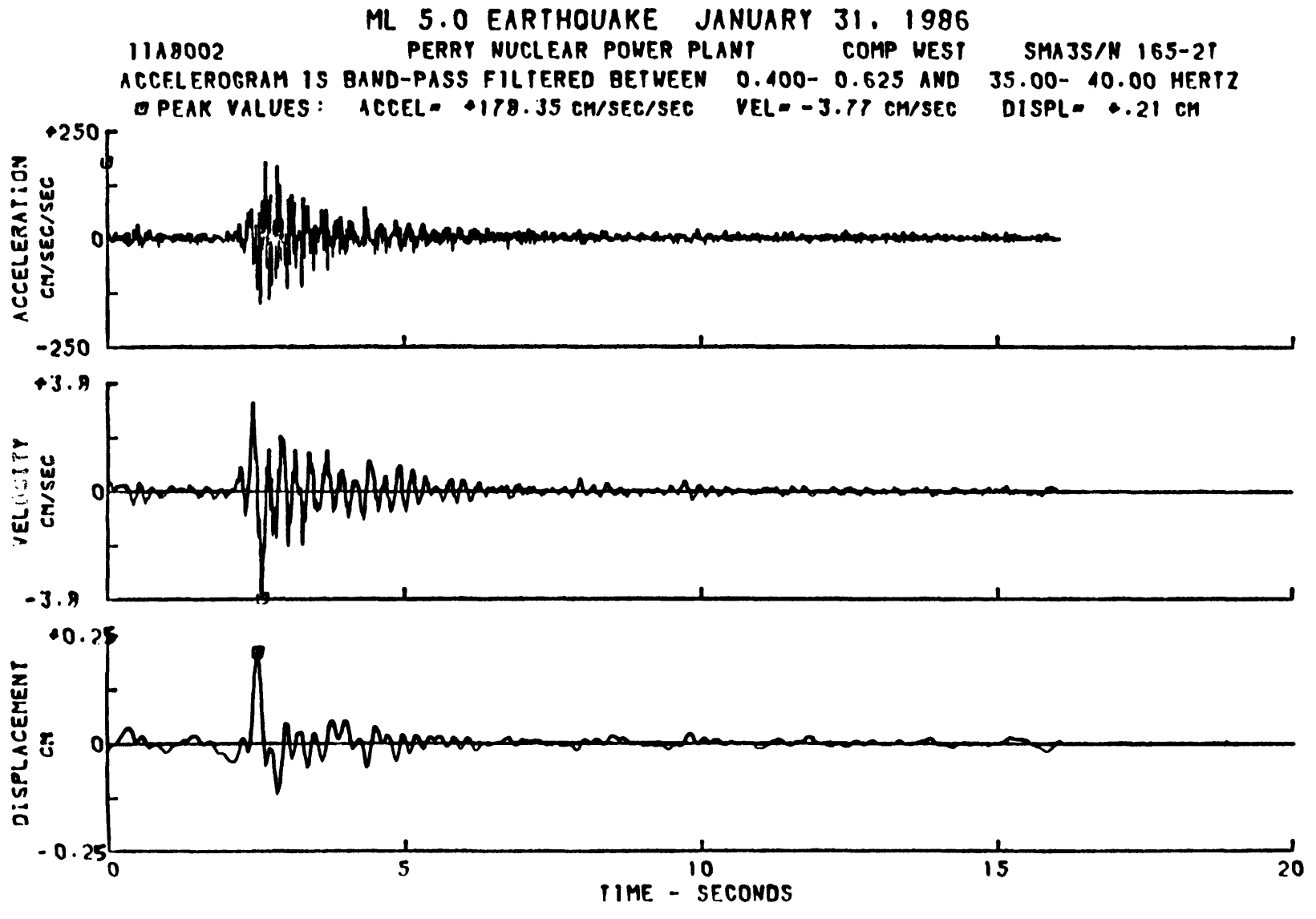
ML 5.0 EARTHQUAKE JANUARY 31, 1986
11A8002 PERRY NUCLEAR POWER PLANT COMP WEST SMA3S/N 165-21
ACCELEROGRAM IS BAND-PASS FILTERED BETWEEN 0.400- 0.625 AND 35.00- 40.00 HERTZ
@ PEAK VALUES: ACCEL= +178.35 CM/SEC/SEC VEL= -3.77 CM/SEC DISPL= +.21 CM
ACCELERATION CM/SEC/SEC
+250
0
-250
VELOCITY CM/SEC
+3.8
0
-3.8
DISPLACEMENT CM
+0.25
0
-0.25
0
5
10
15
20
TIME - SECONDS

Figure 34 C

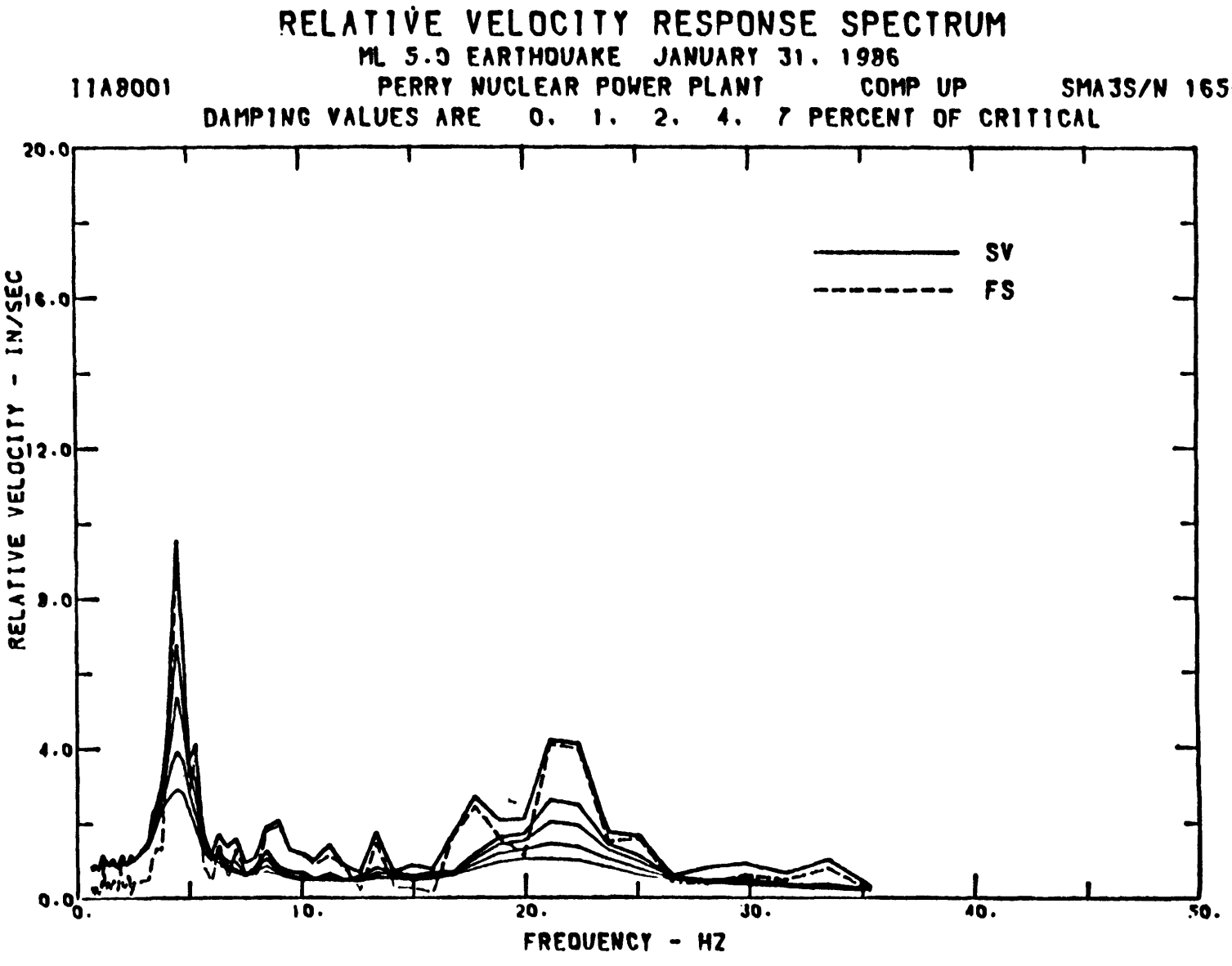

Figure 35 A

KINEMETRICS

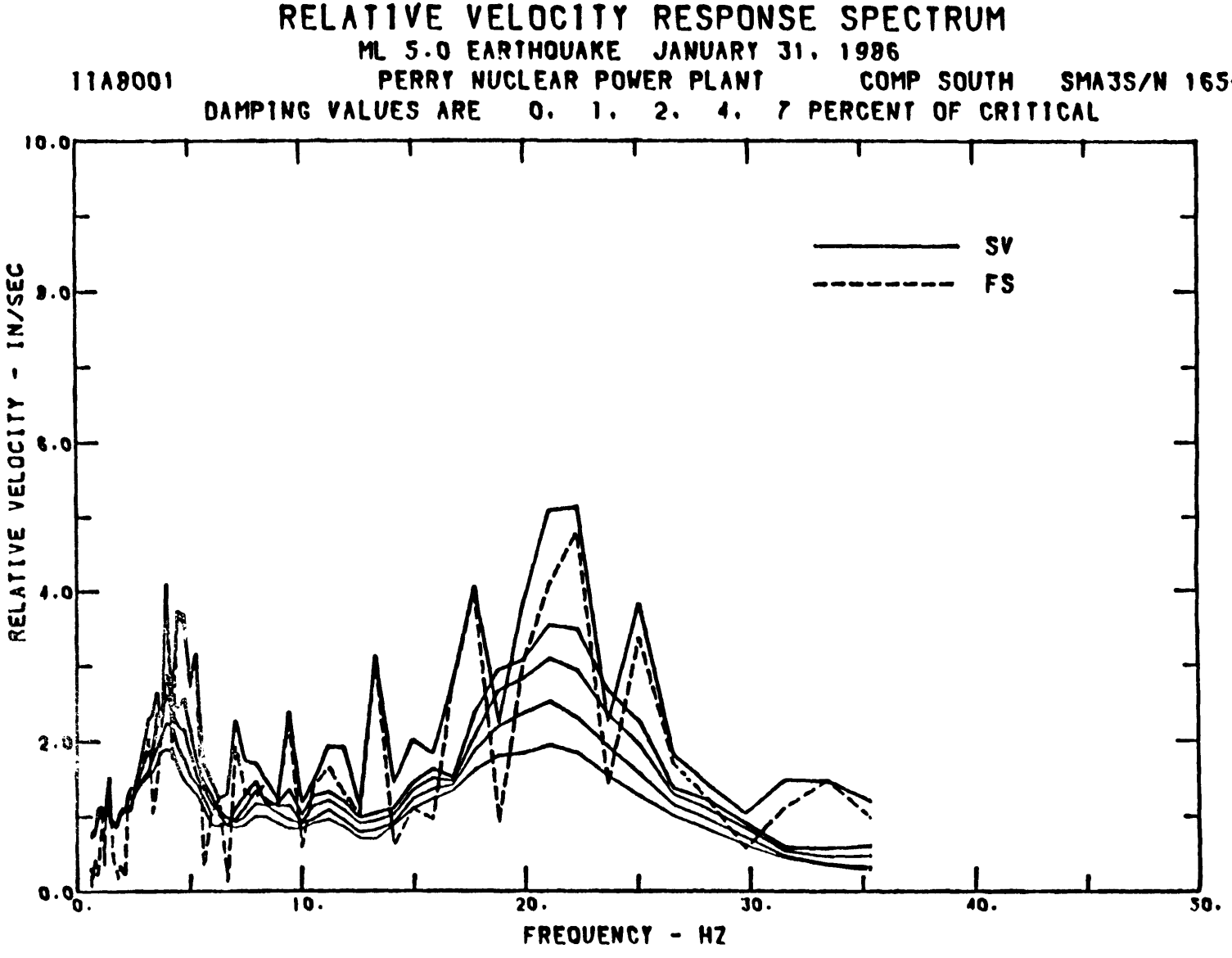

Figure 35 B

KINEMETRICS

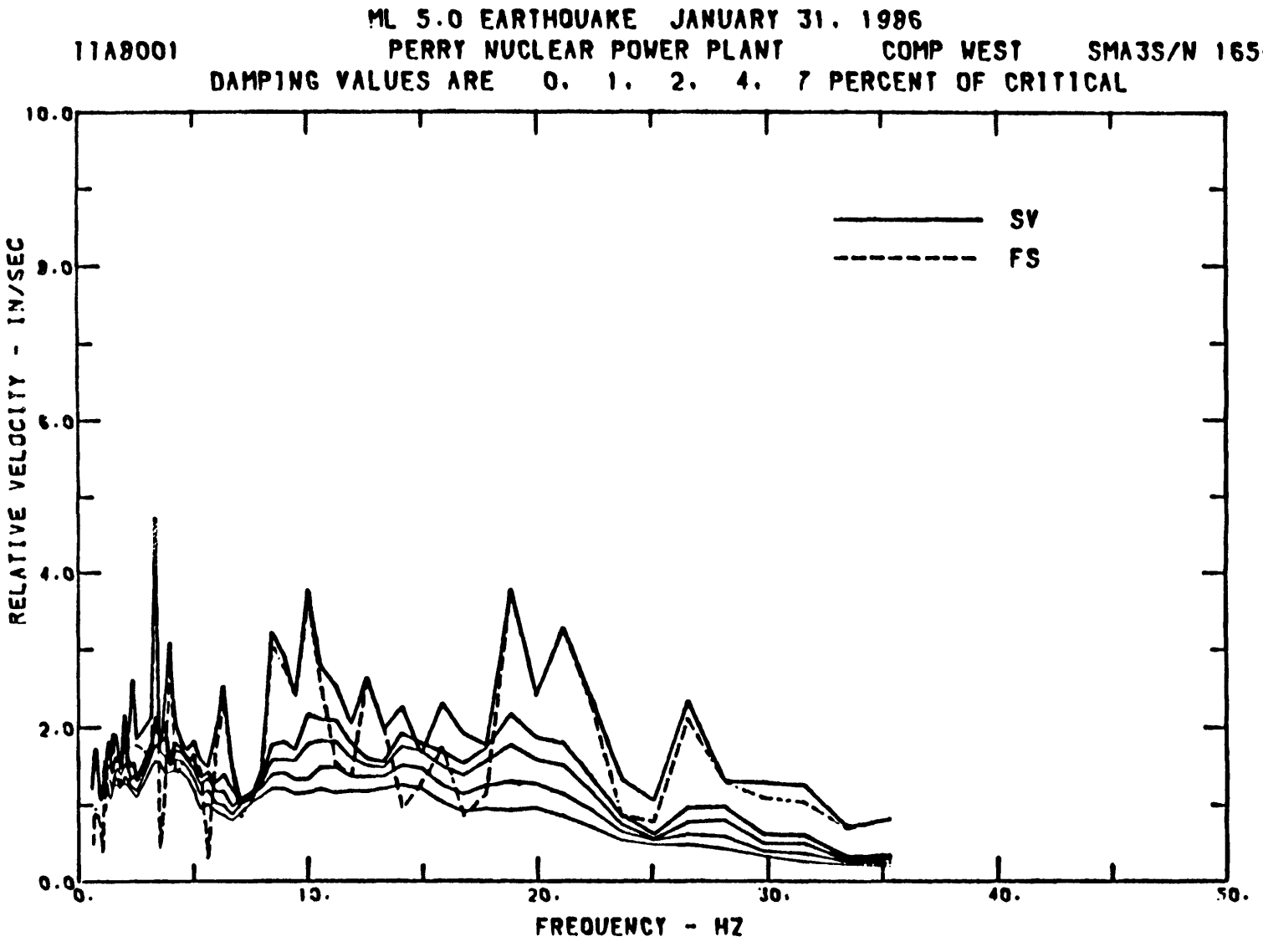

Figure 35 C

KINEMETRICS

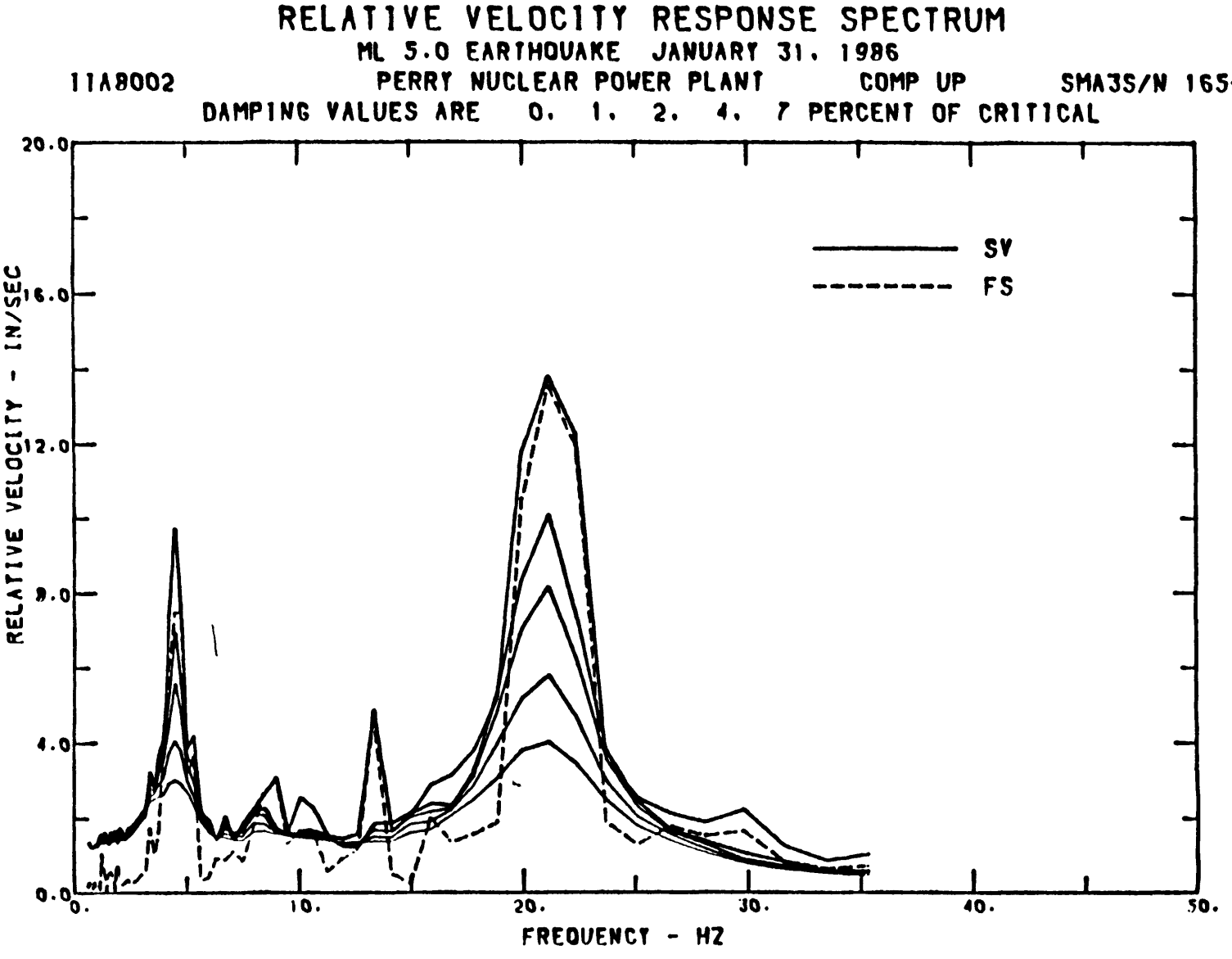

Figure 36 A

KINEMETRICS

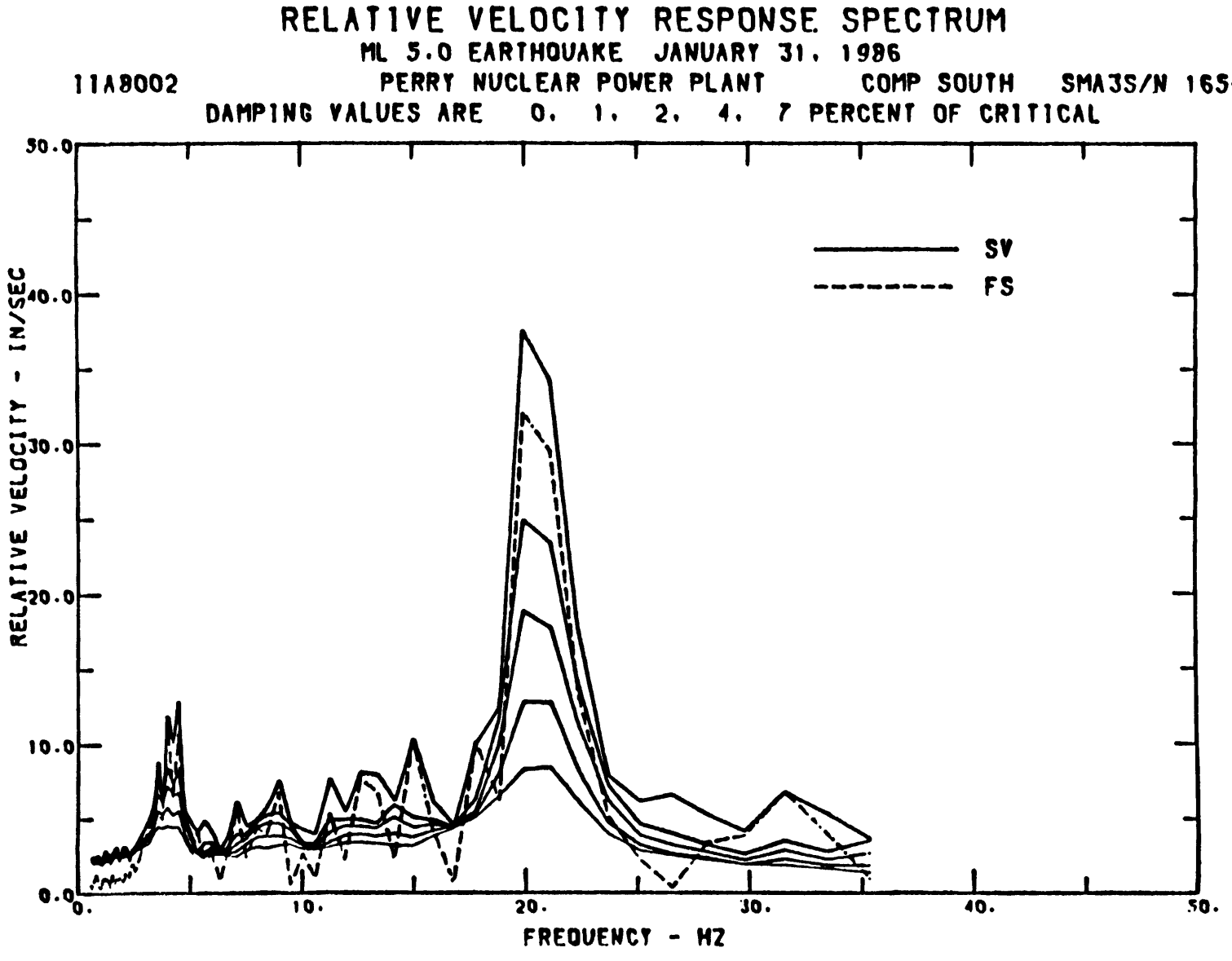

Figure 36 B

KINEMETRICS

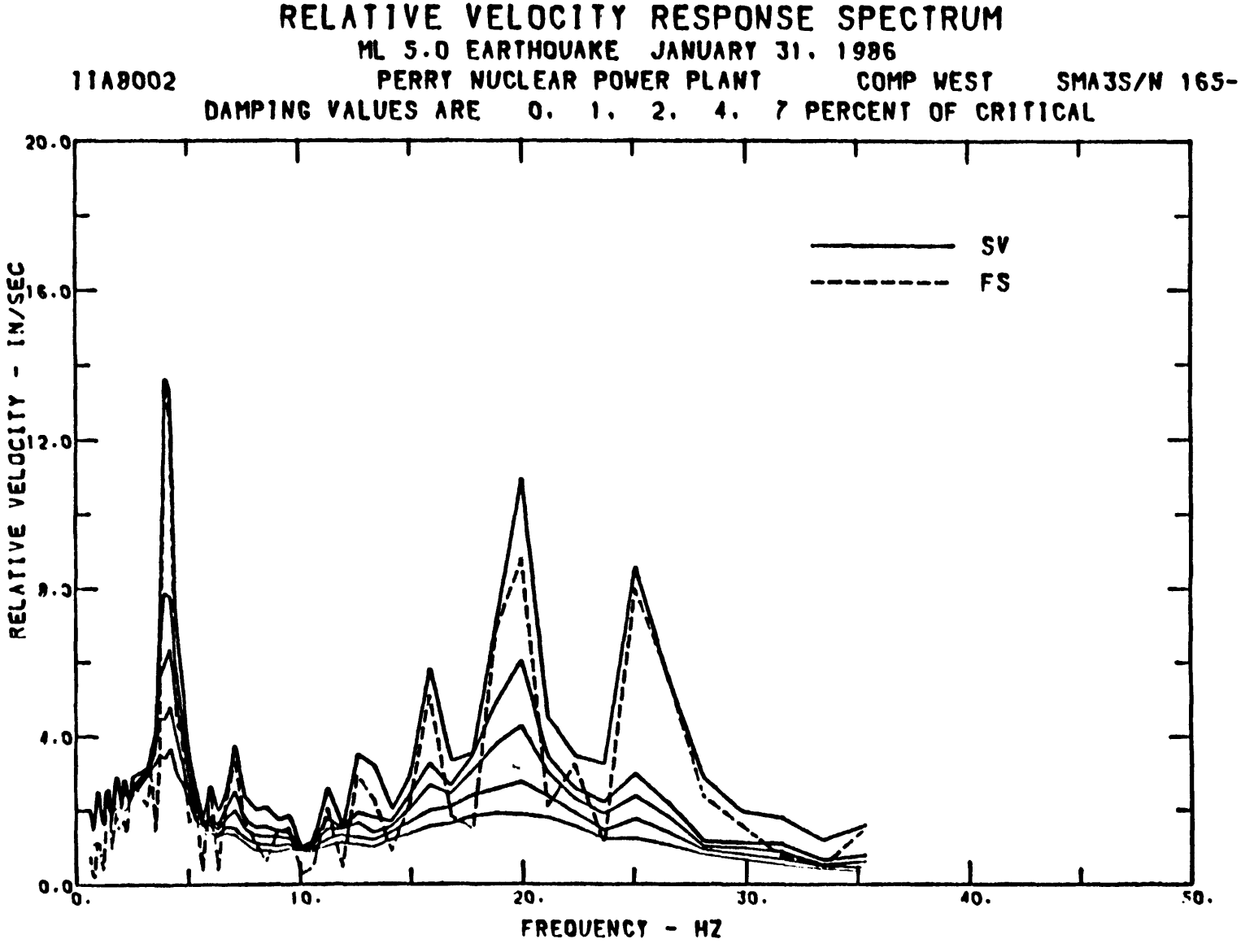
RELATIVE VELOCITY RESPONSE SPECTRUM
ML 5.0 EARTHQUAKE JANUARY 31, 1986
11A8002 PERRY NUCLEAR POWER PLANT COMP WEST SMA3S/N 165-2T
DAMPING VALUES ARE 0. 1. 2. 4. 7 PERCENT OF CRITICAL
SV
FS
RELATIVE VELOCITY - IN/SEC
FREQUENCY - HZ
20.0
16.0
12.0
8.0
4.0
0.0
0.
10.
20.
30.
40.
50.

Figure 36 C

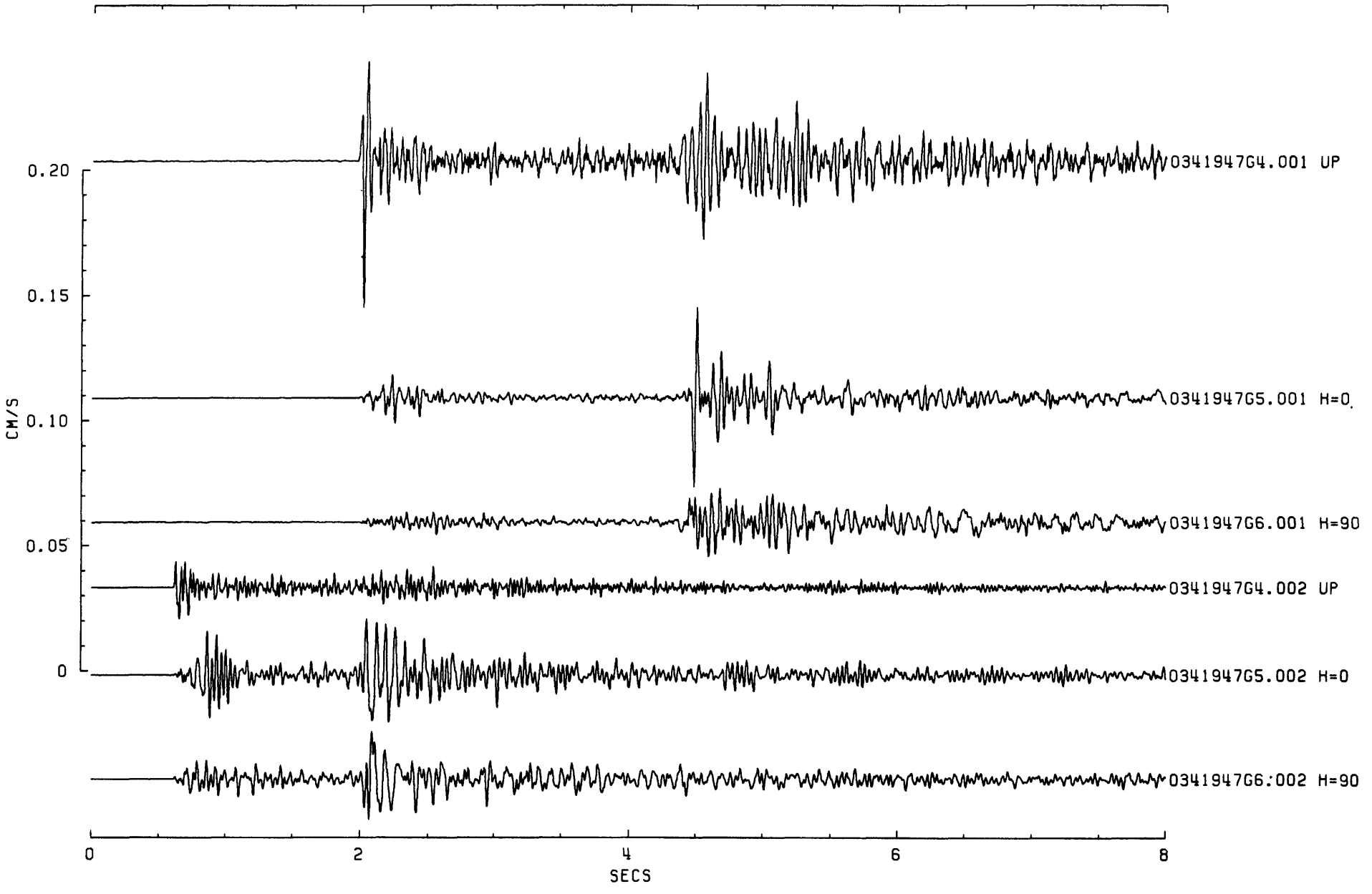
0.20
0.15
0.10
0.05
0
CM/S
0341947G4.001 UP
0341947G5.001 H=0
0341947G6.001 H=90
0341947G4.002 UP
0341947G5.002 H=0
0341947G6.002 H=90
0
2
4
6
8
SECS

Figure 37

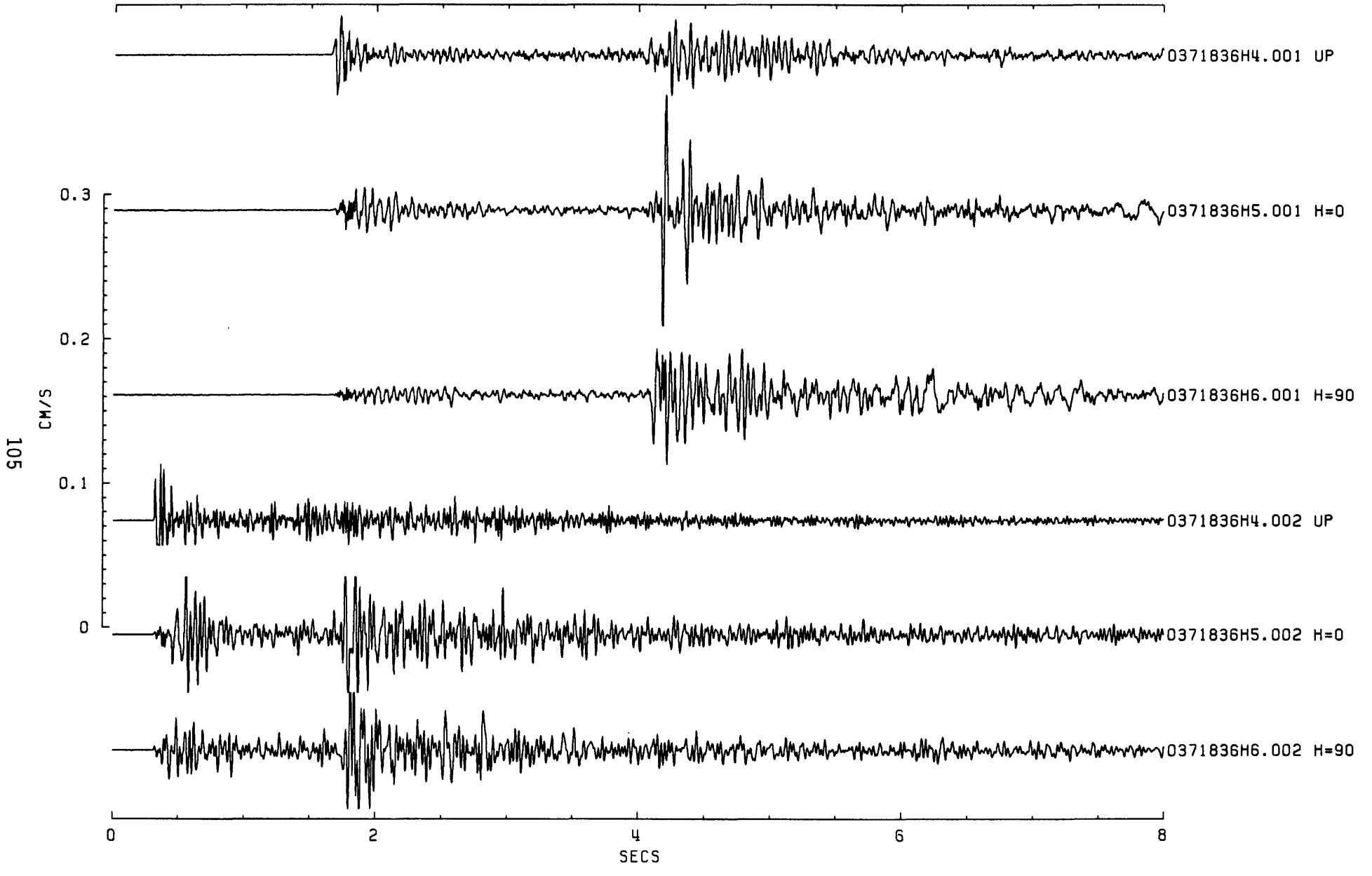
0371836H4.001 UP
0371836H5.001 H=0
0371836H6.001 H=90
0371836H4.002 UP
0371836H5.002 H=0
0371836H6.002 H=90
0.3
0.2
0.1
0
CM/S
0
2
4
6
8
SECS

Figure 38

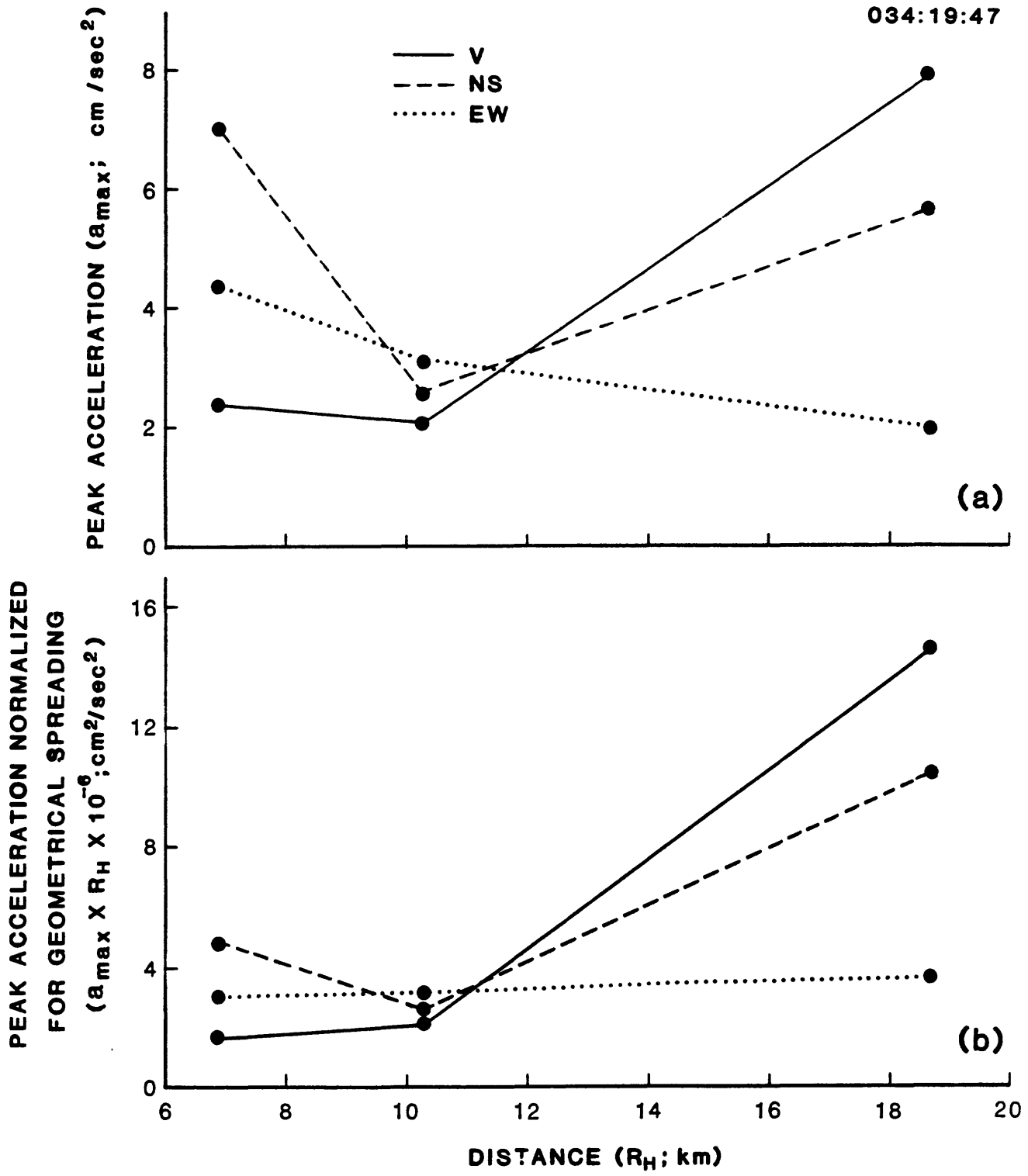
034:19:47
V
NS
EW
PEAK ACCELERATION (a_{max}; cm/sec^2)
(a)
PEAK ACCELERATION NORMALIZED FOR GEOMETRICAL SPREADING ($a_{max} \times R_H \times 10^{-6}$; cm^2/sec^2)
(b)
DISTANCE (R_H; km)

Figure 39

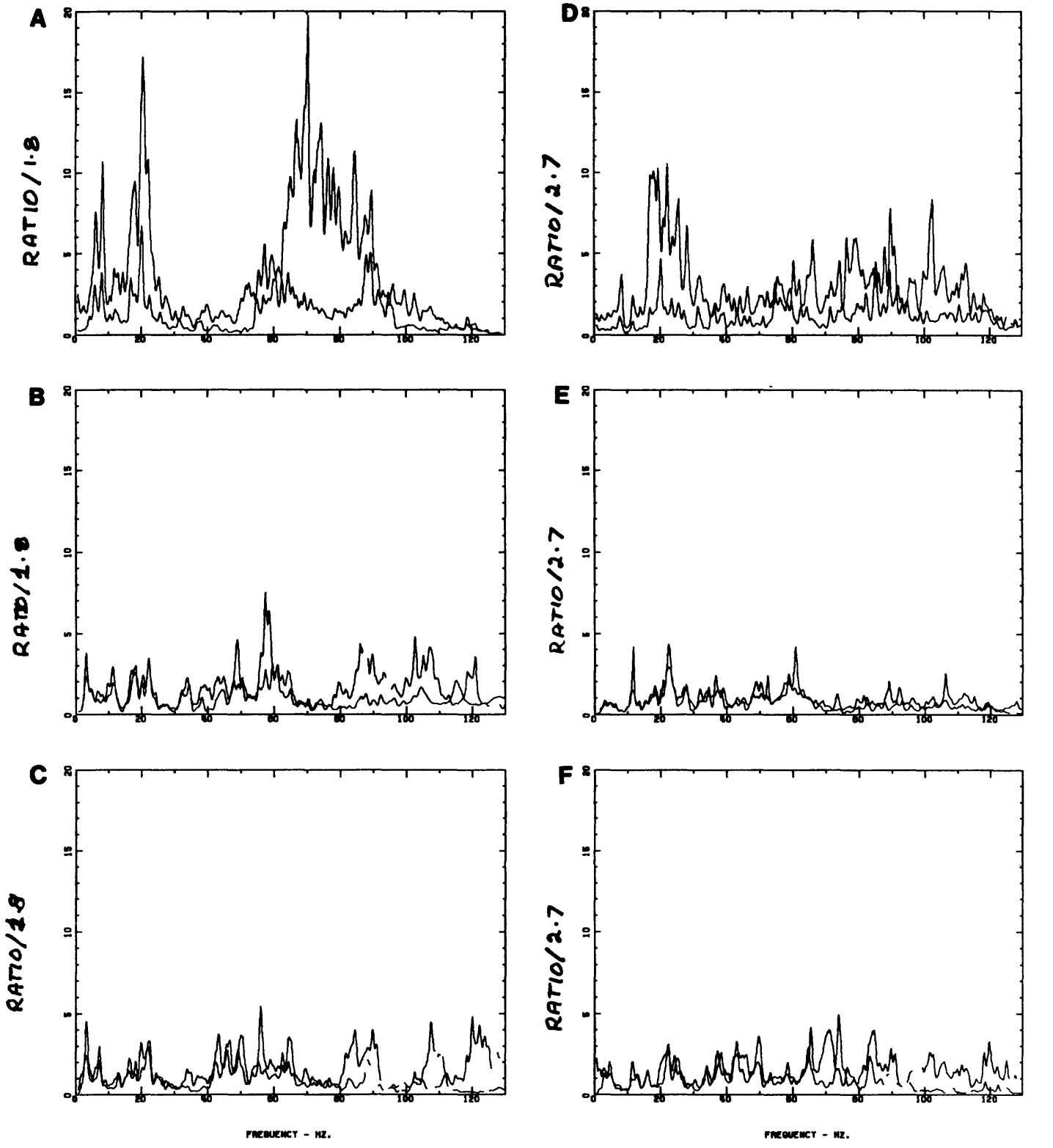
A
RATIO/1.8
D
RATIO/2.7
B
RATIO/1.8
E
RATIO/2.7
C
RATIO/1.8
F
RATIO/2.7
FREQUENCY - HZ.
FREQUENCY - HZ.

Figure 40

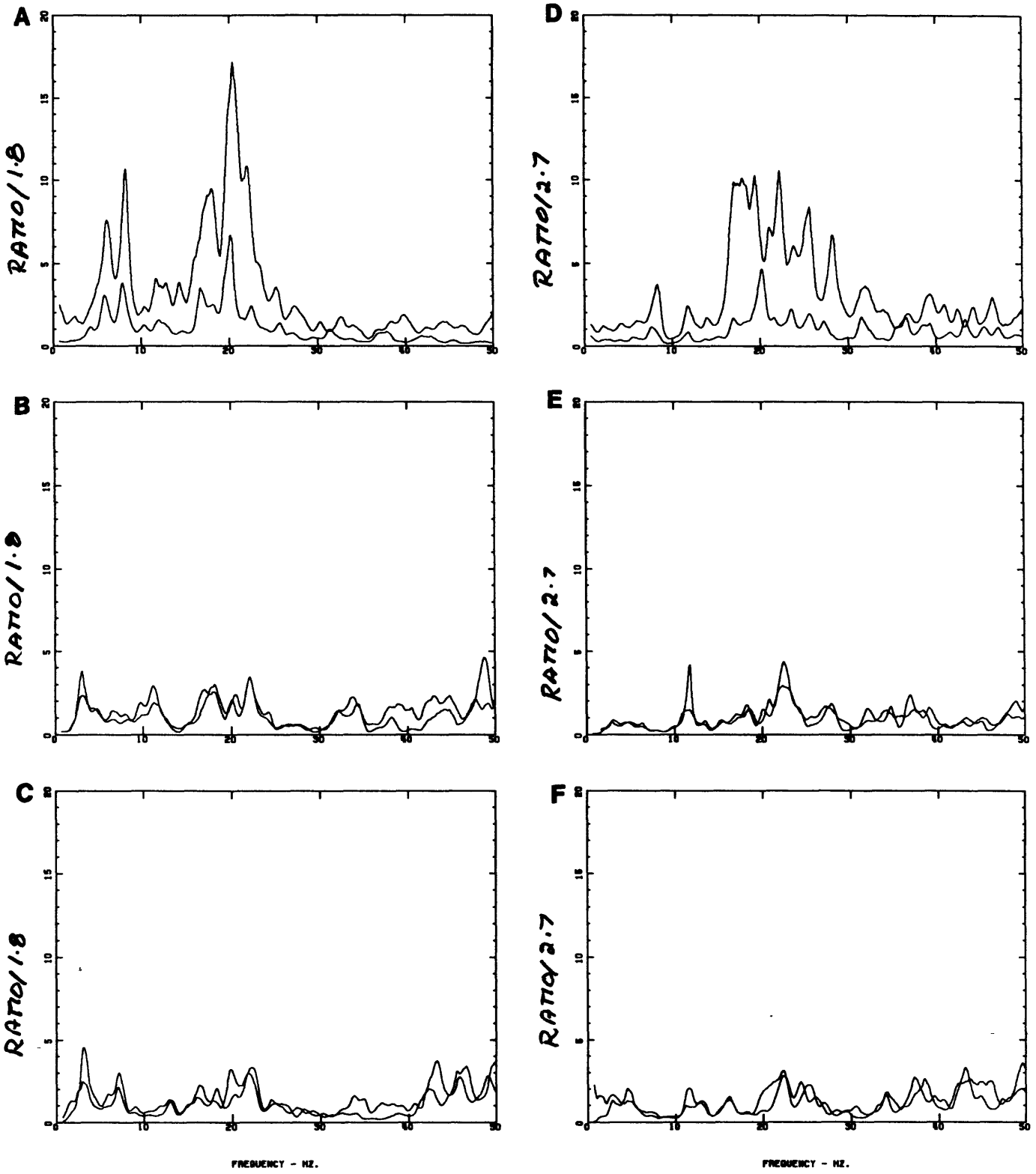
A
RATIO/1.8
D
RATIO/2.7
B
RATIO/1.8
E
RATIO/2.7
C
RATIO/1.8
F
RATIO/2.7
FREQUENCY - HZ.
FREQUENCY - HZ.

Figure 41

APPENDIX A

HISTORICAL AND INSTRUMENTALLY RECORDED SEISMIC EVENTS WITHIN THE STATE OF OHIO 1776 THROUGH 1986

Explanation of Table 1(a) File Format

The data are listed chronologically by date and origin time in Coordinated Universal Time (UTC). Each earthquake entry contains the following information: Geographic coordinates, depth, hypocenter quality with reference sources, magnitudes, and intensity with reference sources. The file has some basic limitations in terms of size (magnitude or intensity) of the earthquakes listed. All felt earthquakes or those with computed magnitudes greater than 2.5 are listed. If no magnitude was computed and the earthquake was felt, it was included in the list. The low-magnitude events located since 1965 with data from dense seismic networks have not been included.

Listed below is an explanation of the symbols and codes that are used in the file listing:

1. Leaders (...) indicate information not available.

2. Latitude and longitude are listed to a thousandth of a degree if they have been published with that precision. A "x" to the right of the longitude indicates that the entry is nontectonic; a "*" indicates the coordinates have been assigned by the compiler; a "?" indicates that published descriptions of the event are inconclusive and it may or may not be an earthquake.

3. Depth of the hypocenter in kilometers.

4. Under the HYPOCENTER heading, the QUAL is defined as:

   a. Determinations of instrumental hypocenters are estimated to be accurate within the degree range of latitude and longitude listed below; each range is letter coded as indicated:

      A = 0.0 - 0.1

      B = 0.1 - 0.2

      C = 0.2 - 0.5

      D = 0.5 - 1.0

      E = 1.0 or larger.

   b. Determinations of noninstrumental epicenters from felt data are estimated to be accurate with the degree ranges of latitude and longitude listed below; each range is letter coded as indicated:

      F = 0.0 - 0.5

      G = 0.5 - 1.0

H = 1.0 - 2.0

I = 2.0 or larger.

5. The reference identification numbers under the HYPOCENTER (REF) and INTENSITY (REF) columns indicate the sources of the hypocenter and intensity. These sources are available on request.

6. The magnitudes are composed of three sections:

a. Under the USGS heading:

The mb values (Gutenberg and Richter, 1956) and the Ms values (Bath, 1966 or Gutenberg, 1945) were published in the Preliminary Determination of Epicenters (PDE) by the National Earthquake Information Center, U. S. Geological Survey and predecessor organizations.

b. Under the heading of OTHER, the associated magnitudes are classified by type and source. The sources are available on request. The magnitude types are identified as:

(1.) ML....(Richter, 1958)

(2.) Mn....(Nuttli, 1973)

(3.) Ms....(Bath, 1966 or Gutenberg, 1945)

(4.) mb....(Gutenberg and Richter, 1956)

(5.) Mnx...[Modified mbLG] (Jones and others, 1977)

(6.) MD....Duration or Coda Length

(7.) m3h...(Lawson and others, 1979)

(8.) Mfa...Magnitude based on felt area attenuation

(9.) UKN...Unknown magnitude

c. Under the MOMENT heading:

The Mw values are computed from the log of the moment in dynes/cm. The source of the contributed value is coded at the right. The formula used in the conversion is from Hanks and Kanamori (1979).

7. Intensity. Values are based on the Modified Mercalli Scale of 1931 (Wood and Neumann, 1931). A letter "F" appears in this column if the quake was felt; but the information was not sufficient or too ambigious to assign a numerical value. A "*" appears to the right of the intensity value if the value was assigned by the compilers.

8. Comments. The comment lines are generally used to list some of the stronger effects caused by those earthquakes with intensities

listed at VI or greater. Other types of comments explains unique feature(s) that occurred as a result of an earthquake. If a source reference follows the comment, then the comment was taken from that reference; otherwise, the comment was taken from the source reference following the intensity assignment.

Data taken from the United States Geological Survey state seismicity files compiled by Stover, C.W., Reagor, G., and Algermissen, S.T. Questions concerning the data should be directed to Carl Stover or Glen Reagor-- Phone (303) 236-1500. These lists are continuously updated and comments on damage are being added.

Table 1(a)--Chronological listing of earthquakes for the state of Ohio through the year 1982.

DATE			ORIGIN TIME (UTC)			LAT.		LONG.			DEPTH (KM)	HYPOCENTER QUAL	REF	MAGNITUDE USGS (mb)	(Ms)	OTHER	MOMENT (Mw)	INTENSITY MM	REF
YEAR	MONTH	DAY	H	M	S														
1776	...	..	14	00	..	39.6	N.	81.9	W.		..	I	116	..	..	.. ..	.. ...	VI	60
	Epicenter near the Muskingum River. The earthquake occurred in the Summer of 1776. Furniture was (nearly) overthrown; rumbling noise; people and animals were frighten; and the duration of the shock was estimated to have lasted two to three minutes.																		
1823	MAY	30	..	..	..	41.5	N.	81.0	W.		..	I	76	..	..	.. ..	.. ...	IV	76
1836	JUL	08	..	..	..	41.5	N.	81.7	W.		..	I	120	..	..	.. ..	.. ...	IV	120
1845	...	..	..	..	..	41.1	N.	84.2	W.	?	..	G	105	..	..	.. ..	.. ...	...	..
	A ridge of ground shifted about 4 feet on a farm in Putnam, Ohio. Not felt.																		
1850	OCT	01	..	..	..	41.4	N.	82.3	W.		..	I	120	..	..	.. ..	.. ...	IV	120
1857	MAR	01	01	40	..	41.8	N.	80.6	W.		..	H	353	..	..	.. ..	.. ...	IV	105
1858	APR	10	12	..	..	41.7	N.	81.3	W.		..	H	105	..	..	.. ..	.. ...	IV	105
1867	JAN	13	..	..	..	41.5	N.	81.7	W.		..	I	120	..	..	.. ..	.. ...	III	120
1872	JUL	23	..	..	..	41.4	N.	82.1	W.		..	G	116	..	..	.. ..	.. ...	III	60
1873	APR	23	04	14	..	39.8	N.	84.2	W.		..	H	116	..	..	.. ..	.. ...	III*	105
1875	JUN	16	12	43	..	40.2	N.	84.0	W.		..	G	38	..	..	.. ..	.. ...	VII	38
	Western Ohio. Most severe at Urbana and Sidney where walls were cracked and chimneys were thrown down. Felt over an estimated area of 40,000 sq miles which included southern Illinois, eastern Missouri, northwestern Kentucky, and southwestern Indiana.																		
1876	JUN	..	..	..	..	40.4	N.	84.2	W.		..	H	105	..	..	.. ..	.. ...	IV*	60
1877	JAN	23	21	..	..	38.8	N.	83.5	W.		..	H	105	..	..	3.6Mfa BAR	.. ...	III	60
1881	AUG	30	03	..	..	39.2	N.	83.6	W.		..	H	116	..	..	.. ..	.. ...	III	105
1882	FEB	09	20	..	..	40.4	N.	84.2	W.		..	H	105	..	..	3.2Mfa BAR	.. ...	V	38
1883	JAN	06	08	..	..	40.4	N.	84.2	W.	*	..	H	105	..	..	.. ..	.. ...	II*	105
1884	MAR	31	19	..	..	39.6	N.	84.8	W.		..	H	116	..	..	.. ..	.. ...	II	105
1884	SEP	19	19	14	..	40.7	N.	84.1	W.		..	G	38	..	..	4.8Mfa BAR	.. ...	VI	38
	Near Lima, Ohio. Slight damage at Lima. Felt area was estimated at 125,000 sq miles. Felt in all states bordering Ohio.																		
1884	DEC	23	23	..	..	40.4	N.	84.2	W.		..	H	105	..	..	.. ..	.. ...	III	60
1885	JAN	18	11	30	..	41.3	N.	81.1	W.		..	H	105	..	..	.. ..	.. ...	III*	105
1885	AUG	15	05	05	..	41.3	N.	81.1	W.		..	H	105	..	..	.. ..	.. ...	III*	105
1886	MAY	03	02	30	..	39.5	N.	82.1	W.		..	H	105	..	..	3.4Mfa BAR	.. ...	V*	131
1889	SEP	..	..	..	..	40.4	N.	84.2	W.		..	H	105	..	..	.. ..	.. ...	III	105
1892	...	..	..	..	..	40.4	N.	84.2	W.		..	H	105	..	..	.. ..	.. ...	IV*	60
1896	MAR	15	07	..	..	40.3	N.	84.2	W.		..	G	105	..	..	.. ..	.. ...	IV	60

1898	OCT	23	..	..	..	41.5	N.	81.7	W.	..	H	105	..	..	..	..	...	..	...	III	116
1899	NOV	12	14	..	..	39.3	N.	83.0	W.	..	H	116	..	..	..	..	...	..	...	IV	105
1900	APR	09	14	..	..	41.4	N.	81.9	W.	..	G	116	..	..	..	..	...	..	...	VI	105
	Berea, Ohio. Two chimneys on one house fell.																				
1901	MAY	17	05	00	..	39.3	N.	82.5	W.	..	G	38	..	..	4.2Mfa	BAR		..	...	V	38
1902	JUN	14	07	..	..	39.4	N.	81.2	W.	..	G	116	..	..	..	..	...	..	...	IV	116
1906	APR	20	18	30	..	41.5	N.	81.7	W.	..	H	105	..	..	..	..	...	..	...	IV	105
1906	APR	23	07	12	..	40.7	N.	83.6	W.	..	H	105	..	..	..	..	...	..	...	IV	116
1906	JUN	27	21	10	..	41.4	N.	81.6	W.	..	G	38	..	..	..	..	...	..	...	V	38
1907	APR	12	19	28	..	41.5	N.	81.7	W.	..	H	105	..	..	..	..	...	..	...	III	173
1914	...	..	..	..	..	40.4	N.	84.2	W.	..	H	105	..	..	..	..	...	..	...	III	105
1925	MAR	27	04	06	..	40.4	N.	84.2	W.	..	H	116	..	..	..	..	...	..	...	V	60
1925	APR	04	..	..	..	39.1	N.	84.5	W.	..	G	105	..	..	..	..	...	..	...	II*	60
1925	OCT	..	..	..	..	40.4	N.	84.2	W.	..	G	105	..	..	..	..	...	..	...	III	105
1926	OCT	26	07	42	..	41.7	N.	83.5	W.	..	G	116	..	..	..	..	...	..	...	III	60
1926	OCT	28	10	00	..	41.7	N.	83.5	W.	..	G	116	..	..	..	..	...	..	...	IV	60
1926	NOV	05	14	53	..	39.1	N.	82.1	W.	..	G	38	..	..	..	..	...	..	...	VII	38
	Southwestern Ohio near Pomeroy. Chimneys were thrown down and a stove was overturned. Some objects were knocked form shelves. Chimneys toppled at Keno, Ohio. Felt throughout Meigs, County, Ohio and Letart, West Virginia-an area estimated at 350 sq miles.																				
1927	JAN	29	..	..	..	40.9	N.	81.2	W.	x ..	H	121	..	..	..	..	...	..	...	V	121
1927	FEB	17	05	30	..	40.8	N.	82.5	W.	..	G	116	..	..	..	..	...	..	...	IV	60
1928	SEP	09	21	..	..	41.5	N.	82.0	W.	..	G	1	..	..	3.7Mfa	BAR		..	...	V	60
1928	OCT	27	..	..	..	40.4	N.	84.1	W.	..	G	116	..	..	3.2Mfa	BAR		..	...	III	60
1929	MAR	08	09	06	..	40.4	N.	84.2	W.	..	C	38	..	..	4.0Mfa	BAR		..	...	V	38
1929	JUN	10	..	..	..	41.5	N.	81.7	W.	..	G	105	..	..	..	..	...	..	...	III	60
1929	SEP	17	19	16	..	41.6	N.	81.5	W.	..	G	116	..	..	..	..	...	..	...	III	173
1930	JUN	26	21	45	..	40.5	N.	84.0	W.	..	G	3	..	..	..	..	...	..	...	IV	60
1930	JUN	27	07	23	..	40.5	N.	84.0	W.	..	G	3	..	..	..	..	...	..	...	IV	60
1930	JUL	11	00	15	..	40.6	N.	83.1	W.	..	G	105	..	..	..	..	...	..	...	IV	60
1930	SEP	29	22	50	..	40.3	N.	84.2	W.	..	G	60	..	..	..	..	...	..	...	III	60
1930	SEP	30	20	40	..	40.3	N.	84.3	W.	..	C	38	..	..	..	..	...	..	...	VII	38
	Near Anna, Ohio. A brief, strong shock was generally felt over a wide area. It caused the chimney at a school house to fall and plaster to crack and fall.																				
1930	OCT	..	..	..	..	40.4	N.	84.2	W.	..	G	116	..	..	..	..	...	..	...	III	60
1931	MAR	21	15	48	..	40.4	N.	84.2	W.	..	G	105	..	..	..	..	...	..	...	III	60
1931	APR	01	00	15	..	40.4	N.	84.1	W.	..	G	105	..	..	..	..	...	..	...	III	60
1931	JUN	10	08	30	..	41.3	N.	84.0	W.	x ..	G	4	..	..	3.7Mfa	BAR		..	...	V	60
1931	SEP	20	23	05	03.4	40.429N.		84.270W.		005	B	349	..	..	4.5Mfa	DG		..	...	VII	38
	Anna, Ohio. Felt over a large portion of Ohio, Indiana, and northern Kentucky-an area estimated at 40,000 sq miles. In the epicentral area chimneys tumbled, plaster fell, windows broken, some cornices were thrown down, and a roof collapsed. Severe damage was also recorded at Botkins, houston, and Sidney (Docekal;105).																				
1931	OCT	08	14	30	..	40.4	N.	84.2	W.	..	G	105	..	..	..	..	...	..	...	III	60
1932	JAN	21	..	..	..	41.1	N.	81.5	W.	..	G	105	..	..	..	..	...	..	...	V	105
1933	FEB	23	03	20	..	40.3	N.	84.2	W.	..	G	105	..	..	3.8Mfa	BAR		..	...	IV	105
1933	MAY	26	..	..	..	41.5	N.	81.4	W.	..	H	121	..	..	..	..	...	..	...	IV	121
1936	JAN	31	07	30	..	41.1	N.	83.2	W.	..	G	116	..	..	..	..	...	..	...	IV	105
1936	OCT	08	16	30	..	39.3	N.	84.4	W.	..	G	105	..	..	3.5Mfa	BAR		..	...	III	60
1936	DEC	26	01	15	..	39.1	N.	84.5	W.	..	G	105	..	..	..	..	...	..	...	III	60
1936	DEC	26	02	05	..	39.1	N.	84.5	W.	..	G	105	..	..	..	..	...	..	...	III	60
1937	MAR	02	14	47	33.3	40.488N.		84.273W.		002	A	349	..	..	4.7Mfa	DG		..	...	VII	38

Western Ohio near Anna and Sidney. This earthquake was felt over an estimated area of 110,000 sq miles in Ohio, Indiana, Michigan, West Virginia, Kentucky, and Canada (Bradley;60). In the area of the highest intensity, plaster fell, and walls cracked in a school house. A number of other buildings and churches experienced similar damage. A number of chimneys fell. At Sidney, the shock was less severe. Two to five shocks were felt in many places.

1937	MAR	03	09	50	..	40.4	N.	84.2	W.		..	G	116	..	..	3.4Mfa	BAR	..	...	V	60
1937	MAR	03	09	55	..	40.4	N.	84.2	W.		..	G	116	..	..	..	..	..	...	III	60
1937	MAR	09	05	44	35.5	40.470	N.	84.280	W.		003	B	349	..	..	4.9Mfa	DG	..	...	VIII	38

Western Ohio. The region around Anna experienced the greatest damage. Chimneys repaired after the March 2 quake were again thrown down, with scarcely a chimney escaping damage. In the Lutheran Church, organ pipes were twisted. Churches and school buildings were badly cracked. At Sidney, a few chimneys fell and there was damage to plaster. Various estimates of the felt area suggest 110,000 to 150,000 sq miles.

1937	APR	23	17	15	..	40.4	N.	84.2	W.		..	G	116	..	..	3.4Mfa	BAR	..	...	III	60
1937	APR	27	17	..	..	40.4	N.	84.2	W.		..	G	116	..	..	3.4Mfa	BAR	..	...	III	60
1937	MAY	02	17	05	..	40.4	N.	84.2	W.		..	G	116	..	..	..	..	..	...	IV	105
1937	OCT	17	04	25	..	39.1	N.	84.5	W.		..	G	105	..	..	..	..	..	...	III	60
1939	MAR	18	11	..	..	40.4	N.	84.2	W.	*	..	G	60	..	..	..	..	..	...	II	60
1939	MAR	18	13	03	..	40.4	N.	84.1	W.		..	G	105	..	..	3.6Mfa	BAR	..	...	III	60
1939	JUN	16	02	20	..	40.4	N.	84.2	W.		..	G	116	..	..	3.4Mfa	BAR	..	...	IV	60
1939	JUL	09	11	50	..	40.4	N.	84.2	W.		..	G	116	..	..	..	..	..	...	II	60
1940	MAY	31	17	00	..	41.1	N.	81.5	W.		..	G	105	..	..	..	..	..	...	II	60
1940	JUN	16	02	30	..	40.9	N.	82.3	W.		..	G	105	..	..	..	..	..	...	IV	105
1940	JUL	28	09	30	..	40.9	N.	82.3	W.		..	G	105	..	..	..	..	..	...	III	105
1940	AUG	15	10	55	..	40.9	N.	82.3	W.		..	G	105	..	..	..	..	..	...	III	105
1940	AUG	19	03	30	..	40.9	N.	82.3	W.		..	G	105	..	..	..	..	..	...	III	105
1943	MAR	09	08	25	24.9	41.623	N.	81.309	W.		007	H	349	..	..	4.5Mn	BAS	..	...	V	105
1944	NOV	13	11	52	..	40.4	N.	84.2	W.		..	G	116	..	..	4.3Mfa	BAR	..	...	III	60
1948	JAN	18	..	..	..	41.7	N.	83.5	W.		..	G	116	..	..	..	..	..	...	III	60
1950	APR	20	..	..	..	39.3	N.	84.2	W.	x	..	G	116	..	..	..	..	..	...	IV	105
1951	DEC	03	07	02	..	41.6	N.	81.4	W.		..	G	116	..	..	3.2Mfa	BAR	..	...	IV	24
1951	DEC	07	21	..	..	41.6	N.	81.4	W.	*	..	G	60	..	..	..	..	..	...	II	60
1951	DEC	21	20	..	..	41.6	N.	81.4	W.		..	G	116	..	..	..	..	..	...	II	60
1952	JUN	20	09	38	08.6	39.540	N.	82.023	W.		009	B	349	..	..	4.1Mfa	DG	..	...	VI	38

Southeaster Ohio near Zanesville. At Zanesville, an old chimney toppled. Felt area was estimated at 10,000 sq miles (Docekal;105).

1953	MAY	07	23	32	..	39.7	N.	82.2	W.	*	..	G	60	..	..	..	..	..	...	IV	60
1953	JUN	12	04	45	..	41.7	N.	83.0	W.		..	G	105	..	..	..	..	..	...	IV	26
1955	MAY	26	18	09	..	41.5	N.	81.7	W.		..	G	38	..	..	..	..	..	...	V	38
1955	JUN	29	01	15	33	41.5	N.	81.7	W.		..	G	38	..	..	..	..	..	...	V	38
1956	JAN	27	12	03	20	40.4	N.	84.2	W.		..	G	105	..	..	4.4ML	OTT	..	...	V	38
1957	JUL	23	13	03	..	38.8	N.	83.8	W.		..	G	105	..	..	..	..	..	...	III	105
1958	MAY	01	22	46	31	41.5	N.	81.7	W.		..	G	38	..	..	..	..	..	...	V	38
1961	FEB	22	09	45	03	41.2	N.	83.4	W.		..	G	38	..	..	4.0Mfa	BAR	..	...	V	38
1967	APR	08	05	40	30.5	39.652	N.	82.535	W.		001	A	349	4.5	..	3.5Mn	GS	..	...	V	38
1968	JUL	26	15	02	53.7	40.4	N.	84.2	W.		..	F	122	3.0	..	..	..	..	...	III	122
1974	SEP	29	02	26	19.1	41.206	N.	83.486	W.		001	B	349	..	..	3.0Mn	SLM	..	...	II	47
1975	FEB	03	10	31	..	41.3	N.	83.2	W.	*	..	F	48	..	..	..	..	..	...	IV	48
1975	FEB	16	23	21	34.4	38.875	N.	82.353	W.		004	A	349	4.4	..	3.0Mn	OG	..	...	IV	48
1977	MAR	09	08	48	17.1	41.0	N.	83.5	W.	x	000	B	97	..	..	..	..	..	...	V	97
1977	JUN	17	15	39	45.9	40.705	N.	84.707	W.		001	C	349	..	..	3.2Mn	AAM	..	...	VI	39

Northwestern Ohio. Slight damage in the form of cracked sidewalks, foundations, and plaster occurred at Celina, Coldwater, Fort Recovery, and Rockford. Felt area was estimated at 200 sq miles (EGM;38).

Table 10(b)--Chronological listing of earthquakes for the state of Ohio, updated from 1983 to present using USGS, National Earthquake Information Service data.

AGENCY	DATE YEAR	MO	DA	ORIGIN TIME	***COORDINATES** LAT.	LONG.	DEPTH	NO pP	STN DEV	*****MAGNITUDE** mb	DBS	Ms	OBS	CONTRIBUTED VALUES	INFORMATION** I	C E	M	F S	PHENOMENA DTSVNWG	IDE	F-E REG	NO. STA	FLG	P
GS	1983	01	22	074657.93*	41.354	-81.191	5.0G		0.41					2.70Mn GS	.	.	.	.	.....		471	11	.	.
~~GS~~	~~1983~~	~~08~~	~~17~~	~~140315.02V~~	~~38.472~~	~~82.772~~	~~11.9G~~							~~3.50Mn GS~~ 3.50MnBLA	~~5~~	~~F~~	.	.	.....		~~491~~	~~32~~	.	.
GS	1984	01	14	201431.29*	41.645	-83.427	5.0G		0.90					2.50CLAAM	4	F	.	.	.....		471	13	.	.
PDE	1985	01	31	164942.20	41.642	-81.109	10.0G		1.01	4.9		11			6	C	.	.	.....		471	71	.	.
PDE	1986	02	07	183622.3+GL	41.645	-81.157	6.2							2.50MnGS	.	F	.	.	.....		471	1	.	.

APPENDIX B

PHASE DATA AND PREFERRED LOCATIONS FOR EARTHQUAKES LOCATED NEAR PAINESVILLE, OHIO FEBRUARY 6 THROUGH MARCH 24, 1986

CRUSTAL MODEL 1

LAYER	VELOCITY KM/SEC	DEPTH KM	THICKNESS KM	VPVS
1	1.800	0.000	0.050	3.000
2	3.000	0.050	0.450	1.900
3	4.200	0.500	0.500	1.800
4	4.500	1.000	0.750	1.780
5	4.750	1.750	0.350	1.760
6	6.150	2.100	17.900	1.740
7	6.700	20.000	20.000	1.730
8	8.100	40.000	1000.000	1.750

THE NEXT MODEL IS FOR S ONLY:

CRUSTAL MODEL 2

LAYER	VELOCITY KM/SEC	DEPTH KM	THICKNESS KM	VPVS
9	0.600	0.000	0.050	0.000
10	1.579	0.050	0.450	0.000
11	2.333	0.500	0.500	0.000
12	2.528	1.000	0.750	0.000
13	2.699	1.750	0.350	0.000
14	3.534	2.100	17.900	0.000
15	3.873	20.000	20.000	0.000
16	4.629	40.000	1000.000	0.000

----------BEGIN----------

86/ 2/ 1 18/54 TEST DATA 86/ 2/ 1 18/54

HORIZONTAL AND VERTICAL SINGLE VARIABLE STANDARD DEVIATIONS (68% - ONE DEGREE OF FREEDOM)
[VALUES TRUNCATED AT 25 KM]

SEH = 0.25 SEH = 0.43 SEZ = 0.89 QUALITY = A
AZ = 25. AZ = -65.

SE OF ORIG = 0.08 TOTAL NUMBER OF ITERATIONS = 5 DMAX = 90.00 SEQUENCE NUMBER =
AT THE CLOSEST STATION USED IN THE SOLUTION BOTH P AND S WERE USED. THE S MINUS P INTERVAL EQUALS 0.52

DATE	ORIGIN	LAT	LONG	DEPTH	MAG	NO	D1	GAP	D	RMS	SEH	SEZ	Q	SQD	ADJ	IN	NR	AVR	AAR	NM	AVXM	SDXM	NF	AVFM	SDFM
860201	1854 49.20	41N38.82	81W 9.42	4.97		21	2	100	1	0.13	0.4	0.9	B	A B	0.07	10	21	0.00	0.09	0		0.0	0		0.0

(- STATION DATA -)				(------ P-WAVE TRAVEL-TIME DATA AND DELAYS -------)						VARI	(---- S-WAVE TRAVEL-TIME DATA --)					(--- MAGNITUDE DATA --)				
STN	DIST	AZM	AIN	PSEC	PRMK	TCOR	O=TTOB	TTCAL	C-DLAY	EDLY=P-RES	P-WT	THIC	SSEC	SRMK	TTOB	TTCAL	S-RES	S-WT	AMX	PR	XMAG	R	FMP	FMAG
wc02	2.3	356	151	50.37	IPC	0	1.17	1.10	1	0.07	2.100		50.89	es3	1.69	1.99	-0.30	0.131						
hqoh	4.5	164	131	50.60	IP	1	1.40	1.33	1	0.07	1.181		51.20	es3	2.00	2.39	-0.39	0.131						
hlh	5.5	37	125	50.77	IPC	0	1.57	1.45	1	0.12	2.100		51.61	is3	2.41	2.60	-0.19	0.131						
hsoh	6.2	159	121	51.05	IP	1	1.85	1.55	1	0.30	1.181			4										
wc04	6.9	179	118	50.89	IPC	0	1.69	1.64	1	0.05	2.100		51.81	es2	2.61	2.94	-0.33	0.525						
choh	6.9	209	118	50.70	IP	1	1.50	1.65	1	-0.15	1.181		52.05	es2	2.85	2.95	-0.09	0.525						
mtoh	9.7	114	110	51.20	IP	1	2.00	2.05	1	-0.05	1.181		52.60	es3	3.40	3.66	-0.26	0.131						
wc03	11.6	36	106	51.49	IPD	0	2.29	2.36	1	-0.07	2.100		53.14	es2	3.94	4.19	-0.25	0.525						
wc01	12.5	254	105	51.72	IPD	0	2.52	2.51	1	0.02	2.100		53.25	es3	4.05	4.44	-0.39	0.131						
hpv	13.6	40	104	51.85	IPD	0	2.65	2.67	1	-0.02	2.100		53.75	is3	4.55	4.73	-0.18	0.131						
gar	15.8	354	102	52.22	IPC	1	3.02	3.02	1	0.00	1.181		54.57	is3	5.37	5.34	0.04	0.131						

QUALITY EVALUATION

DIAGONALS IN ORDER OF STRENGTH	Z	SE	NW	E	NE	SW	N
AVE. OF END POINTS	0.24	0.47	0.60	0.70	0.84	0.85	0.89

NUMBER	RMS	MIN DRMS	AVE DRMS	QUALITY
21	0.13	0.30	0.69	A

----------BEGIN----------

86/ 2/ 2 3/22 TEST DATA 86/ 2/ 2 3/22

HORIZONTAL AND VERTICAL SINGLE VARIABLE STANDARD DEVIATIONS (68% - ONE DEGREE OF FREEDOM)
[VALUES TRUNCATED AT 25 KM]

SEH = 0.12 SEH = 0.13 SEZ = 0.30 QUALITY = A
AZ = -132. AZ = -42.

SE OF ORIG = 0.03 TOTAL NUMBER OF ITERATIONS = 3 DMAX = 90.00 SEQUENCE NUMBER =
AT THE CLOSEST STATION USED IN THE SOLUTION BOTH P AND S WERE USED. THE S MINUS P INTERVAL EQUALS 0.83

DATE	ORIGIN	LAT	LONG	DEPTH	MAG	NO	D1	GAP	D	RMS	SEH	SEZ	Q	SQD	ADJ	IN	NR	AVR	AAR	NM	AVXM	SDXM	NF	AVFM	SDFM
860202	322 48.53	41N38.75	81W 9.53	4.99		24	1	72	1	0.06	0.1	0.3	A	A A	0.32	10	38	0.00	0.05	0		0.0	0		0.0

(- STATION DATA -)				(------ P-WAVE TRAVEL-TIME DATA AND DELAYS -------)					VARI	(---- S-WAVE TRAVEL-TIME DATA --)						(--- MAGNITUDE DATA --)				
STN	DIST	AZM	AIN	PSEC PRMK+TCOR-O=TTOB-TTCAL	C-DLAY-EDLY=P-RES	P-WT	THIC	SSEC	SRMK	TTOB	TTCAL	S-RES	S-WT	AMX	PR	XMAG	R	FMP	FMAG
x03	1.5	330	161	49.62IPC0 1.09 1.05	1 0.04	1.455		50.45	is1	1.92	1.90	0.02	0.818						
wc02	2.4	0	150	49.69IPC0 1.16 1.11	1 0.05	1.455		50.32	s4	1.79	2.01	-0.22	0.000						
haoh	4.5	161	132	49.90IP 1 1.37 1.33	1 0.05	0.818		50.40	es4	1.87	2.38	-0.51	0.000						
hlh	5.7	38	124	50.11IPC1 1.58 1.48	1 0.10	0.818		51.00	is4	2.47	2.67	-0.19	0.000						
choh	6.7	208	119	50.00IP 1 1.47 1.62	1 -0.15	0.818		51.33	es4	2.80	2.90	-0.10	0.000						
wc04	6.8	178	119	50.16IPC0 1.63 1.63	1 0.00	1.455		51.19	s4	2.66	2.92	-0.25	0.000						
howm	7.3	162	117	50.25IPD3 1.72 1.71	1 0.01	0.091		51.45	es4	2.92	3.05	-0.13	0.000						
con	7.4	326	117	50.34IPD1 1.81 1.72	1 0.09	0.818		51.31	is4	2.78	3.08	-0.30	0.000						
x06	8.2	103	114	50.41IPD0 1.88 1.84	1 0.04	1.455		51.75	is0	3.22	3.28	-0.06	1.455						
x02	9.2	1	111	50.54IPC0 2.01 1.99	1 0.02	1.455		51.95	is0	3.42	3.56	-0.14	1.455						
wkr	10.2	119	109	50.67IPD1 2.14 2.13	1 0.01	0.818			4										
x04	11.7	252	106	50.95IPD0 2.42 2.37	1 0.05	1.455		52.66	is0	4.13	4.21	-0.08	1.455						
wc03	11.8	37	106	50.87IPC0 2.34 2.39	1 -0.05	1.455		52.54	is4	4.01	4.24	-0.23	0.000						
wc01	12.4	254	105	51.04IP 1 2.51 2.48	1 0.03	0.818		52.64	s4	4.11	4.39	-0.28	0.000						
min	12.6	220	105	51.00IPC2 2.47 2.52	1 -0.05	0.364		52.92	es4	4.39	4.46	-0.07	0.000						
paoh	12.8	345	105	51.10IP 1 2.57 2.54	1 0.03	0.818		52.80	es4	4.27	4.51	-0.23	0.000						
hpv	13.8	41	104	51.20IPC1 2.67 2.70	1 -0.03	0.818		53.17	is4	4.64	4.78	-0.14	0.000						
wc06	16.0	137	102	51.66EP 3 3.13 3.05	1 0.08	0.091		53.73	is4	5.20	5.39	-0.19	0.000						
x01	17.7	5	100	51.88IPC0 3.35 3.32	1 0.03	1.455			4										
cld	20.1	228	99	52.20EP 3 3.67 3.70	1 -0.03	0.091		54.60	es4	6.07	6.52	-0.45	0.000						

QUALITY EVALUATION

DIAGONALS IN ORDER OF STRENGTH	Z	SE	NW	SW	NE	N	E
AVE. OF END POINTS	0.37	0.72	0.80	0.87	0.90	0.94	0.99

NUMBER	RMS	MIN DRMS	AVE DRMS	QUALITY
24	0.06	0.41	0.84	A

----------BEGIN----------

86/ 2/ 3 19/47 TEST DATA 86/ 2/ 3 19/47

HORIZONTAL AND VERTICAL SINGLE VARIABLE STANDARD DEVIATIONS (68% - ONE DEGREE OF FREEDOM)
[VALUES TRUNCATED AT 25 KM]

SEH = 0.12 SEH = 0.18 SEZ = 0.36 QUALITY = A
AZ = 16. AZ = -74.

SE OF ORIG = 0.03 TOTAL NUMBER OF ITERATIONS = 3 DMAX = 90.00 SEQUENCE NUMBER =
AT THE CLOSEST STATION USED IN THE SOLUTION BOTH P AND S WERE USED. THE S MINUS P INTERVAL EQUALS 0.85

DATE	ORIGIN	LAT	LONG	DEPTH	MAG	NO	D1	GAP	D	RMS	SEH	SEZ	Q	SQD	ADJ	IN	NR	AVR	AAR	NM	AVXM	SDXM	NF	AVFM	SDFM
860203	1947 19.61	41N38.84	81W 9.50	6.10		44	1	73	1	0.10	0.2	0.4	A	A	A	0.17	10	68	0.00	0.07	0		0.0	0		0.0

(- STATION DATA -)				(------ P-WAVE TRAVEL-TIME DATA AND DELAYS -------)						VARI	(---- S-WAVE TRAVEL-TIME DATA --)						(--- MAGNITUDE DATA --)					
STN	DIST	AZM	AIN	PSEC	PRMK	TCOR-O=TTOB-TTCAL		C	DLAY-EDLY=P-RES	P-WT	THIC	SSEC	SRMK	TTOB	TTCAL	S-RES	S-WT	AMX	PR	XMAG	R	FMP	FMAG
x03	1.4	325	166	20.83	IPC0	1.22	1.22	1	0.00	1.470		21.68	is1	2.07	2.19	-0.12	0.827						
wc02	2.2	359	157	20.91	IPC0	1.30	1.26	1	0.04	1.470			4										
elfm	4.3	207	141	21.20	IPD3	1.59	1.43	1	0.16	0.092		22.30	es4	2.69	2.57	0.12	0.000						
cal	4.5	11	139	21.24	IPC1	1.63	1.45	1	0.18	0.827		22.54	is4	2.93	2.61	0.32	0.000						
ham	5.1	164	135	21.16	IPD1	1.55	1.53	1	0.02	0.827		21.66	is4	2.05	2.74	-0.69	0.000						
hlh	5.6	38	132	21.26	IPC1	1.65	1.58	1	0.07	0.827			4										
wsh	5.8	247	131	21.32	IPD1	1.71	1.60	1	0.11	0.827		22.30	is4	2.69	2.86	-0.17	0.000						
bur	6.4	83	128	21.40	IPD1	1.79	1.67	1	0.12	0.827		22.75	is4	3.14	2.99	0.15	0.000						
wc04	6.9	178	126	21.35	IPC0	1.74	1.74	1	0.00	1.470		22.38	s4	2.77	3.11	-0.34	0.000						
con	7.3	325	124	21.47	IPC1	1.86	1.79	1	0.07	0.827			4										
ttr	7.3	205	124	21.52	IPC1	1.91	1.79	1	0.12	0.827		22.92	is4	3.31	3.21	0.10	0.000						
howm	7.5	163	124	21.50	IP-3	1.89	1.81	1	0.08	0.092		22.70	es4	3.09	3.25	-0.16	0.000						
x06	8.2	104	121	21.55	IPD0	1.94	1.92	1	0.02	1.470		22.89	is1	3.28	3.43	-0.15	0.827						
calm	8.8	187	119	21.61	IP+3	2.00	2.01	1	-0.01	0.092		23.00	es4	3.39	3.58	-0.19	0.000						
cot	9.1	147	118	21.72	IPC1	2.11	2.05	1	0.06	0.827		23.16	is4	3.55	3.64	-0.09	0.000						
x02	9.1	0	118	21.60	IPC0	1.99	2.05	1	-0.06	1.470		22.98	is2	3.37	3.64	-0.27	0.367						
cuy	9.8	185	116	21.76	IPC1	2.15	2.15	1	0.00	0.827		23.28	is4	3.67	3.83	-0.16	0.000						
tom	10.0	63	116	21.82	IPD0	2.21	2.17	1	0.04	1.470			4										
hse	10.1	158	115	21.81	IP+1	2.20	2.20	1	0.00	0.827		23.31	is4	3.70	3.90	-0.20	0.000						
cha	11.4	223	113	22.05	IPD0	2.44	2.38	1	0.06	1.470		23.76	es4	4.15	4.22	-0.07	0.000						
mon	11.6	122	112	22.06	IPC1	2.45	2.42	1	0.03	0.827		23.62	is4	4.01	4.29	-0.28	0.000						
wc03	11.6	37	112	21.98	IP 1	2.37	2.42	1	-0.05	0.827		23.78	s4	4.17	4.29	-0.12	0.000						
x04	11.8	252	112	22.19	IPD0	2.58	2.44	1	0.14	1.470			4										
min	12.8	220	110	22.06	IPD0	2.45	2.59	1	-0.14	1.470		23.97	es4	4.36	4.60	-0.24	0.000						
x08	12.9	202	110	22.25	IPC0	2.64	2.60	1	0.04	1.470		24.19	is1	4.58	4.63	-0.05	0.827						
x07	14.0	149	108	22.46	EP-1	2.85	2.77	1	0.08	0.827		24.42	is1	4.81	4.92	-0.11	0.827						
har	14.3	106	108	22.45	IPD1	2.84	2.82	1	0.02	0.827		24.39	is4	4.78	5.01	-0.23	0.000						
lox	14.3	42	108	22.50	IPD1	2.89	2.82	1	0.07	0.827		24.55	is4	4.94	5.01	-0.07	0.000						
hwk	15.5	69	106	22.89	IPC1	3.28	3.03	1	0.25	0.827		25.19	is4	5.58	5.35	0.23	0.000						
wc07	17.0	4	105	22.75	IPC0	3.14	3.25	1	-0.11	1.470		25.03	is4	5.42	5.74	-0.32	0.000						
per	17.1	4	105	22.62	IPC1	3.01	3.27	1	-0.26	0.827		24.60	4	4.99	5.77	-0.78	0.000						
htg	17.3	100	105	22.82	IP 0	3.21	3.29	1	-0.08	1.470		25.52	es4	5.91	5.82	0.10	0.000						
x01	17.5	4	104	22.98	IPC0	3.37	3.33	1	0.04	1.470		25.45	is1	5.84	5.88	-0.04	0.827						
che	19.6	221	103	23.24	IPD0	3.63	3.66	1	-0.03	1.470		25.93	es4	6.32	6.45	-0.13	0.000						
cld	20.2	227	102	23.32	IPD0	3.71	3.76	1	-0.05	1.470			4										
mfd	21.7	161	101	23.62	IPC0	4.01	3.99	1	0.02	1.470		26.52	es4	6.91	7.03	-0.12	0.000						
x09	26.2	187	99	24.32	EP-1	4.71	4.71	1	0.00	0.827		27.70	is1	8.09	8.28	-0.19	0.827						

QUALITY EVALUATION

DIAGONALS IN ORDER OF STRENGTH	Z	SE	NW	E	NE	SW	N
AVE. OF END POINTS	0.29	0.67	0.70	0.75	0.85	0.85	1.07

NUMBER	RMS	MIN DRMS	AVE DRMS	QUALITY
44	0.10	0.32	0.78	A

----------BEGIN----------

86/ 2/ 5 6/34 TEST DATA 86/ 2/ 5 6/34

HORIZONTAL AND VERTICAL SINGLE VARIABLE STANDARD DEVIATIONS (68% - ONE DEGREE OF FREEDOM)
[VALUES TRUNCATED AT 25 KM]

SEH = 0.43 SEH = 0.45 SEZ = 0.46 QUALITY = A
AZ = 14. AZ = -76.

SE OF ORIG = 0.07 TOTAL NUMBER OF ITERATIONS = 5 DMAX = 90.00 SEQUENCE NUMBER =
AT THE CLOSEST STATION USED IN THE SOLUTION BOTH P AND S WERE USED. THE S MINUS P INTERVAL EQUALS 1.74

DATE	ORIGIN	LAT	LONG	DEPTH	MAG	NO	D1	GAP	D	RMS	SEH	SEZ	Q	SQD	ADJ	IN	NR	AVR	AAR	NM	AVXM	SDXM	NF	AVFM	SDFM
860205	634 2.40	41N38.94	81W 9.64	2.07		20	1	49	1	0.21	0.4	0.5	B	B A	0.13	10	31	0.00	0.13	0		0.0	0		0.0

(- STATION DATA -)				(------ P-WAVE TRAVEL-TIME DATA AND DELAYS -------)						VARI	(---- S-WAVE TRAVEL-TIME DATA --)					(--- MAGNITUDE DATA --)				
STN	DIST	AZM	AIN	PSEC PRMK	TCOR	O-TTOB	TTCAL	C-DLAY	EDLY	P-RES	P-WT	THIC	SSEC	SRMK	TTOB	TTCAL	S-RES	S-WT	AMX	PR	XMAG	R	FMP	FMAG
x03	1.1	328	147	2.27IPC1		-0.13	0.60	1		-0.74	1.047		4.01	is2	1.61	1.12	0.48	0.465						
farm	1.6	222	136	3.10IP 3		0.70	0.66	1		0.03	0.116		3.80	es4	1.40	1.24	0.16	0.000						
wc02	2.1	4	127	3.39IPC0		0.99	0.73	1		0.25	1.860		3.92	is4	1.52	1.36	0.15	0.000						
pop	4.8	131	51	3.62IPC1		1.22	1.19	1		0.03	1.047		4.24	is4	1.84	2.15	-0.32	0.000						
x55	4.8	135	51	3.69IPC1		1.29	1.19	1		0.09	1.047		4.60	is1	2.20	2.16	0.03	1.047						
hlh	5.6	41	51	3.77IPD1		1.37	1.31	1		0.05	1.047		4.82	is4	2.42	2.37	0.05	0.000						
cfd	5.9	298	51	3.90IPC0		1.50	1.37	1		0.12	1.860			4										
con	7.0	325	51	4.03IPC1		1.63	1.55	1		0.07	1.047		4.98	is4	2.58	2.79	-0.21	0.000						
wc04	7.1	177	51	3.97 P 1		1.57	1.57	1		0.00	1.047		4.84	es4	2.44	2.81	-0.37	0.000						
ttr	7.4	203	51	4.06IPD1		1.66	1.61	1		0.04	1.047		5.34	is4	2.94	2.89	0.05	0.000						
x02	8.9	2	51	0.00 4		-2.40	1.86	1		-4.26	0.000		5.62	is1	3.22	3.32	-0.10	1.047						
tom	10.1	64	51	4.25IP 2		1.85	2.05	1		-0.20	0.465			4										
monm	10.2	114	51	4.30IPD3		1.90	2.07	1		-0.18	0.116		5.75	es4	3.35	3.69	-0.35	0.000						
wc03	11.6	38	51	4.60IPD0		2.20	2.30	1		-0.10	1.860		6.00	es4	3.60	4.08	-0.49	0.000						
x04	11.6	251	51	4.79IPC2		2.39	2.30	1		0.08	0.465		6.41	is1	4.01	4.09	-0.09	1.047						
wc01	12.3	252	51	4.81IPD0		2.41	2.41	1		-0.01	1.860		6.63	is4	4.23	4.28	-0.05	0.000						
min	12.8	219	51	4.85IP 2		2.45	2.49	1		-0.04	0.465			4										

QUALITY EVALUATION

DIAGONALS IN ORDER OF STRENGTH	Z	SE	NW	NE	N	SW	E
AVE. OF END POINTS	0.18	0.58	0.60	0.76	0.79	0.79	0.81

NUMBER	RMS	MIN DRMS	AVE DRMS	QUALITY
20	0.21	0.24	0.69	B

----------BEGIN----------

86/ 2/ 6 18/36 TEST DATA 86/ 2/ 6 18/36

HORIZONTAL AND VERTICAL SINGLE VARIABLE STANDARD DEVIATIONS (68% - ONE DEGREE OF FREEDOM)
[VALUES TRUNCATED AT 25 KM]

SEH = 0.15 SEH = 0.21 SEZ = 0.44 QUALITY = A
AZ = 5. AZ = -85.

SE OF ORIG = 0.04 TOTAL NUMBER OF ITERATIONS = 4 DMAX = 90.00 SEQUENCE NUMBER =
AT THE CLOSEST STATION USED IN THE SOLUTION BOTH P AND S WERE USED. THE S MINUS P INTERVAL EQUALS 0.87

DATE	ORIGIN	LAT	LONG	DEPTH	MAG	NO	D1	GAP	D	RMS	SEH	SEZ	Q	SQD	ADJ	IN	NR	AVR	AAR	NM	AVXM	SDXM	NF	AVFM	SDFM
860206	1836	22.24	41N38.56	81W 9.64	5.92		43	2	48	1	0.12	0.2	0.4	A	A	A	0.08	10	63	0.00	0.09	0		0.0	0		0.0

(- STATION DATA -)				(------ P-WAVE TRAVEL-TIME DATA AND DELAYS -------)						VARI	(---- S-WAVE TRAVEL-TIME DATA --)					(--- MAGNITUDE DATA --)				
STN	DIST	AZM	AIN	PSEC PRMK+TCOR-O=TTOB-TTCAL C-DLAY-EDLY=P-RES				P-WT	THIC	SSEC	SRMK	TTOB	TTCAL	S-RES	S-WT	AMX	PR	XMAG	R	FMP FMAG
x03	1.7	340	161	23.52IPC0	1.28	1.20	1	0.08	1.592	24.39	is1	2.15	2.17	-0.02	0.896					
wc02	2.8	3	152	23.56IPC0	1.32	1.27	1	0.05	1.592		4									
pop	4.4	124	139	23.75IPD1	1.51	1.42	1	0.09	0.896		4									
ham	4.7	160	137	23.70IPC1	1.46	1.46	1	0.00	0.896	24.33	is4	2.09	2.62	-0.53	0.000					
cal	5.0	12	135	23.81IPC1	1.57	1.49	1	0.08	0.896	25.06	is4	2.82	2.68	0.14	0.000					
wsh	5.4	251	132	23.91IPD1	1.67	1.54	1	0.13	0.896	24.93	is4	2.69	2.75	-0.06	0.000					
hlh	6.1	37	129	23.91IPD1	1.67	1.62	1	0.05	0.896		4									
cfd	6.3	304	128	23.95IPC0	1.71	1.65	1	0.06	1.592	25.00	es4	2.76	2.94	-0.18	0.000					
wc04	6.4	177	127	23.96IP 1	1.72	1.66	1	0.06	0.896		4									
erj	6.6	76	126	23.95IPD1	1.71	1.69	1	0.02	0.896	25.07	is4	2.83	3.02	-0.19	0.000					
ttr	6.8	205	126	24.11IPC1	1.87	1.70	1	0.17	0.896	25.52	is4	3.28	3.04	0.24	0.000					
con	7.6	328	122	24.08IPC1	1.84	1.81	1	0.03	0.896		4									
x06	8.3	100	120	24.13IPD0	1.89	1.92	1	-0.03	1.592	25.49	is1	3.25	3.42	-0.17	0.896					
cot	8.8	144	118	24.34IPC1	2.10	1.99	1	0.11	0.896	25.49	is4	3.25	3.54	-0.29	0.000					
cuy	9.3	184	116	24.42IPC1	2.18	2.06	1	0.12	0.896	25.78	is4	3.54	3.67	-0.13	0.000					
x02	9.6	1	116	24.31IPC0	2.07	2.11	1	-0.04	1.592	25.73	is1	3.49	3.75	-0.26	0.896					
hse	9.7	156	115	24.44EP+1	2.20	2.13	1	0.07	0.896	25.99	is4	3.75	3.78	-0.03	0.000					
tom	10.4	61	114	24.40IPD1	2.16	2.22	1	-0.06	0.896		4									
mon	11.5	119	111	24.71IPD1	2.47	2.39	1	0.08	0.896	26.11	is4	3.87	4.24	-0.37	0.000					
wc01	12.1	255	110	24.78IPD0	2.54	2.48	1	0.06	1.592	26.46	es4	4.22	4.41	-0.19	0.000					
wc03	12.2	36	110	24.71IPD0	2.47	2.49	1	-0.02	1.592	26.66	es4	4.42	4.42	0.00	0.000					
min	12.3	221	110	24.70EP 3	2.46	2.50	1	-0.04	0.100	26.50	es4	4.26	4.45	-0.19	0.000					
x08	12.3	202	110	24.43EP+1	2.19	2.51	1	-0.32	0.896	26.31	is1	4.07	4.47	-0.40	0.896					
x07	13.6	147	108	24.91EPC1	2.67	2.71	1	-0.04	0.896	26.91	is1	4.67	4.82	-0.15	0.896					
fot	13.8	87	108	25.02IPD1	2.78	2.74	1	0.04	0.896	27.02	is4	4.78	4.87	-0.09	0.000					
lox	14.8	41	106	25.07IPD1	2.83	2.90	1	-0.07	0.896	27.09	is4	4.85	5.13	-0.28	0.000					
wc06	15.8	136	105	25.40IPC0	3.16	3.06	1	0.10	1.592	27.48	is4	5.24	5.41	-0.17	0.000					
hwk	15.9	68	105	25.53IPD1	3.29	3.08	1	0.21	0.896	27.93	is4	5.69	5.44	0.25	0.000					
htg	17.4	98	104	25.40EP 3	3.16	3.30	1	-0.14	0.100		4									
wc07	17.5	5	104	25.49IPC0	3.25	3.33	1	-0.08	1.592	27.82	es4	5.38	5.88	-0.30	0.000					
x01	18.0	5	103	25.66IPC0	3.42	3.41	1	0.01	1.592	28.12	is1	5.88	6.01	-0.13	0.896					
che	19.0	221	103	25.80IPD0	3.56	3.57	1	-0.01	1.592	28.47	es4	6.23	6.29	-0.06	0.000					
cld	19.7	228	102	26.00IPD2	3.76	3.68	1	0.08	0.398		4									
mfd	21.3	160	101	26.30IP 2	4.06	3.92	1	0.14	0.398	29.20	es4	6.96	6.91	0.05	0.000					
x09	25.7	187	99	26.89EPD1	4.65	4.62	1	0.03	0.896	30.25	is1	8.01	8.13	-0.12	0.896					
x11	54.8	172	94	31.62IPU1	9.38	9.34	1	0.04	0.308		4									

QUALITY EVALUATION

DIAGONALS IN ORDER OF STRENGTH	Z	E	SE	NW	NE	SW	N
AVE. OF END POINTS	0.29	0.70	0.73	0.75	0.78	0.81	1.09

NUMBER	RMS	MIN DRMS	AVE DRMS	QUALITY
43	0.12	0.34	0.78	A

----------BEGIN----------

86/ 2/ 7 15/20 TEST DATA 86/ 2/ 7 15/20

HORIZONTAL AND VERTICAL SINGLE VARIABLE STANDARD DEVIATIONS (68% - ONE DEGREE OF FREEDOM)
[VALUES TRUNCATED AT 25 KM]

SEH = 0.13 SEH = 0.16 SEZ = 0.56 QUALITY = A
AZ = 11. AZ = -79.

SE OF ORIG = 0.04 TOTAL NUMBER OF ITERATIONS = 4 DMAX = 90.00 SEQUENCE NUMBER =
S AND P ARE NOT BOTH USED AT CLOSEST STATION

DATE	ORIGIN	LAT	LONG	DEPTH	MAG	NO	D1	GAP	D	RMS	SEH	SEZ	Q	SQD	ADJ	IN	NR	AVR	AAR	NM	AVXM	SDXM	NF	AVFM	SDFM
860207	1520 20.20	41N39.06	81W 9.24	4.59		27	2	42	1	0.08	0.2	0.6	A	A	A	0.07	10	46	0.00	0.06	0	0.0	0	0.0	

(- STATION DATA -)				(------ P-WAVE TRAVEL-TIME DATA AND DELAYS -------)								VARI	(---- S-WAVE TRAVEL-TIME DATA --)						(--- MAGNITUDE DATA --)					
STN	DIST	AZM	AIN	PSEC	PRMK	TCOR	O=TTOB	TTCAL	C-DLAY	EDLY	=P-RES	P-WT	THIC	SSEC	SRMK	TTOB	TTCAL	S-RES	S-WT	AMX	PR	XMAG	R	FMP	FMAG
wc02	1.9	348	154	21.29	PC1		1.09	1.01	1		0.08	0.938		21.64	es4	1.44	1.84	-0.40	0.000						
cal	4.0	7	132	21.51	IPC1		1.31	1.23	1		0.08	0.938		22.38	is4	2.18	2.21	-0.03	0.000						
pop	4.6	138	128	21.51	IPC1		1.31	1.29	1		0.02	0.938		22.17	is4	1.97	2.32	-0.35	0.000						
hlh	5.0	38	125	21.59	IPD1		1.39	1.35	1		0.04	0.938		22.34	is4	2.14	2.43	-0.29	0.000						
ham	5.4	169	123	21.56	ip	1	1.36	1.40	1		-0.04	0.938		22.46	is4	2.26	2.53	-0.27	0.000						
erj	5.9	83	120	21.77	IPD1		1.57	1.48	1		0.09	0.938		22.71	is4	2.51	2.65	-0.14	0.000						
wsh	6.2	245	118	21.76	IPD1		1.56	1.52	1		0.04	0.938		22.82	is4	2.62	2.73	-0.11	0.000						
cfd	6.3	294	118	21.70	IP	1	1.50	1.54	1		-0.04	0.938		22.60	es4	2.40	2.75	-0.35	0.000						
con	7.2	320	114	21.91	IPC1		1.71	1.66	1		0.05	0.938		22.86	is4	2.66	2.97	-0.31	0.000						
wc04	7.3	181	114	21.91	IPD1		1.71	1.68	1		0.03	0.938		23.16	es4	2.96	3.00	-0.04	0.000						
ttr	7.8	206	112	22.04	IPD1		1.84	1.75	1		0.09	0.938		23.45	is4	3.25	3.13	0.12	0.000						
x06	8.0	108	112	22.01	IPC1		1.81	1.77	1		0.04	0.938		23.22	is1	3.02	3.18	-0.16	0.938						
x02	8.7	358	110	22.12	IPC2		1.92	1.88	1		0.04	0.417		23.39	is1	3.19	3.37	-0.18	0.938						
cuy	10.3	187	106	22.39	IPD1		2.19	2.13	1		0.06	0.938		23.89	is4	3.69	3.79	-0.10	0.000						
wc03	11.1	37	105	22.45	IPD0		2.25	2.26	1		-0.01	1.668		24.05	es4	3.85	4.02	-0.17	0.000						
mon	11.6	124	104	22.56	IPC1		2.36	2.33	1		0.03	0.938		24.09	is4	3.89	4.14	-0.25	0.000						
wc01	12.9	252	103	22.80	IPD0		2.60	2.55	1		0.05	1.668		24.57	es4	4.37	4.51	-0.15	0.000						
fat	13.3	91	102	22.83	EPD1		2.63	2.60	1		0.03	0.938		24.71	is4	4.51	4.61	-0.10	0.000						
min	13.3	220	102	22.70	IP	1	2.50	2.61	1		-0.11	0.938			4										
x08	13.4	203	102	22.78	EPD1		2.58	2.62	1		-0.04	0.938		24.66	is1	4.46	4.64	-0.19	0.938						
lax	13.8	42	102	22.85	IPD1		2.65	2.68	1		-0.03	0.938		24.92	is4	4.72	4.75	-0.03	0.000						
wc06	16.1	140	100	23.30	IPC0		3.10	3.06	1		0.04	1.668		25.43	es4	5.23	5.40	-0.18	0.000						
x01	17.1	3	99	0.00	4		-20.20	3.21	1		-23.41	0.000		25.84	is1	5.64	5.67	-0.03	0.938						
mfd	21.9	162	97	24.20	IP	1	4.00	3.99	1		0.01	0.938			4										

QUALITY EVALUATION

DIAGONALS IN ORDER OF STRENGTH	Z	NW	SE	E	SW	NE	N
AVE. OF END POINTS	0.24	0.74	0.75	0.81	0.85	0.85	1.08

NUMBER	RMS	MIN DRMS	AVE DRMS	QUALITY
27	0.08	0.29	0.80	B

```
----------BEGIN----------
86/ 2/10   20/ 6                                TEST DATA                                86/ 2/10   20/ 6

                                HORIZONTAL AND VERTICAL SINGLE VARIABLE STANDARD DEVIATIONS (68% - ONE DEGREE OF FREEDOM)
                                [VALUES TRUNCATED AT 25 KM]
                                     SEH =   0.16          SEH =   0.22          SEZ =   0.62   QUALITY = A
                                     AZ  =    -5.          AZ  =   -95.

SE OF ORIG =   0.05  TOTAL NUMBER OF ITERATIONS =   4   DMAX =  90.00   SEQUENCE NUMBER =
S AND P ARE NOT BOTH USED AT CLOSEST STATION

 DATE    ORIGIN      LAT      LONG    DEPTH    MAG NO D1 GAP D  RMS  SEH  SEZ Q SQD  ADJ IN NR  AVR  AAR NM AVXM SDXM NF AVFM SDFM
860210 20 6 13.49 41N39.16  81W 9.27   4.97        26  2  69 1 0.09  0.2  0.6 A A A 0.06 10 44 0.00 0.08  0       0.0  0       0.0

(- STATION DATA -) (------ P-WAVE TRAVEL-TIME DATA AND DELAYS -------) VARI (---- S-WAVE TRAVEL-TIME DATA --)(--- MAGNITUDE DATA --)
 STN  DIST AZM AIN PSEC PRMK+TCOR-O=TTOB-TTCAL C-DLAY-EDLY=P-RES  P-WT THIC SSEC SRMK  TTOB TTCAL S-RES S-WT AMX PR XMAG R  FMP FMAG
wc02   1.7 348 158 14.54IPC0        1.05  1.06 1          -0.01 1.719      14.89 es4  1.40  1.91 -0.51 0.000
cal    3.8   8 136 14.89IPC1        1.40  1.25 1           0.15 0.967      15.76 is4  2.27  2.25  0.02 0.000
pop    4.7 139 130 14.87IPC1        1.38  1.35 1           0.03 0.967      15.54 is4  2.05  2.43 -0.38 0.000
hlh    4.9  40 129 14.93IPD1        1.44  1.38 1           0.06 0.967      15.97 is4  2.48  2.47  0.01 0.000
ham    5.6 169 125 14.86IPC1        1.37  1.46 1          -0.09 0.967      15.06 is4  1.57  2.64 -1.07 0.000
erj    6.0  85 123 15.06IPC1        1.57  1.50 1           0.07 0.967      16.24 is4  2.75  2.72  0.03 0.000
wsh    6.3 243 121 15.16IPD1        1.67  1.56 1           0.11 0.967      16.76 is4  3.27  2.79  0.48 0.000
con    7.0 320 118 15.21IPC1        1.72  1.67 1           0.05 0.967      22.86 is4  9.37  2.98  6.39 0.000
wc04   7.5 181 116 15.15IPD0        1.66  1.73 1          -0.07 1.719      15.93 es4  2.44  3.10 -0.66 0.000
ttr    8.0 205 114 15.35IPD1        1.86  1.80 1           0.06 0.967      16.68 is4  3.19  3.21 -0.02 0.000
x06    8.1 109 114 15.36IPC1        1.87  1.81 1           0.05 0.967      16.62 is1  3.13  3.24 -0.11 0.967
x02    8.5 358 113 15.42IPC1        1.93  1.88 1           0.05 0.967      16.72 is1  3.23  3.35 -0.12 0.967
x02    8.5 358 113 15.48   2        1.99  1.88 1           0.11 0.430      16.74 is2  3.25  3.35 -0.10 0.430
cot    9.4 150 111 15.54IPC1        2.05  2.01 1           0.04 0.967      16.91 is4  3.42  3.60 -0.18 0.000
cuy   10.4 187 109 15.72EPC2        2.23  2.16 1           0.07 0.430      17.39 is4  3.90  3.87  0.03 0.000
wc03  11.0  37 107 15.67IPD0        2.18  2.26 1          -0.08 1.719      17.35 es4  3.86  4.02 -0.16 0.000
mon   11.7 125 106 15.91IPC1        2.42  2.37 1           0.05 0.967          4
wc01  12.9 251 105 15.95 P 1        2.46  2.56 1          -0.11 0.967      17.78 es4  4.29  4.55 -0.26 0.000
fot   13.3  92 104 16.19EPC2        2.70  2.63 1           0.07 0.430      18.21 is4  4.72  4.65  0.07 0.000
lox   13.7  43 104 16.09IPD1        2.60  2.68 1          -0.08 0.967      18.34 is4  4.85  4.75  0.10 0.000
hwk   15.1  71 102 16.62IPC1        3.13  2.90 1           0.23 0.967      18.98 is4  5.49  5.13  0.36 0.000
wc06  16.3 140 101 16.50IPC0        3.01  3.10 1          -0.09 1.719          4
x01   16.9   4 101  0.00   4      -13.49  3.19 1         -16.68 0.000      19.07 is1  5.58  5.64 -0.06 0.967

                    QUALITY EVALUATION

DIAGONALS IN ORDER OF STRENGTH       Z     E    SW    NE    SE    NW     N
AVE. OF END POINTS                0.23  0.68  0.69  0.71  0.73  0.76  0.99


          NUMBER       RMS  MIN DRMS  AVE DRMS   QUALITY
             26      0.09      0.27      0.72         B
```

----------BEGIN----------

86/ 2/23 3/29 TEST DATA 86/ 2/23 3/29

HORIZONTAL AND VERTICAL SINGLE VARIABLE STANDARD DEVIATIONS (68% - ONE DEGREE OF FREEDOM)
[VALUES TRUNCATED AT 25 KM]

SEH = 0.24 SEH = 0.28 SEZ = 0.73 QUALITY = A
AZ = -19. AZ = -109.

SE OF ORIG = 0.07 TOTAL NUMBER OF ITERATIONS = 4 DMAX = 90.00 SEQUENCE NUMBER =
AT THE CLOSEST STATION USED IN THE SOLUTION BOTH P AND S WERE USED. THE S MINUS P INTERVAL EQUALS 0.55

DATE	ORIGIN	LAT	LONG	DEPTH	MAG	NO	D1	GAP	D	RMS	SEH	SEZ	Q	SQD	ADJ	IN	NR	AVR	AAR	NM	AVXM	SDXM	NF	AVFM	SDFM
860223	329 48.46	41N39.06	81W 9.44	4.77		16	2	95	1	0.08	0.3	0.7	B	A B	0.07	10	16	0.00	0.06	0		0.0	0		0.0

(- STATION DATA -)				(------ P-WAVE TRAVEL-TIME DATA AND DELAYS -------)						VARI	(---- S-WAVE TRAVEL-TIME DATA --)						(--- MAGNITUDE DATA --)					
STN	DIST	AZM	AIN	PSEC	PRMK	TCOR-O=TTOB-TTCAL		C-DLAY-EDLY=P-RES	P-WT	THIC	SSEC	SRMK	TTOB	TTCAL	S-RES	S-WT	AMX	PR	XMAG	R	FMP	FMAG
wc02	1.8	356	155	49.55	IPC0	1.09	1.04 1	0.06	2.586		50.10	s3	1.64	1.88	-0.24	0.162						
pop	4.7	136	128	49.82	IPC0	1.36	1.33 1	0.03	2.586		50.47	is3	2.01	2.40	-0.39	0.162						
hlh	5.2	40	125	49.86	EPD0	1.40	1.39 1	0.01	2.586		50.81	is3	2.35	2.50	-0.15	0.162						
con	7.0	322	116	50.14	IPC0	1.68	1.65 1	0.03	2.586		51.14	is3	2.68	2.95	-0.27	0.162						
ttr	7.7	204	114	50.29	EP 1	1.83	1.75 1	0.08	1.455		51.54	is3	3.08	3.12	-0.04	0.162						
wc03	11.3	38	106	50.66	EP 3	2.20	2.30 1	-0.10	0.162		52.28	s3	3.82	4.08	-0.26	0.162						
wc01	12.6	252	104	50.91	IPD0	2.45	2.51 1	-0.06	2.586		52.79	is3	4.33	4.45	-0.12	0.162						
wc06	16.3	139	101	51.48	EP 3	3.02	3.09 1	-0.07	0.162		53.71	es3	5.25	5.47	-0.22	0.162						

QUALITY EVALUATION

DIAGONALS IN ORDER OF STRENGTH	Z	NW	NE	N	SE	SW	E
AVE. OF END POINTS	0.26	0.61	0.66	0.66	0.68	0.71	0.72

NUMBER	RMS	MIN DRMS	AVE DRMS	QUALITY
16	0.08	0.28	0.64	B

----------BEGIN----------

86/ 2/24 16/55 TEST DATA 86/ 2/24 16/55

HORIZONTAL AND VERTICAL SINGLE VARIABLE STANDARD DEVIATIONS (68% - ONE DEGREE OF FREEDOM)
[VALUES TRUNCATED AT 25 KM]

SEH = 0.33 SEH = 0.46 SEZ = 3.54 QUALITY = C
AZ = 1. AZ = -89.

SE OF ORIG = 0.22 TOTAL NUMBER OF ITERATIONS = 5 DMAX = 90.00 SEQUENCE NUMBER =
AT THE CLOSEST STATION USED IN THE SOLUTION BOTH P AND S WERE USED. THE S MINUS P INTERVAL EQUALS 0.64

DATE	ORIGIN	LAT	LONG	DEPTH	MAG	NO	D1	GAP	D	RMS	SEH	SEZ	Q	SQD	ADJ	IN	NR	AVR	AAR	NM	AVXM	SDXM	NF	AVFM	SDFM
860224	1655	6.37	41N38.96	81W 9.81	3.72		10	5	126	1	0.09	0.5	3.5	C	C	B	0.32	10	12	0.00	0.05	0		0.0	0		0.0

(- STATION DATA -)				(------ P-WAVE TRAVEL-TIME DATA AND DELAYS -------)							VARI	(---- S-WAVE TRAVEL-TIME DATA --)					(--- MAGNITUDE DATA --)				
STN	DIST	AZM	AIN	PSEC	PRMK	TCOR	O=TTOB	TTCAL	C-DLAY	EDLY=P-RES	P-WT	THIC	SSEC	SRMK	TTOB	TTCAL	S-RES	S-WT	AMX	PR	XMAG	R	FMP	FMAG
pop	5.0	130	116	7.68	IPD	0	1.31	1.28	1	0.04	2.759		8.32	is3	1.95	2.30	-0.35	0.172						
hlh	5.7	43	112	7.75	IPC	0	1.38	1.37	1	0.01	2.759		8.65	is3	2.28	2.49	-0.20	0.172						
con	6.9	326	108	7.94	IPC	0	1.57	1.56	1	0.01	2.759		9.34	is3	2.97	2.81	0.17	0.172						
ttr	7.3	201	106	8.07	EP	2	1.70	1.64	1	0.07	0.690		8.97	is3	2.60	2.93	-0.33	0.172						
wc03	11.7	39	99	0.00		4	-6.37	2.33	1	-8.69	0.000		10.25	es3	3.88	4.13	-0.25	0.172						
wc01	12.1	252	99	7.95	EP	4	1.58	2.39	1	-0.80	0.000		10.35	es3	3.98	4.25	-0.26	0.172						

QUALITY EVALUATION

DIAGONALS IN ORDER OF STRENGTH	Z	NE	E	SW	NW	N	SE
AVE. OF END POINTS	0.16	0.58	0.60	0.66	0.66	0.70	0.73

NUMBER	RMS	MIN DRMS	AVE DRMS	QUALITY
10	0.09	0.21	0.62	B

----------BEGIN----------

86/ 2/28 1/39 TEST DATA 86/ 2/28 1/39

HORIZONTAL AND VERTICAL SINGLE VARIABLE STANDARD DEVIATIONS (68% - ONE DEGREE OF FREEDOM)
[VALUES TRUNCATED AT 25 KM]

SEH = 0.28 SEH = 0.39 SEZ = 0.87 QUALITY = A
AZ = 6. AZ = -84.

SE OF ORIG = 0.08 TOTAL NUMBER OF ITERATIONS = 5 DMAX = 90.00 SEQUENCE NUMBER =
AT THE CLOSEST STATION USED IN THE SOLUTION BOTH P AND S WERE USED. THE S MINUS P INTERVAL EQUALS 0.60

DATE	ORIGIN	LAT	LONG	DEPTH	MAG	NO	D1	GAP	D	RMS	SEH	SEZ	Q	SQD	ADJ	IN	NR	AVR	AAR	NM	AVXM	SDXM	NF	AVFM	SDFM
860228	139 34.07	41N39.11	81W 9.59	4.31		12	2	92	1	0.08	0.4	0.9	B	A B	0.05	10	13	0.00	0.04	0		0.0	0		0.0

(- STATION DATA -)				(------ P-WAVE TRAVEL-TIME DATA AND DELAYS -------)						VARI	(---- S-WAVE TRAVEL-TIME DATA --)					(--- MAGNITUDE DATA --)				
STN	DIST	AZM	AIN	PSEC PRMK+TCOR-O=TTOB-TTCAL		C-DLAY-EDLY=P-RES		P-WT	THIC	SSEC	SRMK	TTOB	TTCAL	S-RES	S-WT	AMX	PR	XMAG	R	FMP FMAG
wc02	1.7	3	154	35.10IPC0	1.03	0.96	1	0.07	2.560	35.70	es3	1.63	1.75	-0.12	0.160					
pop	5.0	135	123	35.45EP 2	1.38	1.31	1	0.07	0.640	36.05	is3	1.98	2.38	-0.40	0.160					
hlh	5.3	43	120	35.43IPD0	1.36	1.36	1	0.00	2.560	36.21	is3	2.14	2.45	-0.31	0.160					
wc09	6.8	177	114	35.70IP 4	1.63	1.58	1	0.05	0.000		4									
con	6.8	323	113	35.65IPC0	1.58	1.58	1	0.00	2.560	36.60	is3	2.53	2.84	-0.31	0.160					
ttr	7.7	202	110	35.78IPD0	1.71	1.71	1	0.00	2.560	37.13	is3	3.06	3.08	-0.02	0.160					
wc01	12.5	251	102	36.60EP+3	2.53	2.47	1	0.06	0.160	38.30	es3	4.23	4.38	-0.15	0.160					

QUALITY EVALUATION

DIAGONALS IN ORDER OF STRENGTH	Z	NW	E	SE	SW	NE	N
AVE. OF END POINTS	0.26	0.51	0.53	0.65	0.67	0.67	0.71

NUMBER	RMS	MIN DRMS	AVE DRMS	QUALITY
12	0.08	0.27	0.59	B

```
----------BEGIN----------------------------------------------------------------------------------------
86/ 3/ 8    20/42                                  TEST DATA                                  86/ 3/ 8    20/42

                                  HORIZONTAL AND VERTICAL SINGLE VARIABLE STANDARD DEVIATIONS (68% - ONE DEGREE OF FREEDOM)
                                  [VALUES TRUNCATED AT 25 KM]
                                       SEH =   0.34          SEH =   0.35          SEZ =   0.98   QUALITY = A
                                       AZ  =  -56.           AZ  =   34.

SE OF ORIG =   0.07  TOTAL NUMBER OF ITERATIONS =   4   DMAX =  90.00   SEQUENCE NUMBER =
AT THE CLOSEST STATION USED IN THE SOLUTION BOTH P AND S WERE USED.  THE S MINUS P INTERVAL EQUALS      0.45

 DATE    ORIGIN      LAT      LONG    DEPTH    MAG NO D1 GAP D  RMS  SEH  SEZ Q SQD  ADJ IN NR  AVR  AAR NM AVXM SDXM NF AVFM SDFM
860308 2042 49.49 41N38.72  81W 9.36   4.42        12  2 102 1 0.10  0.4  1.0 B A B 0.11 10 12 0.00 0.09  0       0.0  0       0.0

(- STATION DATA -) (------ P-WAVE TRAVEL-TIME DATA AND DELAYS -------) VARI (---- S-WAVE TRAVEL-TIME DATA --)(--- MAGNITUDE DATA --)
 STN  DIST AZM AIN PSEC PRMK+TCOR-O=TTOB-TTCAL C-DLAY-EDLY=P-RES  P-WT THIC SSEC SRMK  TTOB TTCAL S-RES S-WT AMX PR XMAG R  FMP FMAG
wc02   2.5 355 145 50.60IPC0        1.11  1.04 1            0.07 1.882      51.05 es3  1.56  1.88 -0.32 0.118
wc09   6.1 180 117 50.90IP 0        1.41  1.48 1           -0.07 1.882      51.90 es3  2.41  2.66 -0.25 0.118
wc08   7.6 292 112 51.30IPC0        1.81  1.71 1            0.10 1.882      52.60 es3  3.11  3.07  0.04 0.118
wc03  11.7  36 103 51.75IPD0        2.26  2.35 1           -0.09 1.882      53.50 is3  4.01  4.17 -0.16 0.118
wc01  12.6 254 102 51.90IPC0        2.41  2.49 1           -0.07 1.882      53.80 es3  4.31  4.41 -0.10 0.118
wc06  15.8 138 100 52.60IPC0        3.11  3.00 1            0.12 1.882      54.75 es3  5.26  5.30 -0.04 0.118

                        QUALITY EVALUATION

DIAGONALS IN ORDER OF STRENGTH        Z    NE    NW    SW    SE     N     E
AVE. OF END POINTS                 0.22  0.66  0.69  0.73  0.77  0.77  0.89


              NUMBER       RMS  MIN DRMS  AVE DRMS   QUALITY
                 12      0.10      0.28      0.72         B
```

```
----------BEGIN-----------------------------------------------------------------------------------------
86/ 3/12    8/55                                  TEST DATA                                  86/ 3/12    8/55

                                  HORIZONTAL AND VERTICAL SINGLE VARIABLE STANDARD DEVIATIONS (68% - ONE DEGREE OF FREEDOM)
                                  [VALUES TRUNCATED AT 25 KM]
                                       SEH =   0.30          SEH =   0.71          SEZ =   0.38   QUALITY = A
                                       AZ  =  -115.          AZ  =  -25.

SE OF ORIG =   0.13  TOTAL NUMBER OF ITERATIONS =   9   DMAX =  90.00   SEQUENCE NUMBER =
S AND P ARE NOT BOTH USED AT CLOSEST STATION

 DATE    ORIGIN      LAT      LONG     DEPTH    MAG NO D1 GAP D  RMS  SEH  SEZ Q SQD  ADJ IN NR  AVR  AAR NM AVXM SDXM NF AVFM SDFM
860312  855 26.59 41N43.64  81W10.25   2.00        10  1 216 1 0.06  0.7  0.4 C B D 0.24 10 10-0.01 0.04  0       0.0  0       0.0

(- STATION DATA -) (------ P-WAVE TRAVEL-TIME DATA AND DELAYS -------) VARI (---- S-WAVE TRAVEL-TIME DATA --)(--- MAGNITUDE DATA --)
 STN  DIST AZM AIN PSEC PRMK+TCOR-O=TTOB-TTCAL C-DLAY-EDLY=P-RES  P-WT THIC SSEC SRMK  TTOB TTCAL S-RES S-WT AMX PR XMAG R  FMP FMAG
x02    1.1  79 146 25.55IPC9       -1.04  0.59 1          -0.04 2.647      25.97 is1  0.42  0.46 -0.04  SMP
wc02   6.7 171  51 28.16IP 1         1.57  1.51 1           0.06 2.647      29.23 is3  2.64  2.71 -0.07 0.294
wc03   8.0  87  51 28.35EP 3         1.76  1.73 1           0.03 0.294      29.56 es3  2.97  3.09 -0.12 0.294
wc08   8.6 223  51 28.40EP 3         1.81  1.82 1          -0.01 0.294      29.65 es3  3.06  3.25 -0.19 0.294
wc09  15.2 175  51 29.47EP 1         2.88  2.89 1          -0.01 2.647            4
wc01  16.5 221  51 29.70EP 3         3.11  3.11 1           0.00 0.294      32.00 es3  5.41  5.49 -0.08 0.294

                     QUALITY EVALUATION

DIAGONALS IN ORDER OF STRENGTH        Z    NW    SE    N    SW    E    NE
AVE. OF END POINTS                 0.39  0.69  0.69  0.75  0.82  0.85  0.87


           NUMBER      RMS  MIN DRMS  AVE DRMS   QUALITY
               10     0.06      0.64      0.77         A
```

```
----------BEGIN-----------------------------------------------------------------------------------------
86/ 3/24   13/42                                  TEST DATA                                  86/ 3/24   13/42

                                  HORIZONTAL AND VERTICAL SINGLE VARIABLE STANDARD DEVIATIONS (68% - ONE DEGREE OF FREEDOM)
                                  [VALUES TRUNCATED AT 25 KM]
                                       SEH =   0.22          SEH =   0.24          SEZ =   0.69   QUALITY = A
                                       AZ  =   -42.          AZ  =  -132.

SE OF ORIG =   0.05  TOTAL NUMBER OF ITERATIONS =   4   DMAX =  90.00   SEQUENCE NUMBER =
AT THE CLOSEST STATION USED IN THE SOLUTION BOTH P AND S WERE USED.  THE S MINUS P INTERVAL EQUALS      0.70

 DATE    ORIGIN      LAT      LONG    DEPTH    MAG NO D1 GAP D  RMS  SEH  SEZ Q SQD  ADJ IN NR  AVR  AAR NM AVXM SDXM NF AVFM SDFM
860324 1342 41.20 41N38.05  81W 9.97   4.92        12  4  97 1 0.06  0.2  0.7 B A B 0.13 10 12 0.00 0.05  0       0.0  0       0.0

(- STATION DATA -) (------ P-WAVE TRAVEL-TIME DATA AND DELAYS -------) VARI (---- S-WAVE TRAVEL-TIME DATA --)(--- MAGNITUDE DATA --)
 STN  DIST AZM AIN PSEC PRMK+TCOR-O=TTOB-TTCAL C-DLAY-EDLY=P-RES  P-WT THIC SSEC SRMK  TTOB TTCAL S-RES S-WT AMX PR XMAG R  FMP FMAG
wc02   3.8   9 136 42.45IPCO        1.25  1.23 1           0.01 1.882      43.15 es3  1.95  2.23 -0.28 0.118
wc09   4.9 170 128 42.65IPCO        1.45  1.37 1           0.08 1.882      43.45 es3  2.25  2.45 -0.21 0.118
wc08   7.5 303 116 42.90IPCO        1.70  1.72 1          -0.02 1.882      44.07 es3  2.87  3.08 -0.21 0.118
wc01  11.5 259 106 43.55IPDO        2.35  2.33 1           0.01 1.882      45.25 es3  4.05  4.14 -0.10 0.118
wc03  13.2  35 104 43.85IPDO        2.65  2.61 1           0.04 1.882      45.80 es3  4.60  4.62 -0.02 0.118
wc06  15.5 132 102 44.10IPCO        2.90  2.97 1          -0.07 1.882      46.33 es3  5.13  5.25 -0.12 0.118

                    QUALITY EVALUATION

DIAGONALS IN ORDER OF STRENGTH        Z    NE    SW    NW     N    SE     E
AVE. OF END POINTS                 0.22  0.68  0.71  0.72  0.77  0.83  0.90


           NUMBER       RMS  MIN DRMS  AVE DRMS   QUALITY
              12      0.06      0.29      0.73         B
```

AVERAGE RMS OF ALL EVENTS = 0.10

XXXXX CLASS/	A	B	C	D	TOTAL XXXXX
NUMBER/	12.0	0.0	1.0	0.0	13.0
P/	92.3	0.0	7.7	0.0	

INCLUDE ONLY CLASS B AND BETTER IN THE FOLLOWING STATISTICS.

	P RESIDUALS				S RESIDUALS				S-P RESIDUALS				X-MAG RES			F-MAG RES			
STATION	N	WT	AVE	SD	N	WT	AVE	SD	N	WT	AVE	SD	N	AVE	SD	N	AVE	SD	STATION
bur	1	0.8	0.12	0.00	0	0.0	0.00	0.00	0	0.0	0.00	0.00	0	0.00	0.00	0	0.00	0.00	bur
cal	4	0.9	0.12	0.04	0	0.0	0.00	0.00	0	0.0	0.00	0.00	0	0.00	0.00	0	0.00	0.00	cal
calm	1	0.1	-0.01	0.00	0	0.0	0.00	0.00	0	0.0	0.00	0.00	0	0.00	0.00	0	0.00	0.00	calm
cfd	3	1.5	0.07	0.06	0	0.0	0.00	0.00	0	0.0	0.00	0.00	0	0.00	0.00	0	0.00	0.00	cfd
cha	1	1.5	0.06	0.00	0	0.0	0.00	0.00	0	0.0	0.00	0.00	0	0.00	0.00	0	0.00	0.00	cha
che	2	1.5	-0.02	0.01	0	0.0	0.00	0.00	0	0.0	0.00	0.00	0	0.00	0.00	0	0.00	0.00	che
choh	2	1.0	-0.15	0.01	1	0.5	-0.09	0.00	0	0.0	0.00	0.00	0	0.00	0.00	0	0.00	0.00	choh
cld	3	0.7	-0.02	0.05	0	0.0	0.00	0.00	0	0.0	0.00	0.00	0	0.00	0.00	0	0.00	0.00	cld
con	8	1.3	0.04	0.03	2	0.2	-0.29	0.02	0	0.0	0.00	0.00	0	0.00	0.00	0	0.00	0.00	con
cot	3	0.9	0.07	0.03	0	0.0	0.00	0.00	0	0.0	0.00	0.00	0	0.00	0.00	0	0.00	0.00	cot
cuy	4	0.8	0.06	0.05	0	0.0	0.00	0.00	0	0.0	0.00	0.00	0	0.00	0.00	0	0.00	0.00	cuy
elfm	1	0.1	0.16	0.00	0	0.0	0.00	0.00	0	0.0	0.00	0.00	0	0.00	0.00	0	0.00	0.00	elfm
erj	3	0.9	0.06	0.03	0	0.0	0.00	0.00	0	0.0	0.00	0.00	0	0.00	0.00	0	0.00	0.00	erj
farm	1	0.1	0.03	0.00	0	0.0	0.00	0.00	0	0.0	0.00	0.00	0	0.00	0.00	0	0.00	0.00	farm
fot	3	0.8	0.04	0.02	0	0.0	0.00	0.00	0	0.0	0.00	0.00	0	0.00	0.00	0	0.00	0.00	fot
gar	1	1.2	0.00	0.00	1	0.1	0.04	0.00	0	0.0	0.00	0.00	0	0.00	0.00	0	0.00	0.00	gar
ham	4	0.9	-0.03	0.05	0	0.0	0.00	0.00	0	0.0	0.00	0.00	0	0.00	0.00	0	0.00	0.00	ham
haoh	2	1.0	0.06	0.02	1	0.1	-0.39	0.00	0	0.0	0.00	0.00	0	0.00	0.00	0	0.00	0.00	haoh
har	1	0.8	0.02	0.00	0	0.0	0.00	0.00	0	0.0	0.00	0.00	0	0.00	0.00	0	0.00	0.00	har
hlh	9	1.4	0.05	0.04	3	0.2	-0.22	0.07	0	0.0	0.00	0.00	0	0.00	0.00	0	0.00	0.00	hlh
howm	2	0.1	0.05	0.03	0	0.0	0.00	0.00	0	0.0	0.00	0.00	0	0.00	0.00	0	0.00	0.00	howm
hpv	2	1.5	-0.02	0.01	1	0.1	-0.18	0.00	0	0.0	0.00	0.00	0	0.00	0.00	0	0.00	0.00	hpv
hse	2	0.9	0.04	0.04	0	0.0	0.00	0.00	0	0.0	0.00	0.00	0	0.00	0.00	0	0.00	0.00	hse
hsoh	1	1.2	0.30	0.00	0	0.0	0.00	0.00	0	0.0	0.00	0.00	0	0.00	0.00	0	0.00	0.00	hsoh
htg	2	0.8	-0.09	0.02	0	0.0	0.00	0.00	0	0.0	0.00	0.00	0	0.00	0.00	0	0.00	0.00	htg
hwk	3	0.9	0.23	0.02	0	0.0	0.00	0.00	0	0.0	0.00	0.00	0	0.00	0.00	0	0.00	0.00	hwk
lox	4	0.9	-0.03	0.06	0	0.0	0.00	0.00	0	0.0	0.00	0.00	0	0.00	0.00	0	0.00	0.00	lox
mfd	3	0.9	0.03	0.04	0	0.0	0.00	0.00	0	0.0	0.00	0.00	0	0.00	0.00	0	0.00	0.00	mfd
min	5	0.7	-0.10	0.04	0	0.0	0.00	0.00	0	0.0	0.00	0.00	0	0.00	0.00	0	0.00	0.00	min
mon	4	0.9	0.05	0.02	0	0.0	0.00	0.00	0	0.0	0.00	0.00	0	0.00	0.00	0	0.00	0.00	mon
monm	1	0.1	-0.18	0.00	0	0.0	0.00	0.00	0	0.0	0.00	0.00	0	0.00	0.00	0	0.00	0.00	monm
mtoh	1	1.2	-0.05	0.00	1	0.1	-0.26	0.00	0	0.0	0.00	0.00	0	0.00	0.00	0	0.00	0.00	mtoh
paoh	1	0.8	0.03	0.00	0	0.0	0.00	0.00	0	0.0	0.00	0.00	0	0.00	0.00	0	0.00	0.00	paoh
per	1	0.8	-0.26	0.00	0	0.0	0.00	0.00	0	0.0	0.00	0.00	0	0.00	0.00	0	0.00	0.00	per
pop	6	1.2	0.04	0.03	2	0.2	-0.39	0.01	0	0.0	0.00	0.00	0	0.00	0.00	0	0.00	0.00	pop
tom	3	0.9	-0.03	0.09	0	0.0	0.00	0.00	0	0.0	0.00	0.00	0	0.00	0.00	0	0.00	0.00	tom
ttr	7	1.2	0.06	0.05	2	0.2	-0.03	0.01	0	0.0	0.00	0.00	0	0.00	0.00	0	0.00	0.00	ttr
wc01	11	1.4	-0.01	0.05	6	0.2	-0.14	0.10	0	0.0	0.00	0.00	0	0.00	0.00	0	0.00	0.00	wc01
wc02	12	1.9	0.07	0.06	6	0.2	-0.19	0.10	0	0.0	0.00	0.00	0	0.00	0.00	0	0.00	0.00	wc02
wc03	11	1.4	-0.05	0.05	5	0.2	-0.19	0.08	0	0.0	0.00	0.00	0	0.00	0.00	0	0.00	0.00	wc03
wc04	7	1.4	0.01	0.04	1	0.5	-0.33	0.00	0	0.0	0.00	0.00	0	0.00	0.00	0	0.00	0.00	wc04
wc06	7	1.3	0.02	0.09	3	0.1	-0.13	0.08	0	0.0	0.00	0.00	0	0.00	0.00	0	0.00	0.00	wc06
wc07	2	1.5	-0.09	0.02	0	0.0	0.00	0.00	0	0.0	0.00	0.00	0	0.00	0.00	0	0.00	0.00	wc07
wc08	3	1.4	0.03	0.06	3	0.2	-0.14	0.10	0	0.0	0.00	0.00	0	0.00	0.00	0	0.00	0.00	wc08
wc09	3	2.1	0.00	0.06	2	0.1	-0.23	0.02	0	0.0	0.00	0.00	0	0.00	0.00	0	0.00	0.00	wc09
wkr	1	0.8	0.01	0.00	0	0.0	0.00	0.00	0	0.0	0.00	0.00	0	0.00	0.00	0	0.00	0.00	wkr
wsh	4	0.9	0.10	0.04	0	0.0	0.00	0.00	0	0.0	0.00	0.00	0	0.00	0.00	0	0.00	0.00	wsh
x01	3	1.5	0.03	0.02	4	0.9	-0.07	0.04	0	0.0	0.00	0.00	0	0.00	0.00	0	0.00	0.00	x01
x02	6	1.1	0.00	0.05	7	0.9	-0.16	0.06	1	2.6	-0.04	0.00	0	0.00	0.00	0	0.00	0.00	x02
x03	4	1.4	-0.10	0.30	4	0.8	0.04	0.20	0	0.0	0.00	0.00	0	0.00	0.00	0	0.00	0.00	x03
x04	3	1.1	0.09	0.04	2	1.3	-0.08	0.01	0	0.0	0.00	0.00	0	0.00	0.00	0	0.00	0.00	x04
x06	5	1.3	0.02	0.03	5	1.0	-0.12	0.05	0	0.0	0.00	0.00	0	0.00	0.00	0	0.00	0.00	x06
x07	2	0.9	0.02	0.06	2	0.9	-0.13	0.02	0	0.0	0.00	0.00	0	0.00	0.00	0	0.00	0.00	x07
x08	3	1.1	-0.08	0.15	3	0.9	-0.21	0.14	0	0.0	0.00	0.00	0	0.00	0.00	0	0.00	0.00	x08
x09	2	0.9	0.01	0.02	2	0.9	-0.15	0.04	0	0.0	0.00	0.00	0	0.00	0.00	0	0.00	0.00	x09
x11	1	0.3	0.04	0.00	0	0.0	0.00	0.00	0	0.0	0.00	0.00	0	0.00	0.00	0	0.00	0.00	x11
x55	1	1.0	0.09	0.00	1	1.0	0.03	0.00	0	0.0	0.00	0.00	0	0.00	0.00	0	0.00	0.00	x55

*U.S. GOVERNMENT PRINTING OFFICE: 1986-491-405:40006